공학박사 학위논문

MATHEMATICAL MODELING-BASED APPROACH TO CARDIOPULMONARY RESUSCITATION

심폐소생술에 대한 수학적 모델링 기반의 접근

2021 년 8 월

서울대학교 대학원

협동과정 바이오엔지니어링 전공

신 동 아

심폐소생술에 대한 수학적 모델링 기반의 접근

지도 교수 이 정 찬

이 논문을 공학박사 학위논문으로 제출함
2021 년 08 월

서울대학교 대학원
협동과정 바이오엔지니어링
신 동 아

신동아의 공학박사 학위논문을 인준함
2021 년 08 월

위 원 장		김 희 찬
부위원장		이 정 찬
위 원		서 길 준
위 원		박 중 열
위 원		최 성 욱

Ph. D. Dissertation

MATHEMATICAL MODELING-BASED APPROACH TO CARDIOPULMONARY RESUSCITATION

BY

DONG AH SHIN

AUGUST 2021

INTERDISCIPLINARY PROGRAM IN

BIOENGINEERING

THE GRADUATE SCHOOL

SEOUL NATIONAL UNIVERSITY

MATHEMATICAL MODELING-BASED APPROACH TO CARDIOPULMONARY RESUSCITATION

Academic adviser Jung Chan Lee
Submitting a Ph.D. Dissertation of Engineering
August 2021

Interdisciplinary Program in Bioengineering
Graduate School, Seoul National University

Dong Ah Shin

Confirming the Ph.D. Dissertation written by
Dong Ah Shin
August 2021

Chair
Hee Chan Kim, Ph. D.

Vice Chair
Jung Chan Lee, Ph.D.

Examiner
Gil Joon Suh, M.D. / Ph. D.

Examiner
Joong Yull Park, Ph. D.

Examiner
Seong Wook Choi, Ph. D.

ABSTRACT

MATHEMATICAL MODELING-BASED APPROACH TO CARDIOPULMONARY RESUSCITATION

Dong Ah Shin

Interdisciplinary Program in Bioengineering

The Graduate School

Seoul National University

For a long time, many studies based on mathematical modeling have been conducted to understand cardiopulmonary resuscitation (CPR) physiology. However, some aspects of the existing CPR model do not reflect the current CPR physiology appropriately. If the generalized CPR model does not suitably reflect the hemodynamic phenomena of current CPR, errors may exist in the hemodynamic interpretation. In addition, it is suggested that the one-size-fits-all CPR specified in the guidelines is not suitable, and the direction of recent CPR research is shifting toward personalized CPR. However, in personalized CPR, it is difficult to use preclinical or clinical trial approaches because various factors associated with the patient and environment interact and affect the patient. Therefore, this study was conducted with three goals to provide insight into the hemodynamics during CPR through a simulation-based approach.

The first objective was to develop an improved generalized CPR model that can reflect the current CPR physiology. The modified CPR model

proposed herein added superior and inferior vena cava compartments in the thoracic cavity of the existing model, as well as a "hybrid pump" mechanism. To compare the hemodynamic effects of the existing and modified models, various maneuvers such as the active compression-decompression CPR combined with the impedance threshold device, head-up tilt, and head-down tilt were simulated. Additionally, the modified model was compared with an animal model to confirm that it reflects the current CPR physiology more than the existing model does. The comparison showed that the pressure waveform and coronary perfusion pressure (CPP) were more appropriately reflected than in the existing model. Therefore, it was verified that the improved model developed in this study is a generalized CPR model that reflects the current CPR physiology more accurately.

The second goal was to verify the hemodynamic effects on the reduced thoracic elasticity and compression position—which are the current issues of the existing CPR technique—through simulation based on the improved model. The reduced elasticity of the thorax was simulated to decrease linearly for 1 min immediately after the start of CPR. The results show that as the elasticity of the thorax decreased, the pressure amplitude of the aorta and vena cava decreased during compression, along with the venous return and blood flow. Furthermore, a simple simulation was performed by adjusting the compression ratio between the ventricle and atrium with the thoracic pump factor to compare the hemodynamic difference according to the compression position. Consequently, when the atrium was compressed more than the ventricle, the stroke volume and CPP decreased, indicating that hemodynamics was limited. Therefore, it was demonstrated that a change in the pressure amplitude and CPP during compression could potentially enable estimation of the change in the elasticity of the thorax and assist in determining the position of compression.

Finally, this study attempted to present the possibility of a personalized CPR model. Cardiovascular parameters were estimated for different patients using a genetic algorithm. Additionally, it was confirmed that

patient-specific cardiovascular models could be constructed with different sets of parameters for each patient. Furthermore, incorporating the CPR model into the patient-specific cardiovascular model revealed that the hemodynamic effect of chest compression varies according to the cardiovascular parameter configuration. The hemodynamic changes for different compression conditions were compared in a pig model. From the results, it was shown that various hemodynamics occurred depending on the compression condition when using the personalized CPR model. Thus, it is possible to determine the optimal compression condition for the patient-specific from this.

In conclusion, this study showed that the modified CPR model is a generalized model that reflects the current CPR physiology more accurately. It also proved that hemodynamic interpretation can address the limitations of the current CPR technique through the modified model. Additionally, by presenting the possibility of a patient-specific CPR model based on this, this study can serve as the basis for research on personalized CPR modeling.

Keywords: Mathematical modeling, Cardiopulmonary resuscitation, Patient-specific CPR, Optimal compression position, Coronary perfusion pressure, Parameter estimation

Student Number: 2015-22886

CONTENTS

List of Tables

List of Figures

CHAPTER 1

Introduction

1.1 Basic understanding of cardiovascular system

1.1.1 Cardiac output

The cardiovascular system is a closed-loop composed of the heart and blood vessels, which play an essential role in regulating the body's metabolism, such as supplying oxygen, removing carbon dioxide, and supplying nutrients through blood flow. In the cardiovascular system, the heart is the central organ and acts like a pump that discharges blood through regular contractions and relaxation. Cardiac output (CO) is the product of the heart rate (BPM) and stroke volume (SV), and refers to the amount of blood flow generated for 1 minute [1]. The SV occurs when the heart contracts once in a stable state, which in a normal person is usually 60 – 80 ml. A pressure-volume curve can represent the work done by the heart during one ejection, and according to the cardiac cycle; it can be represented as shown in Figure 1.1 [2].

In the pressure-volume curve, the cardiac cycle is divided into four stages. The first stage (Point 4 → Point 1) is the ventricular filling or diastolic phase, in which the volume of the ventricle increases as the heart relaxes when the bicuspid valve opens. The second stage is the isovolumetric contraction stage. As the bicuspid valve is closed, the pressure increases by the contraction of the heart in the same end-diastolic volume (EDV) state. When the increasing systolic pressure of the ventricle begins to become greater than the aortic pressure, the aortic valve opens at Point 2, and blood is ejected from the ventricle (the third stage, the ejection phase). At this time, the ventricle pressure

reaches the peak and then decreases as the volume decreases, and the aortic valve closes again at the point when the ventricular pressure becomes equal to the aortic pressure (Point 3). All valves are closed in the isovolumetric diastolic step until Point 4 during the decrease of the ventricular pressure. In the pressure-volume curve, the width represents the difference between the EDV and end-systolic volume (ESV), which is SV.
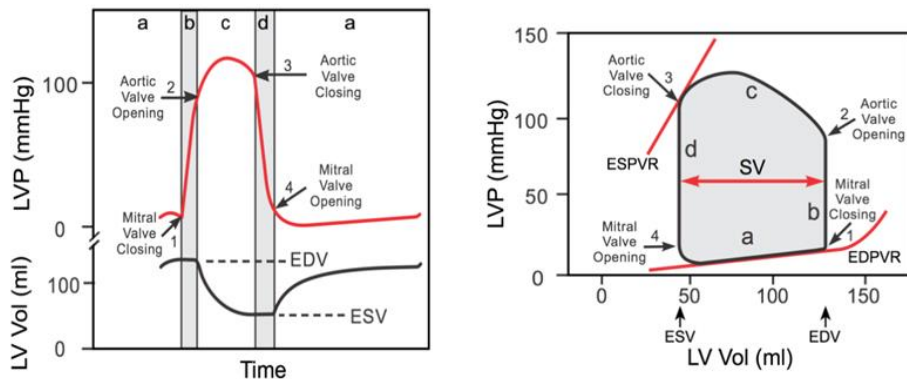
Figure 1.1 Diagram of cardiac cycle and pressure-volume curve. Adapted from www.CVphysiology.com with permission of Richard E. Klabunde [2].

The pressure-volume curve is an essential tool that can visually depict changes in the state and work of the ventricle and is affected by changes in the preload, afterload, and inotropy applied to the ventricle [1, 3].
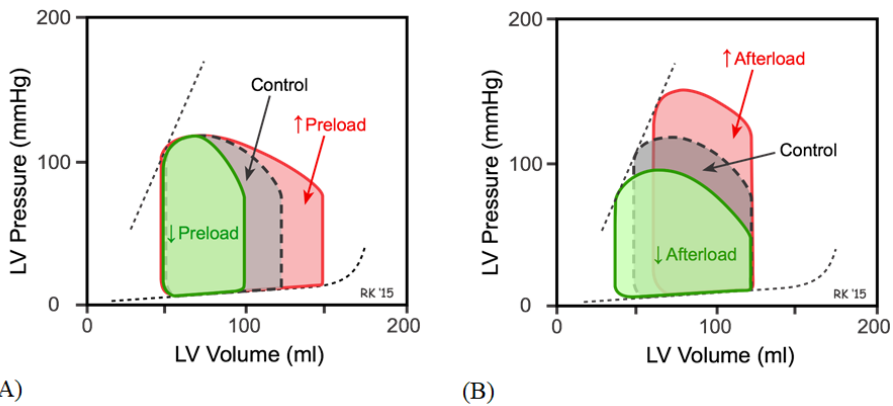
Figure 1.2 Pressure-volume curve change according to preload and afterload. (A) Preload, (B) Afterload. Adapted from www.CVphysiology.com with permission of Richard E. Klabunde [3].

Preload refers to the extent to which the sarcomere of the myocardium is stretched during the diastolic phase and directly indicates the degree of the ventricular filling [4]. Therefore, when the preload increases, the SV increases owing to Frank-Starling law, and when it decreases, the SV decreases, as shown in Figure 1.2. The afterload refers to the pressure that the heart must overcome to discharge blood during contraction [4]. As the aortic and pulmonary artery pressure increase, the heart must overcome it, and ejection must occur, which causes an increase in the afterload proportionally. Therefore, when the aortic pressure increases, the isovolumetric contraction stage is prolonged because the ventricle must create a higher pressure to overcome the aortic pressure, and the SV decreases because ejection occurs at a higher pressure. Conversely, when the aortic pressure decreases, the afterload decreases, resulting in an increase in

the SV. Inotropy refers to the extent to which the myocardium is stretched; when inotropy increases, the SV increases by increasing the ventricular pressure development and ejection rate [4]. Therefore, the preload, afterload, and inotropy interact to influence changes in the heart condition.

1.1.2 Venous return and Frank-Starling's law
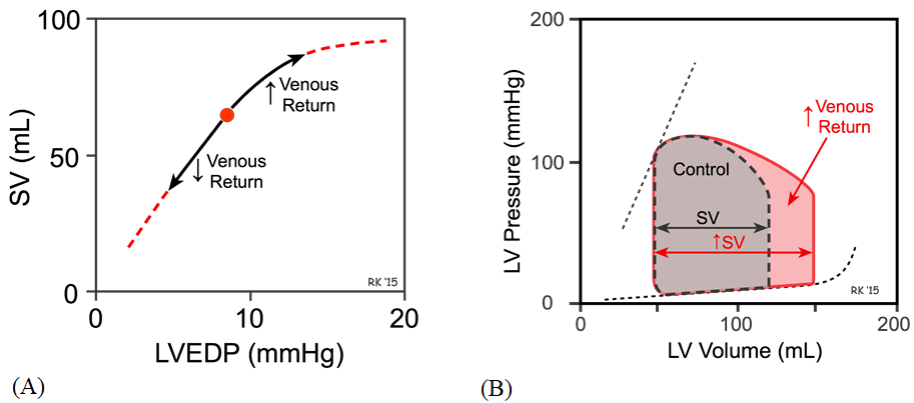
Figure 1.3 (A) SV change curve according to venous return change by Frank-starling law. (B) PV curve change due to venous return change. Adapted from www.CVphysiology.com with permission of Richard E. Klabunde [5].

Venous return refers to the blood flow to the heart, and in the normal cardiovascular system, it has the same amount as the cardiac output because it is a closed-loop [6, 7]. If the CO and venous return are not the same, blood accumulates in the systemic or pulmonary circulation. Frank-Starling's law controls the balance of the blood volume (Fig. 1.3(A)). Frank-Starling's law

states   that as the end-diastolic volume increases, the myocardial fibers become more stretched, and the contractile force of the ventricle increases [4, 5, 8].

When the blood volume returning to the right atrium increases owing to an increase in the venous return, the preload of the right ventricle increases, which increases the pulmonary circulation and SV in the right ventricle. Accordingly, when the venous return of the pulmonary vein increases, the preload of the left ventricle increases, and the volume at the end of the diastolic phase increases. Moreover, according to Frank-starling's law, the SV increases to reach the same end-systolic volume under the condition of constant afterload and isotropy (Fig. 1.3(B)). Therefore, the venous return plays an important role in regulating SV, and is determined by dividing the pressure gradient between the vena cava and right atrium by the vascular resistance. Because the pressure gradient inducing the venous return is relatively low (<10mmHg), even a slight pressure change in the vein or right atrium can significantly change the venous return. Factors affecting the venous return include muscle pumps, changes in venous compliance and resistance, vena cava compression, gravity, and respiratory activity [6, 9, 10]. For an example of respiratory activity, when the lungs expand during inhalation on spontaneous breathing, the pressure in the right atrium slightly decreases, and the pressure in the veins increases by abdominal pressure. Thus, the pressure gradient increases, and venous return increases during inhalation. Therefore, because the venous return is sensitive to

intrathoracic pressure, it can be easily affected by mechanical ventilation or cardiopulmonary resuscitation.

1.1.3 Blood circulatory system
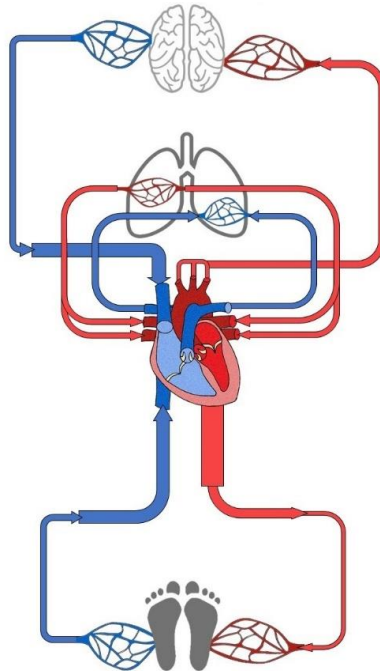
Figure 1.4 Blood circulatory system.

The heart's movement produces blood circulation. The blood circulation system can be divided into systemic circulation, pulmonary circulation, and coronary artery circulation systems (Fig. 1.4) [11]. Systemic circulation starts from the left ventricle, passes through the arteries, capillaries, and veins in sequence, and returns to the right atrium; this process transfers oxygenated blood from the heart to the body. Pulmonary circulation starts in

the right ventricle and passes through the pulmonary artery and lungs. Carbon dioxide delivered from the veins is exchanged for oxygen in the lungs, and oxygenated blood is supplied through the pulmonary veins. Coronary artery circulation starts in the aortic arch and supplies nutrients and oxygen to the heart tissue. Because problems with coronary circulation can lead to several cardiac dysfunctions, coronary artery perfusion is an important indicator in clinical applications [12]. Therefore, clinically, coronary perfusion pressure is commonly used as an indicator to predict the degree of coronary artery perfusion, which is calculated as the difference between the aortic pressure and right atrial pressure in the diastolic phase [13].
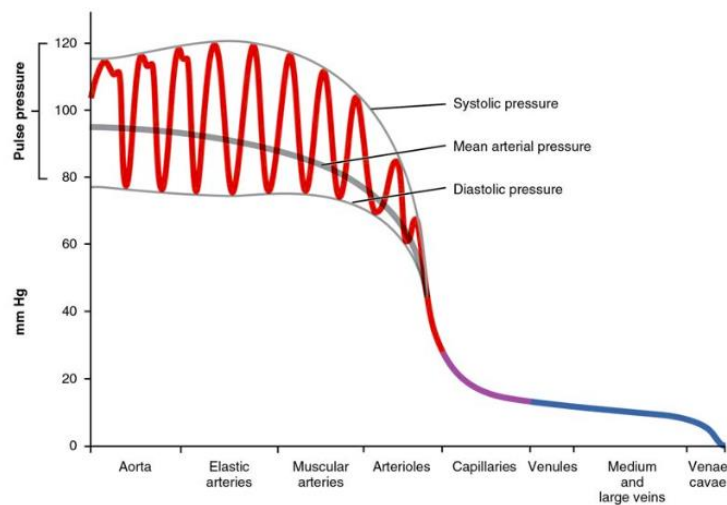
Figure 1.5 Systemic blood pressure. Adapted from https://openstax.org/books/anatomy-and-physiology/pages/20-2-blood-flow-blood-pressure-and-resistance [14].

The blood flow is caused by the pressure difference between the ends of each blood vessel. Therefore, the produced blood flow is directly proportional to the pressure difference, and the blood pressure decreases from the aorta to arterioles and veins. The blood pressure of the systemic circulation is shown in Figure 1.5, which shows that the pressure drops from the arteries to the arterioles, and it drops sharply from the capillaries to the veins [11].

The hemodynamic parameters of the normal cardiovascular system [15], such as the blood pressure, cardiac output, and heart rate, have values in the ranges listed in Table 1.

Parameters		Value	Units
Arterial Blood Pressure	Systolic (SBP)	100 – 140	mmHg
	Mean (BP or MAP)	70 – 105	mmHg
	Diastolic (DBP)	60 – 80	mmHg
Central venous pressure (CVP)		0 – 6	mmHg
Right atrial pressure (RAP)		0 – 8	mmHg
Stroke volume (SV)		50 – 100	ml
Cardiac Output (CO)		4 - 8	L/min
Heart Rate (HR)		60 - 100	beats

Table 1.1 Ranges of normal hemodynamic parameters

1.2 Cardiopulmonary resuscitation

1.2.1 Basic concept for cardiopulmonary resuscitation

Cardiopulmonary resuscitation (CPR) is an emergency treatment that artificially circulates blood and helps in breathing when a cardiac arrest occurs. It helps to delay brain damage and restore normal activities of the heart by circulating a patient's blood [16]. Cardiac arrest is when the pump function of the heart stops, and oxygen is not supplied to various organs such as the brain and lungs through blood circulation. Patients that do not receive CPR within a reasonable time right after cardiac arrest can experience a sharp decline in survival and death [17]. In the AHA guidelines [16, 18], chest compressions are initiated by placing the hand on the inter-nipple line; in adults, it is recommended to perform compressions of 100–120 times per minute at a depth of 5–6 cm [18].

Blood circulation during CPR is formed by the compression of the chest cavity, unlike the normal cardiovascular system, not by the thrust of the heart itself, and is caused by pressure gradients between the compression area and area where it is not compressed. Therefore, during CPR, the SV is generated per compression, and CO can be expressed by multiplying the number of compressions by the SV. For the pressure during CPR, both the aortic pressure (ABP) and right atrial pressure (RAP) increase as shown in Figure 1.6, and the RAP is similar to or higher than the ABP [19-21]. Because the high

RAP limits coronary perfusion during the compression phase in CPR, the coronary perfusion pressure (CPP) is calculated as the pressure gradient between ABP and RAP in the relaxation phase [13, 19, 22].
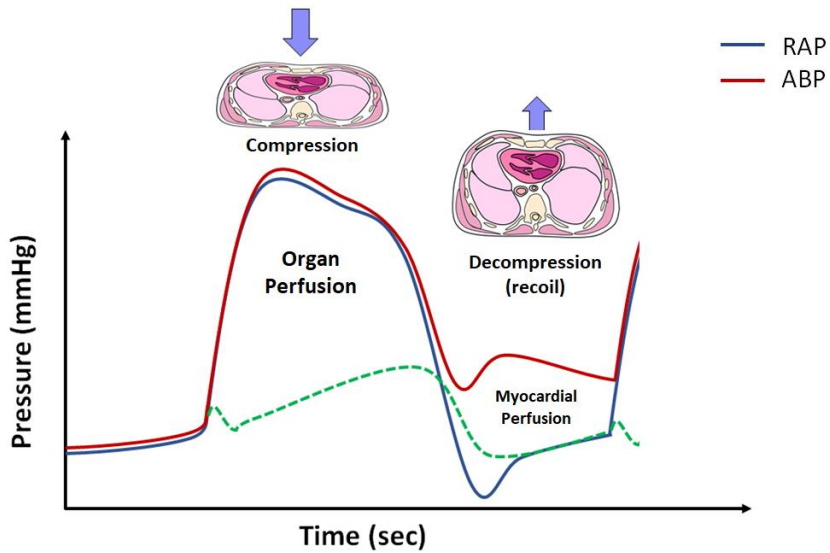
Figure 1.6 Blood pressure waveform during CPR.

During CPR, the venous return is manually affected by the recoil phase of the thoracic cavity because the heart cannot function normally [7]. The negative pressure formed inside the thoracic cavity by the recoil phase decreases the pressure of the atrium and blood vessels in the thoracic cavity and creates the venous return. Therefore, when the recoil phase is incomplete by thoracic injuries such as rib fractures during CPR, the venous return could be

reduced. In standard CPR (S-CPR), because the recoil phase is passively dependent on the recoil of the thorax, if an appropriate recoil phase is not formed, the venous return and the resulting stroke volume are limited. To improve this, a new treatment for controlling intrathoracic pressure is proposed. This therapy is referred to intrathoracic pressure regulation (IPR), and is a method that creates negative pressure in the thoracic cavity during the recoil phase. Active compression-decompression CPR (ACD-CPR) is one of the IPR techniques that artificially lifts the thoracic cavity in the recoil phase using a suction device [18]. Because ACD-CPR creates negative pressure inside the thoracic cavity, it is possible to form a larger venous return than S-CPR [18, 23]. Another of the IPR techniques is the use an impedance threshold valve (ITV) device [23-25]. The device prevents ambient air from entering the lungs during the recoil phase and continuously maintains negative pressure in the chest. It has been demonstrated in several animal and clinical trials that this IPR technique improves the venous return and CPP during CPR.

1.2.2 Theories of CPR mechanism

There is still a debate on the mechanisms by which blood flow is formed and maintained during CPR. The representative CPR mechanisms are the "cardiac pump theory" and "thoracic pump theory". The "cardiac pump" theory assumes that blood flow occurs as the ventricles are directly compressed. In contrast, the "thoracic pump" theory considers the heart as a simple conduit, and also assumes that the intrathoracic pressure is increased by chest compression, which creates the blood pressure and blood flow in the heart and blood vessels [26, 27].
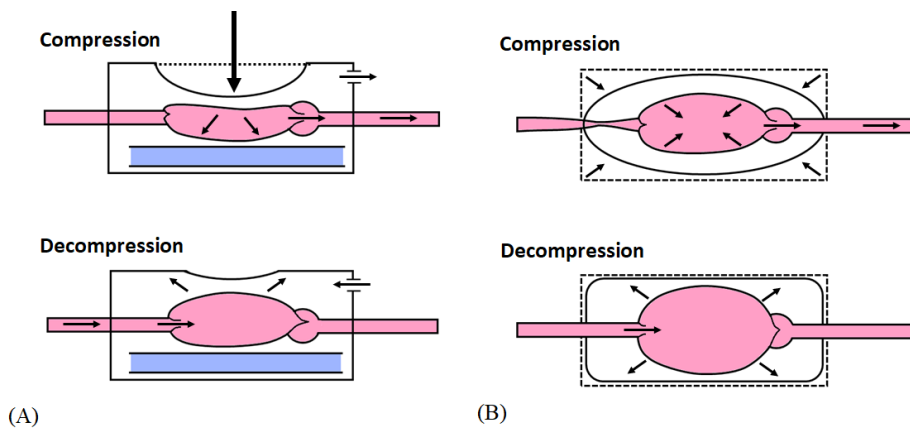
Figure 1.7 Diagram of CPR mechanisms. (A) Cardiac pump, (B) Thoracic pump.

Additionally, there are the "respiratory pump theory" and "left atrial pump theory" [27]. The "respiratory pump theory" states that blood flow is formed by the interaction between the heart and lungs, and the "left atrial pump theory" states that because it compresses the left atrium, a forward flow occurs through the open mitral valve and at the same time pulmonary blood flow in the pulmonary veins occur in the reverse direction.

1.3 Mathematical modeling for CPR

1.3.1 Basic concept of lumped parameter model for cardiovascular system

For centuries, researches have been conducted to understand the hemodynamics of the cardiovascular system. In 1738, Daniel Bernoulli published the Bernoulli equation, which link blood pressure and blood flow velocity. Moreover, in 1840, Poiseuille published the Hagen-Poiseuille equation, which describes the relationship between the pressure drop and flow rate under constant flow conditions [11, 15, 28].
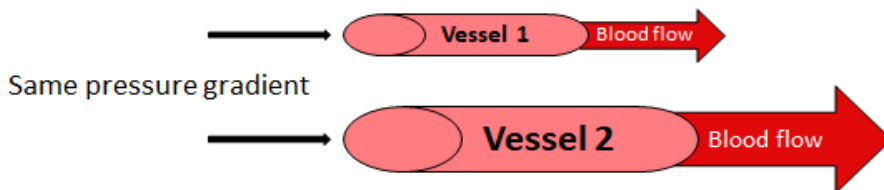
Figure 1.8 Diagram of Hagen-Poiseuille equation for blood flow.

The resistance of blood vessels is related to the diameter, length, and viscosity of the blood vessels and can be expressed as Eq. (1.1) according to the Poiseuille equation (Fig. 1.8).

$$R = \frac{8\mu l}{\pi r^4} = \frac{\Delta P}{Q} \qquad \text{Eq. (1.1)}$$

Where R is the resistance of the vessels, μ is the viscosity of blood, r is the radius of the vessel, l is the length of the vessel, ΔP is the pressure changes in each vessel, and Q is the flow of each vessel.

In 1890 the famous "Frank-starling law" and "Windkessel effect" were published by Otto Frank. The Windkessel effect is a theory for the compliance of blood vessels [11, 29]. Compliance indicates the degree of expansion and contraction of the vessel wall according to pressure changes (Eq. (1.2)) [14].

$$C = \frac{\Delta V}{\Delta P} \qquad \text{Eq. (1.2)}$$

Where C is the compliance of the vessels, ΔP is the pressure changes in each vessel, and ΔV is the volume changes in each vessel.

Arteries with high elasticity expand and store blood during systole because of an increase in blood pressure. The stored blood is discharged again to provide a circulating force, which is indicated as a capacitor in the Windkessel model. This Windkessel model became the basis for an electrical analog model or lumped parameter (LP) model of the cardiovascular system [30].

(A)

(B)
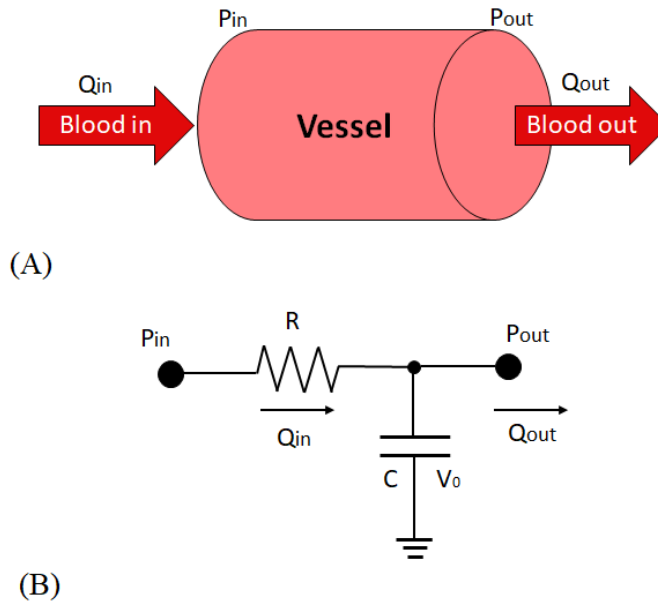
Figure 1.9 Electrical circuit of blood vessel element.

The LP model can provide physical insight into the cardiovascular system with a low computational cost and simple manner, and ultimately lead to improved treatment. Therefore, many studies using the LP model have been performed over the past several decades to understand the relationship between the pressure and flow rate in the cardiovascular system's normal or various pathological conditions [31-35]. The LP model represents each blood vessel and heart of the cardiovascular system as one compartment [36, 37]. The compartment of the blood vessel is represented by an electrical circuit consisting of resistance and capacitance (Fig. 1.9). Each compartment can be expressed as the relationship between the blood pressure and blood flow rate

using Eq. (1.1 and 1.2). Furthermore, when the volume is obtained through the flow rate of the corresponding compartment, the pressure can be calculated. In the LP model, the ventricular compliance is represented by a variable capacitance, as shown in Figure 1.10, which is simulated as a chamber with valves at the inlet and outlet. The diodes represent the valves [37].
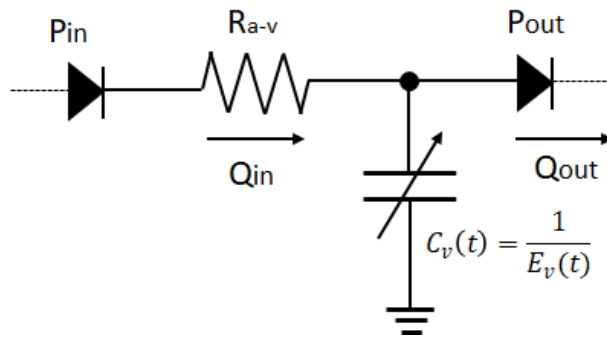
Figure 1.10 Electrical circuit of the ventricle.

To define the ventricle contraction, which changes with time, the compliance value of the end-systolic phase $(E_{es} = 1/C_{es})$ and end-diastolic phase $(E_d = 1/C_d)$ should be defined. In a normal ventricle, E_{es} has a value of $1.7 \sim 6.7$ mmHg/ml, and E_d has a value of $0.1 \sim 0.6$ mmHg/ml [36, 37].
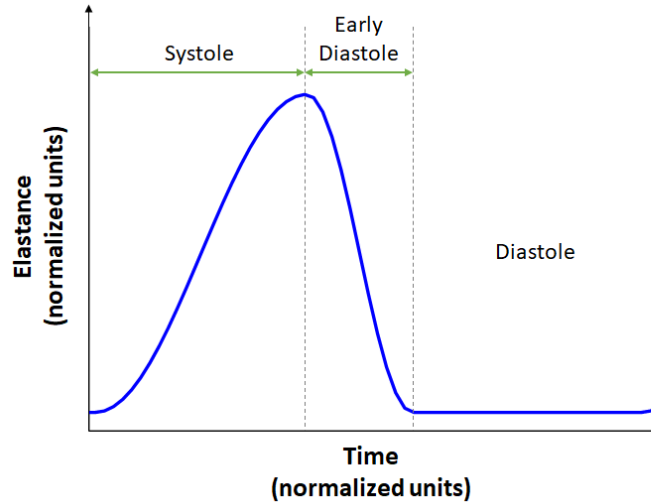
Figure 1.11 Normalized time-varying elastance of ventricle.

The ventricular compliance $(E(t) = 1/C(t))$ changes during the systolic phase to reach the end-systolic compliance along with the half-sine wave. During the initial diastolic phase, the half-cosine wave is followed to reach the end-diastolic compliance. Moreover, during the remaining diastolic phase, the end-diastolic compliance is maintained. Figure 1.11 shows the normalized time-varying compliance (elastance) of the ventricle represented as Eq. (1.3). Additionally, the atrium can be simulated as a variable compliance model in the same way as the ventricle. However, most LP models represent a constant for atrial compliance except for studies on the hemodynamic response to exercise because it does not act dominantly on the heart's contraction [37].

$E(t)$

$$= \begin{cases} E_d + \dfrac{E_{es}-E_d}{2} \cdot \left(1 - cos\left(\dfrac{\pi \cdot t}{T_s}\right)\right) & 0 \leq t \leq T_s \\[3mm] E_d + \dfrac{E_{es}-E_d}{2} \cdot \left(1 + cos\left(\dfrac{2\pi \cdot (t - T_s)}{T_s}\right)\right) & T_s < t \leq \dfrac{3}{2}T_s \\[3mm] E_d & \dfrac{3}{2}T_s < t \end{cases}$$

Eq. (1.3)

1.3.2 Previous studies on CPR modeling

The study of CPR based on LP modeling began with the electrical circuit model proposed by Babbs in the 1980s [38]. The initial study defined the cardiac arrest status and cardiac and thoracic pump mechanism through electrical circuits. In cardiac arrest, cardiac compliance has constant compliance, unlike normal cardiac models. From this study until the early 2000s, research on CPR modeling was led by Babbs, and studies on various CPR techniques such as ACD-CPR and interposed abdominal compression CPR (IAC-CPR) were conducted [39]. In 2005, a thoracic cavity model was proposed as a spring-damper system[40], and the transmission of external force was expressed as displacement rather than simply converting the external force into pressure. In this model, a compression depth of 5 cm was applied according to the AHA guidelines. Moreover, a hybrid pump mechanism that combines a cardiac pump and thoracic pump was proposed. In this mechanism, the left and

right ventricles were directly pressed by the cardiac pump, and the thoracic pump factor was added to the aorta, pulmonary artery, and atria in the thoracic cavity to control the change the intrathoracic pressure. In 2006, the optimal duty ratio and compression rate were suggested through studies on various duty ratios and compression rates on the CPR techniques [41]. The duty ratio represents the ratio of the time the pulse is on in one cycle, and in CPR, it is the time to compress the chest during one chest compression cycle. Since then, studies on CPR have been conducted by several works based on Babbs' model. In a 2011 study by Yvette Koeken et al.[42], the hemodynamic effects of various compression profiles such as the sine, trapezoidal, and square waves were compared. Furthermore, this study suggested that blood flow may be restricted when blood vessels in the thoracic cavity collapse owing to strong compression. In 2012, a study by Yanru Zhang et al. analyzed the effect of IAC-CPR on pulmonary circulation [43]. This study suggested that although IAC-CPR is excellent in improving hemodynamics, the pulmonary pressure is significantly increased by abdominal compression, which has the possibility of developing pulmonary edema. In 2017, two research teams conducted a study on applying a passive leg raising (PLR) maneuver during CPR [44, 45]. PLR is a maneuver that has been used to improve hemodynamic response by increasing cardiac output in patients with circulatory disorders. These studies suggested that hemodynamics can be improved when applied during CPR.

1.4 Motivation and objectives

In the past decades, many clinical and theoretical studies on various cardiopulmonary resuscitation (CPR) techniques have been performed for hemodynamic improvement and the return of spontaneous circulation (ROSC) recovery during CPR [22]. However, approximately 20 to 140 patients in every 100,000 suffer from cardiac arrest every year, and the survival rate of out-of-hospital cardiac arrest (OHCA) patients that receive CPR is approximately 20%. Additionally, the in-hospital cardiac arrest (IHCA) survival rate is still not high at approximately 40% [46]. To improve the ROSC and insufficient survival rate of CPR, it is necessary to understand hemodynamics during CPR, and through this, the CPR technique can be improved.

Mathematical modeling has the advantage of ideally approaching various techniques and phenomena of CPR that are clinically difficult to identify. Therefore, in this study, a mathematical modeling-based study was conducted to provide theoretical insights on the hemodynamics of CPR; the approach was made through three objectives.

First, because the existing CPR model does not reflect the current CPR physiology, this study proposed an improved CPR model. Various simulation studies have been performed to understand the hemodynamic principle of CPR based on CPR mechanisms. Most of these studies were based on the lumped parameter model proposed by Babbs [39-45]. In the Babbs's model, a "hybrid

22

pump" mechanism that combines the "cardiac pump" theory and "thoracic pump" theory was used, and the degree of "thoracic pump" was adjusted by the thoracic pump factor [40]. This model has contributed significantly to the basic understanding of the hemodynamics of CPR; however, there are still some aspects not reflecting the current CPR physiology in this model. First, in the compression phase of CPR, the peak value of the RAP should be greater than or equal to that of the ABP [19, 20, 22]. However, Babbs's original model has a considerably low RAP peak value. Because the RAP affects the venous return and coronary artery perfusion, even small changes have a significant effect on the pressure gradient that determines it [7]. Therefore, a proper RAP must be reflected to fully predict the venous return and coronary artery perfusion. Second, under normal cardiac conditions, when the aortic valve opens in the systolic phase, the coronary blood flow is limited. However, when the valve closes in the diastolic phase, it increases, forming a retrograde flow. Thus, coronary blood flow occurs dominantly in the diastolic phase [47-49]. During CPR, the aortic valve opens in the compression phase and closes in the relaxation phase in terms of the thoracic and cardiac pump mechanisms. Therefore, as in the normal cardiac condition, coronary perfusion increases dominantly in the relaxation phase when the aortic valve is closed [13, 50], and according to this principle, the CPP during CPR is calculated as the difference between the ABP and RAP in the relaxation phase [13, 20, 51]. However, the existing simulation model does not reflect coronary perfusion during CPR

because it shows the dominant result of coronary perfusion in the compression phase.

Therefore, through this study, an improved CPR model of the hybrid pump mechanism that can solve the aforementioned problems is proposed. Animal experiments were conducted to verify whether the modified CPR model better reflects the current CPR physiology. The pressure waveforms obtained from these were compared with those from the simulation results. Further, to compare the difference between the proposed and existing CPR model, various CPR techniques were simulated, such as active compression-decompression with an impedance threshold valve device (ACD–CPR+ITD) and the patient's body positions (Head-up tilt and Head-down tilt). ACD–CPR+ITV has been clinically proven to increase coronary perfusion [23, 24]. Therefore, it was simulated to compare the effect of increasing coronary perfusion with the conventional model. However, although there are few clinical studies of changes in the patient's body position during CPR, recent animal studies have shown that when CPR is performed in the head-up position, cerebral and coronary perfusion is augmented by venous return changes [52, 53]. Therefore, the change in body positions was simulated to compare the venous return and perfusion of the existing and proposed model.

a. Number of the unsuccesfully resuscitated with and without SCI by gender and age groups

	male without SCI	male with SCI	female with SCI	female without SCI	age group
>90 yr	0	13	21	5	>90 yr
80-89	14	126	187	10	80-89
70-79	30	343	190	11	70-79
60-69	40	340	100	6	60-69
50-59	49	291	67	13	50-59
40-49	34	101	24	9	40-49
30-39	23	40	14	2	30-39
18-29	22	15	4	5	18-29

■ male with SCI □ male without SCI ■ female with SCI □ female without SCI

b. Percentage of patients sustaining CPR-related SCI and average number of SCI by gender and age groups

age group	male avg	male without SCI	male with SCI	female with SCI	female without SCI	female avg
>90 yr	12,46	0%	100%	81%	19%	11,57
80-89	12,78	10%	90%	95%	5%	12,20
70-79	12,13	8%	92%	95%	5%	11,48
60-69	11,34	11%	89%	94%	6%	10,43
50-59	10,10	14%	86%	84%	16%	9,63
40-49	8,64	25%	75%	73%	27%	7,00
30-39	5,83	37%	63%	88%	13%	5,93
18-29	4.67	59%	41%	44%	56%	2.25

■ male with SCI □ male without SCI ■ female with SCI □ female without SCI

Figure 1.12 Percentage of population for unsuccessfully resuscitated and CPR-related chest injury. Adapted from Kralj et al. Resuscitation. 2015; Vol.93 136-141 [54].

Second, this study focused on determining the hemodynamic effects on several issues of existing CPR techniques through simulation. The first issue is 'the reduction in the CPR effect upon reducing the thoracic elasticity due to rib fracture'. Current guidelines recommend performing chest compressions of 5–6 cm. However, through animal experiments, recent studies have suggested that the compression depth specified in the current guidelines increases thoracic

injuries (Fig. 1.12); thus, the hemodynamic effects are reduced upon reducing the thoracic elasticity [55, 56].
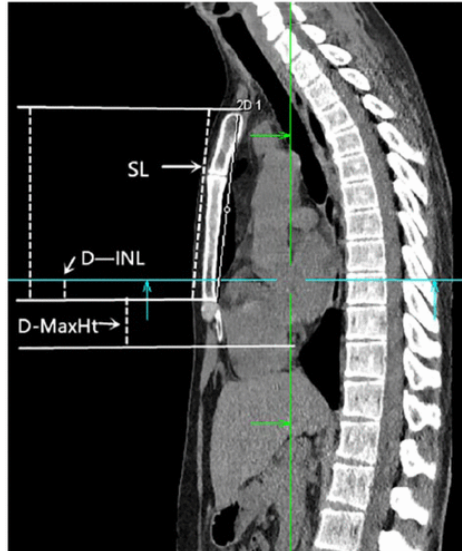
Figure 1.13 The sagittal image of chest-computed tomography. Adapted from Jiang et al. Hong Kong J. Emerg. Med. 2020; Vol.27(4) 197-201 [57].

The second issue is 'Is the current compression point the optimal compression point?'. The current guideline recommends the inter-nipple line (INL) as the compression point. However, recent studies suggest that the current compression position can compress the aorta and pulmonary arteries in anatomy [58-60]. Additionally, because the maximum depth of the left ventricle is below the INL [57, 61], they proposed the compression position should be below the INL (Fig. 1.13). If the compression position compresses the atrium

more than the ventricle, the aorta and pulmonary arteries can be compressed together by the anatomical position, limiting blood flow. Therefore, this study attempted to verify the hemodynamic effects according to the compression position and the decrease in the elasticity of the thoracic cavity through simulation.

Finally, this study presents the possibility of establishing a personalized CPR model. Recently, research is underway to advance CPR techniques into personalized CPR [62-65]. However, clinically, it is difficult to understand the factors that affect hemodynamics because various factors interact environmentally. Furthermore, it is time-consuming and expensive. Therefore, this study presents the possibility of a patient-specific CPR model through parameter estimation of the cardiovascular system [66]. Babbs conducted a study to provide an optimal waveform for compression during CPR [41]. However, because the cardiovascular state, elasticity of the thorax, and heart's position vary among people, the optimal waveform and optimal strategy may vary depending on the individual. In addition, the resistance and compliance of the blood vessels that consist of the cardiovascular system are patient-specific, causing each patient to have different hemodynamic characteristics. Therefore, if the patient-specific cardiovascular parameters can be estimated, it becomes possible to predict the SV and CPP through each patient's cardiovascular status when CPR is applied. The elasticity of the thorax

and compression position mentioned in the second section can also vary considerably depending on the patient. The elasticity of the thoracic cavity varies according to geometry, body shape, age, and gender [67]. Because the stiffness of the ribs increases with age, the risk of injury increases; thus, the uniform compression depth recommended in the current guidelines may not be appropriate. Likewise, the heart's position may vary from patient to patient. For example, in obese patients, the heart's position is displaced compared to a health person owing to abdominal obesity [68]; the compression position may also have to be changed from the compression position suggested by the current guideline. Therefore, if the elasticity of the thorax and compression position can be individually reflected for each patient, it will be possible to increase the understanding of hemodynamics during CPR and to lay the basis for personalized CPR. For these reasons, in this study, the parameters of each cardiovascular system were estimated using a genetic algorithm (GA) to generate a patient-specific cardiovascular system [69, 70]. Moreover, different elasticity and compression positions were applied to the patient-specific cardiovascular model, and the possibility of a personalized CPR model was verified through the animal model established previously.

CHAPTER 2

Materials and Methods

2.1 Modified CPR model based on general cardiovascular model

First, to develop a CPR model that can reflect the current CPR physiology, the modified CPR model was developed and performed comparative verification with the existing model through various maneuver and animal experiments.

CPR model of this study originated from the cardiovascular model proposed by Babbs, and was modified to reflect CPR physiology. Matlab software (The MathWorks, Inc., MA, USA) was used for modeling and simulation, and the 4th and 5th order Runge-Kutta methods were used at constant time intervals to solve the differential equations. The time-step used in the calculation was 0.001s.

2.1.1 Modified hybrid CPR model

The model proposed by Babbs (Original model) consists of 4 cardiac chambers and 10 vascular compartments [40]. The pressure gradient in each compartment is caused by changes in the input and output blood flow to the compliance of each compartment (Eq. (2.1)). Blood flow is proportional to the pressure difference between the two compartments, and inversely proportional to the vascular resistance between the two compartments according to Ohm's

law (Eq. (2.2)). Each compartment has its own compliance and resistance values, and the values based on a 70 kg adult male were used.

$$\frac{dP_1}{dt} = \frac{1}{C_1}(Q_{in} - Q_{out}) \qquad (2.1)$$

$$Q_{in} = \frac{1}{R_{in}}(P_2 - P_1) \qquad (2.2)$$

To simulate chest compression, the structure of the thoracic cavity was represented by the spring–damper system, and a pressure gradient was generated in the compartments of the thoracic cavity as the depth of the chest changed by an external force. The cardiac pump mechanism was applied to the left and right ventricles to cause a direct pressure change, and at the same time, the thoracic pump mechanism was applied by allowing intrathoracic pressure to be transmitted to the left and right atrium, aorta, and pulmonary artery. The thoracic pump factor ($f_{tp} = 0.75$) was applied to adjust the scale of the transmitted intrathoracic pressure.

As shown in Figure 2.1, the model proposed in this study (Hybrid model) was constructed by adding the superior and inferior vena cava compartments of the thoracic cavity to the original model, and all blood vessels in the thoracic cavity were subjected to pressure changes of intrathoracic pressure. The CPR pump mechanism used a hybrid pump mechanism similar to the Babbs model. In this model, only the ventricle was compressed directly,

and the atrium received a change in intrathoracic pressure through the thoracic pump factor. However, in the hybrid model, both the atrium and ventricle were directly compressed and simultaneously subjected to changes in the intrathoracic pressure. Thus, f_{tp} was applied equally to all cardiac chambers, and f_{tp} in this model indicates that cardiac pumps and thoracic pumps mediate all compartments within the thoracic cavity simultaneously (which means hybrid pump). The thoracic pump factor ranges from $0 < f_{tp} <= 1$, and when $f_{tp} = 0$, this model is no longer identical to Babbs' pure cardiac model.
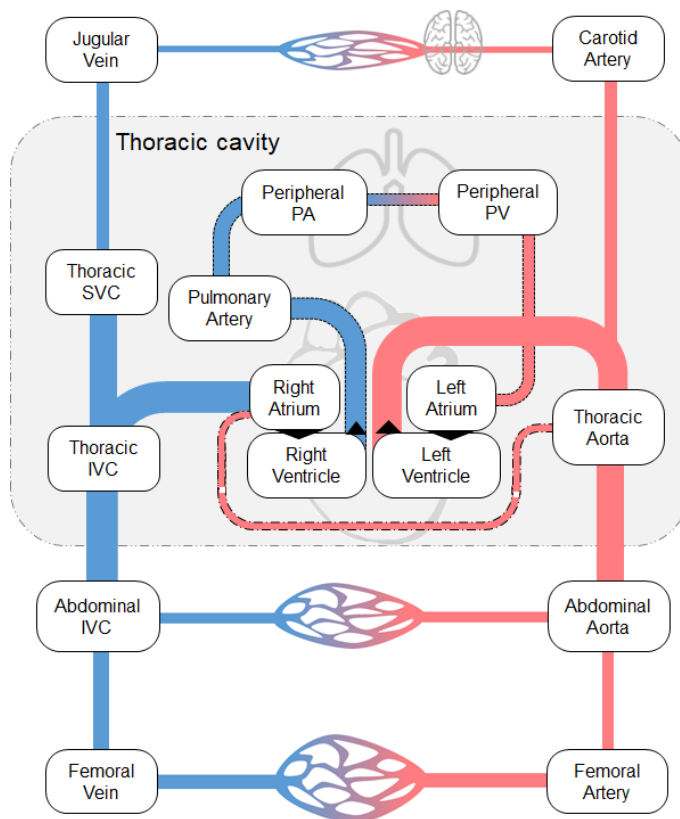
Figure 2.1 Diagram of the hybrid model composed of 16 compartments.

Figure 2.2 show schematics of the hybrid pump mechanism of the hybrid model, and the pressure and blood flow directions of the heart, arteries, and veins were plotted when the chest is compressed and relaxed, respectively. Table 2.1 shows the compliance and resistance of the newly added thoracic superior and inferior vena cava [37], and the same parameters of the remaining compartments were used as in the original model.
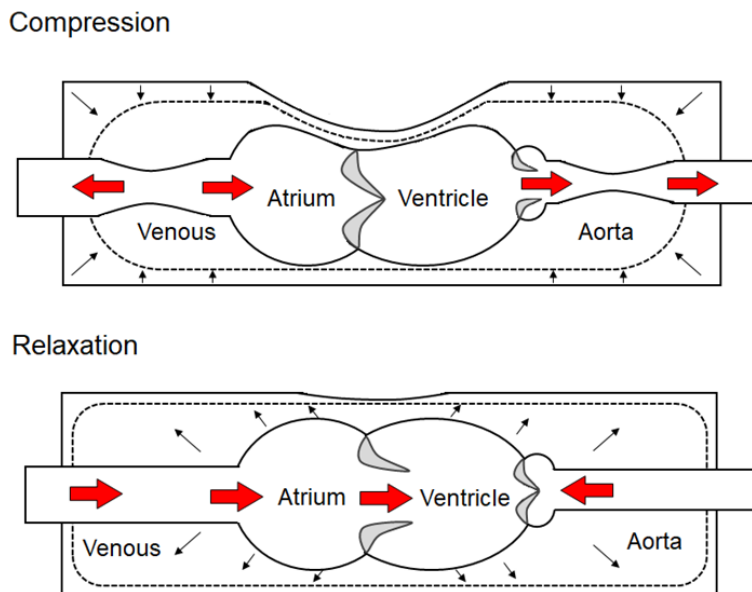
Figure 2.2 Conceptual diagram of the hybrid pump mechanism. Cross-sectional views during compression and relaxation, including both the left and right cardiac chambers. The thick red arrows indicate the direction of blood flow, while the thin arrows indicate the direction in which pressure acts within the thoracic cavity.

Table 2.1 Added model parameters.

Resistances	Value [mmHg/L/s]	Definition
R_{Tho_SVC}	10	Resistance between the thoracic superior vena cava and the right atrium
R_{Tho_IVC}	5	Resistance between the thoracic inferior vena cava and the right atrium
Compliances	Value [L/mmHg]	Definition
C_{Tho_SVC}	0.014	Compliance of the thoracic superior vena cava
C_{Tho_IVC}	0.007	Compliance of the thoracic inferior vena cava
C_{Ab_IVC}	0.014	Compliance of the abdominal inferior vena cava

2.1.2 Simulations of various maneuvers for CPR model

2.1.2.1 Active compression-decompression CPR with an impedance threshold valve (ACD-CPR+ITV)

To compare the CPP difference between the original model and the hybrid model, we simulated ACD–CPR+ITV (Figure 2.3), which has been clinically proven to improve coronary perfusion [23, 24, 71]. ACD–CPR is recommended to be used with an ITV device, as during the relaxation phase, it creates greater negative pressure in the thoracic cavity than the standard CPR (S–CPR). Therefore, ACD–CPR and ITV were simulated together [18].

ACD–CPR alternately delivers positive and negative pressure on the thoracic cavity. To simulate this, in the compression phase, an external force of 400 N was applied with a half-sine wave to compress the chest by about 5 cm, and in the relaxation phase, the chest was lifted by about 2 cm using 25 % of the external force [39].

The ITV device is attached to an endotracheal tube or a ventilation mask, and in the relaxation phase during CPR serves to prevent inhalation caused by negative pressure [24]. To simulate the effects caused by the ITV device, airway airflow was set to zero when the difference between ambient and lung pressure was less than 0 [40].
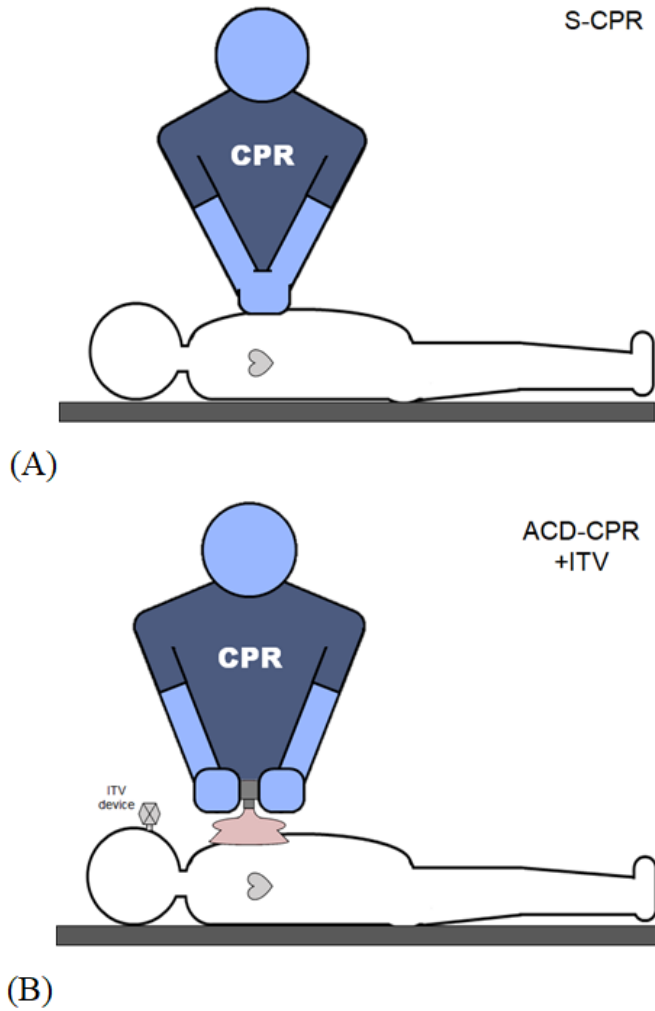
Figure 2.3 Schematics of CPR techniques. (A) standard cardiopulmonary resuscitation (S–CPR), and (B) active compression–decompression CPR with an impedance threshold valve device (ACD–CPR+ITV).

2.1.2.3 Head-up tilt (HUT) and head-down tilt (HDT)

To compare venous return, and cerebral and coronary perfusion that occur according to body position changes during CPR, we compared the hybrid model with the original model by applying the HUT and HDT models [72]. In the supine position, gravity does not affect blood pressure changes, but during HUT, blood is pulled to the lower extremities by gravity, therefore the pressure of the blood vessels in the upper body relatively decreases, and the pressure in the lower body increases (Fig. 3(a)). Conversely, during HDT, gravity acts on the upper body, reducing blood pressure in the lower body (Fig. 3(b)). In order to simulate the effect of gravity according to the body position, the distance between the upper and lower body compartments from the thoracic cavity was set, and hydrostatic pressure was applied to the compartments except for the thoracic cavity, according to the tilt angle [72, 73].

$$Q = \frac{P_{in} - P_{out} + \rho g h \sin \theta}{R} \qquad (2.3)$$

where, ρ is the blood density, g is the constant of gravitational acceleration, h is the distance between thoracic cavity and extra-thoracic compartments, and θ (degree) is the tilt angle.
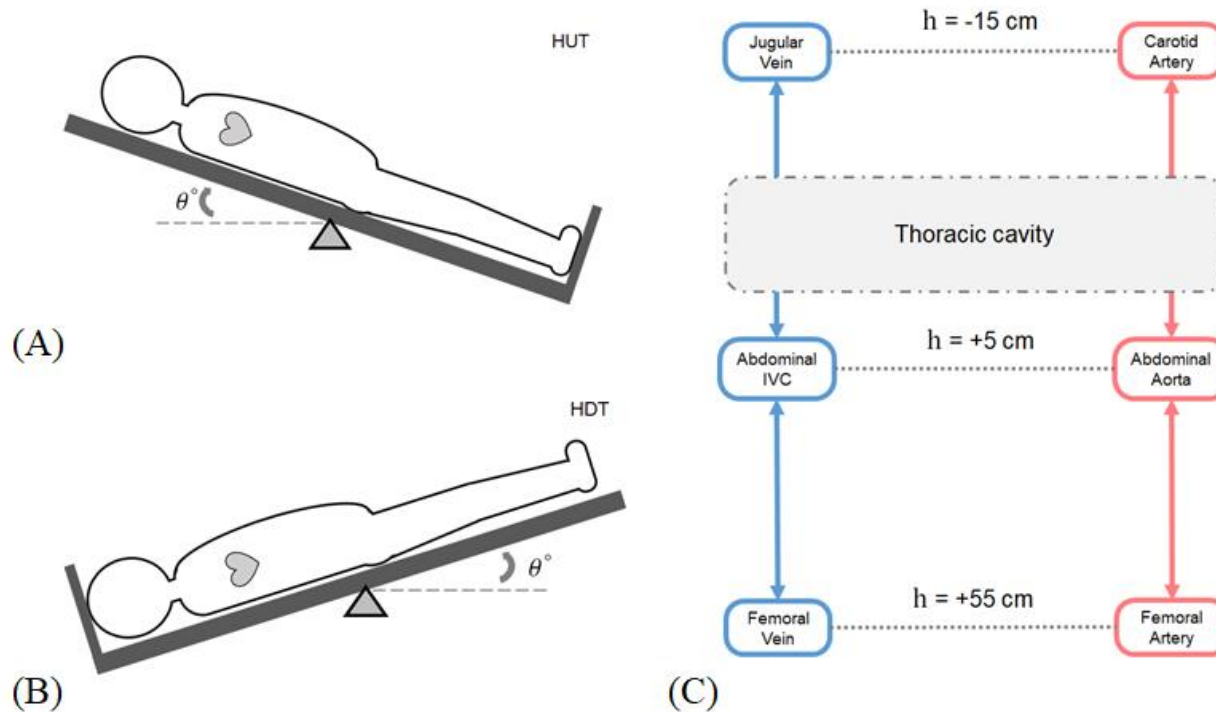
Figure 2.4 Schematics of (A) head-up-tilt (HUT) and (B) head-down-tilt (HDT). (C) Diagram representing the distance of each compartment from the thoracic cavity used to determine the hydrostatic pressure in each compartment (not scaled).

2.1.3 Animal experiments for hemodynamic data acquisition

In this study, to verify whether the modified CPR model adequately reflects the current CPR physiology, hemodynamic data were obtained from pig animal experiments for CPR (Fig. 2.5) and compared with simulation results. Pigs are similar to humans because the thoracic cavity and the abdominal cavity are separated from the diaphragm, so they are the most commonly used animals for CPR experiments [74].
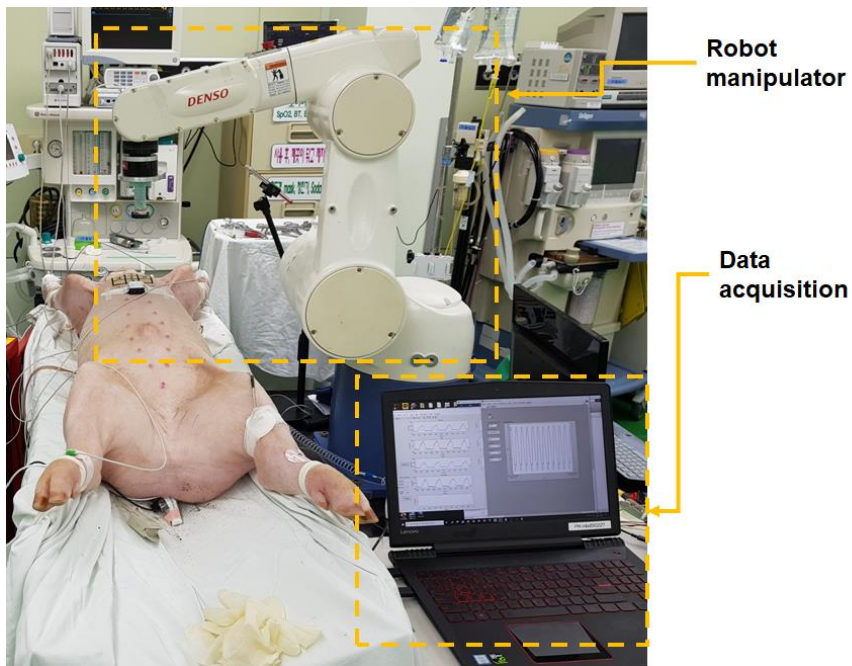
Figure 2.5 Animal experiments for hemodynamic data acquisition during CPR using robot manipulator.

Pigs between 37 and 45 kg were used, and all experimental procedures were performed with the approval of the Institutional Animal Care and Use Committee of Seoul National University (IACUC No. 19-0158-S1A0). Animals were induced to anesthesia by intramuscular injection of 5 mg/kg of

Zoletil (zolazepam and tiletamin; Virbac Korea, Republic of Korea), and intubated for mechanical ventilation. Anesthesia was maintained through inhalation of 1%–1.5% of isoflurane with an initial respiratory rate 15 / min. For measuring pressure, Arrow Seldinger Arterial Catheter (20 Gauge; Teleflex Inc., USA) and Swan-Ganz catheter (7.5 Fr; Edwards Lifesciences Corporation, USA) were placed in the right carotid artery and right atrium, respectively.

2.1.3.1 Experimental protocol
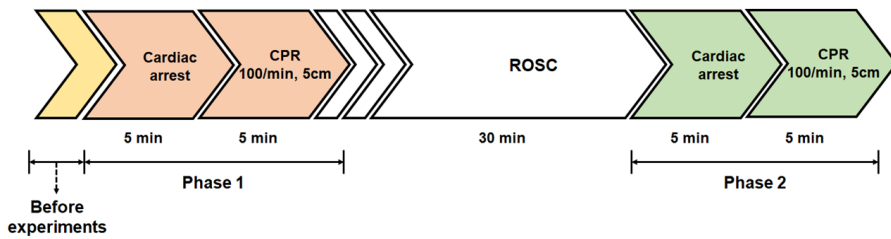
Figure 2.6 Timeline for experiments.

The experimental protocol was divided into two phases as shown in Figure 2.6, and CPR was performed for 5 minutes after cardiac arrest for 5 minutes in each phase. Cardiac arrest was induced by inserting a pacing catheter into the right ventricle and delivering direct current to a 9V battery to generate ventricular fibrillation. Chest compression was uniformly provided with a duty ratio of 50, 100 / min of compression rate, and 5 cm of depth using a robotic manipulator (VM-6083G model, Denso Co., Ltd., Japan). External defibrillation (step 2, 200J) was performed using a Zoll R series defibrillator (Zoll Medical, USA) every minute until the ROSC after the end of one-phase. After stabilizing for 30 minutes after ROSC, a two-phase experiment was conducted in the same manner.

2.1.3.2 Data acquisition

During the experiment, arterial blood pressure (ABP) and right atrial pressure (RAP) from the patient monitor were collected in real-time, and all data acquisition were performed with a data acquisition card (NI-USB 6003, National Instruments, Austin, TX, USA) and an acquisition program (MATLAB, The MathWorks, Inc., MA, USA) with a sampling frequency of 500Hz. The data used in this study were the steady-state data before cardiac arrest and the data within the initial 5-second of one-phase CPR. The experiment was performed on a total of 3 pigs, and in this study, data were acquired and used from two pigs to which the pressure waveform under normal conditions before the start of the experiment can be applied.

2.2 Simulation-based approach to current issues in CPR using modified hybrid CPR model

In this section, simulations were performed to theoretically verify the hemodynamic effects of the two issues currently in CPR, 'the adverse effect of reduced elasticity of thorax' and 'compression position'.

2.2.1 Reduced elasticity of thorax
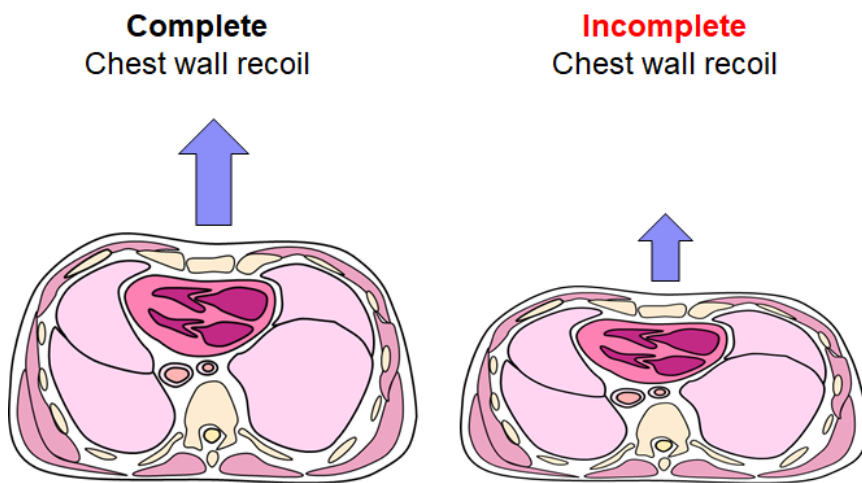
Figure 2.7 Incomplete thoracic recoil due to reduced thoracic elasticity.

$$P_{external} = f_{tp}E_{chset}(\dot{x}_1\Delta t) \qquad \text{Eq. (2.4)}$$

The reduction in the elasticity of the thorax occurs within 1 to 2 minutes after the initial compression begins [75, 76]. Therefore, to simulate this, the elasticity (E_{chset}) of the thorax was linearly decreased with time for 1 minute from the time 10 seconds after the start of compression. The initial elasticity decreased linearly from 37 kPa to 15 kPa for 1 minute, and changes in ABP, CVP, CPP, and venous return were verified over the entire time. The

42

thoracic elasticity was varied within the modulus of the mediastinal organs in Babbs' paper [40, 74]. The simulation was carried out for 90 seconds.

2.2.2 Ventricle-atrium compression ratio (VAR) for compression position
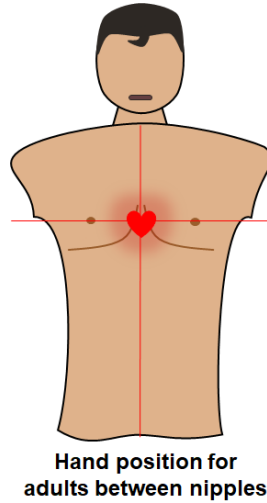
Figure 2.8 Chest compression position for adults during CPR.

Changing the compression position can lead to a change in the compression ratio between the ventricle and the atrium due to the sternum's hinge motion[61, 77]. For example, when compression is applied to the lower part of the sternum, a greater pressure gradient may be formed by the sternum's hinge motion, resulting in greater pressure in the ventricle site. Therefore, to compare the hemodynamic changes according to the compression position, the position's change was simply simulated with the compression ratio (ventricular-atrial compression ratio, VAR) between the ventricle and the atrium and modulated the VAR by changing f_{tp} of the ventricle and atrium. The f_{tp} was applied differently based on the atrium and ventricle, while the same ratio was applied equally to the left and right sides. Also, considering the anatomical position, the same f_{tp} for the atrium was applied for the great vessels in the

thoracic cavity [78]. The VAR changes were performed only in the hybrid model.

2.3 Parameter estimation of simple cardiovascular model for patient-specific CPR model

In this section, to develop a patient-specific CPR model, parameters for the cardiovascular system were estimated, and simulations were performed applying different elasticities of the thorax and compression positions in the personalized cardiovascular model. To avoid the estimation of unknown parameters, in this study, the simplest cardiovascular system was constructed that can be estimated using hemodynamic indices provided in the open dataset. Scipy.integrate.odeint from Python SciPy package (www.scipy.org) was used to solve the ordinary differential equations for the simple cardiovascular system.

The patient-specific cardiovascular parameters were estimated from a large multi-parameter ICU database (PhysioNet's MIMIC II database) [79]. The MIMIC II database contains several physiological indices such as an electrocardiogram (ECG), ABP, CVP, CO, and heart rate with more than 2000 records. The database was collected from 48 medical, surgical, and coronary intensive care beds in tertiary hospitals for adult patients aged 18 to 90 years or older.

2.3.1 Simple cardiovascular model

As shown in Figure 2.9, a simple cardiovascular system is composed of four compartments, consisting of the left heart, artery, vein, and capillary. The vascular compartment is composed of resistance and compliance. The equation for each blood vessel was the same as the blood flow and pressure gradient equation in Section 2.1.
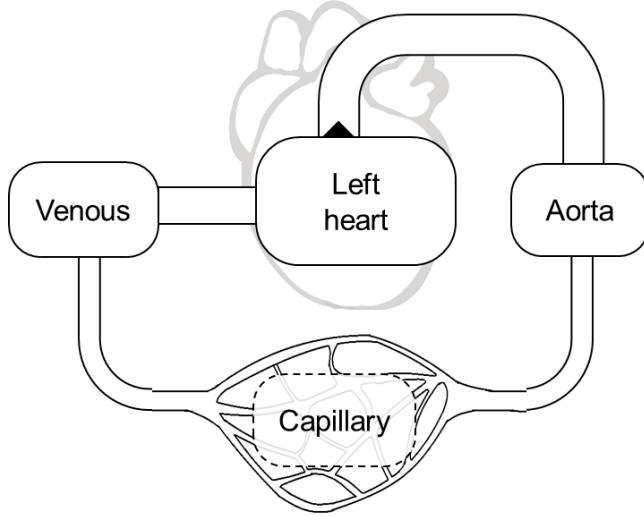
Figure 2.9 Diagram of simple cardiovascular system composed of 4 compartments.

In this model, the heart has a time-varying elastance to reflect different heart conditions for each patient. The time-varying elastance is the same as that in Eq. (2.5).

$$E(t)$$

$$= \begin{cases} E_d + \dfrac{E_{es}-E_d}{2} \cdot \left(1 - cos\left(\dfrac{\pi \cdot t}{T_s}\right)\right) & 0 \le t \le T_s \\ E_d + \dfrac{E_{es}-E_d}{2} \cdot \left(1 + cos\left(\dfrac{2\pi \cdot (t - T_s)}{T_s}\right)\right) & T_s < t \le \dfrac{3}{2}T_s \\ E_d & \dfrac{3}{2}T_s < t \end{cases} \qquad \text{Eq. (2.5)}$$

where Ts is the end-systolic time, E_{es} is the end-systolic elastance, and E_d is the end-diastolic elastance.

2.3.2 Genetic algorithm for parameter estimation

A genetic algorithm (GA) is the technique for solving optimization problems based on the evolutionary process. In this study, a GA was used to estimate the parameters of the cardiovascular system (Fig. 2.10) [70].
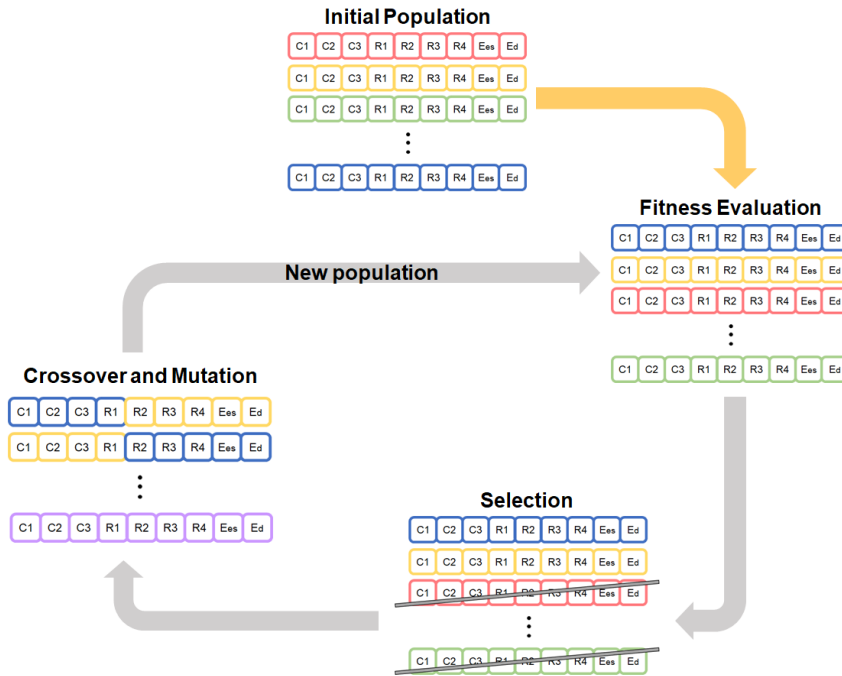
Figure 2.10 Conceptual diagram of genetic algorithm

To create an initial population, the parameter sets were randomly generated. The parameter sets consisted of nine parameters: resistance and compliance of each blood vessel, end-systolic elastance, and end-diastolic elastance of the left heart. The range of the parameters was defined to a value multiplied by five times of each parameter as the upper bound, and a value divided by five times of each parameter for have the lower bound. 10,000 parameter sets were randomly generated within the parameter range. By substituting the generated parameters into the differential equation, the results

for systolic blood pressure (SBP), diastolic blood pressure (DBP), central venous pressure (CVP), and SV, which are target hemodynamic indexes for each parameter set, are obtained. 70 parameter sets were obtained by excluding values that were too low or too high compared to those within a range in normal hemodynamic conditions, which were defined as the initial population.

Figure 2.11 shows the flow chart of GA. Because parents are the basis for the next generation, two sets (n=35) were selected through tournament selection. The selected parents had two children per parent through mating. The offspring underwent a crossover with a crossover rate of 0.4 and a mutation with a mutation rate of 0.8. One-point crossover was used for the crossover, and uniform mutation was used for the mutation so that the mutation could occur only within a specified parameter range. Finally, the fitness was calculated as the average error rate between the simulated results of the differential equation calculated through the parameter set and actual target hemodynamic indices (Eq. (2.6)).

$$Mean\ Error\ [\%] = \left[\frac{Target_{ABP,CVP,SV} - Simulated_{ABP,CVP,SV}}{Target_{ABP,CVP,SV}} \times 100 \right] \quad \text{Eq. (2.6)}$$

Because the GA evaluates candidate solutions over several generations, it can be computationally expensive. Therefore, in this study, a cardiovascular model with simple parameters was adopted for rapid computation. Additionally, to shorten the time required to reach the optimal solution, the generation size was limited to 70 individuals, and the evolution was limited to 30 generations for optimization; the maximum solution calculation time did not exceed 50 s.

2.3.3 Application of CPR model to patient-specific cardiovascular model

For a personalized CPR model, the CPR model was simulated on a patient-specific cardiovascular model. The modified hybrid model proposed in this study was applied to the CPR model, and the chest compression was transmitted to the heart, artery, and vein, excluding the capillary. To indicate cardiac arrest, the compliance of the heart was represented as a constant, and this value was applied as $C_{LV} = 1/E_d$.
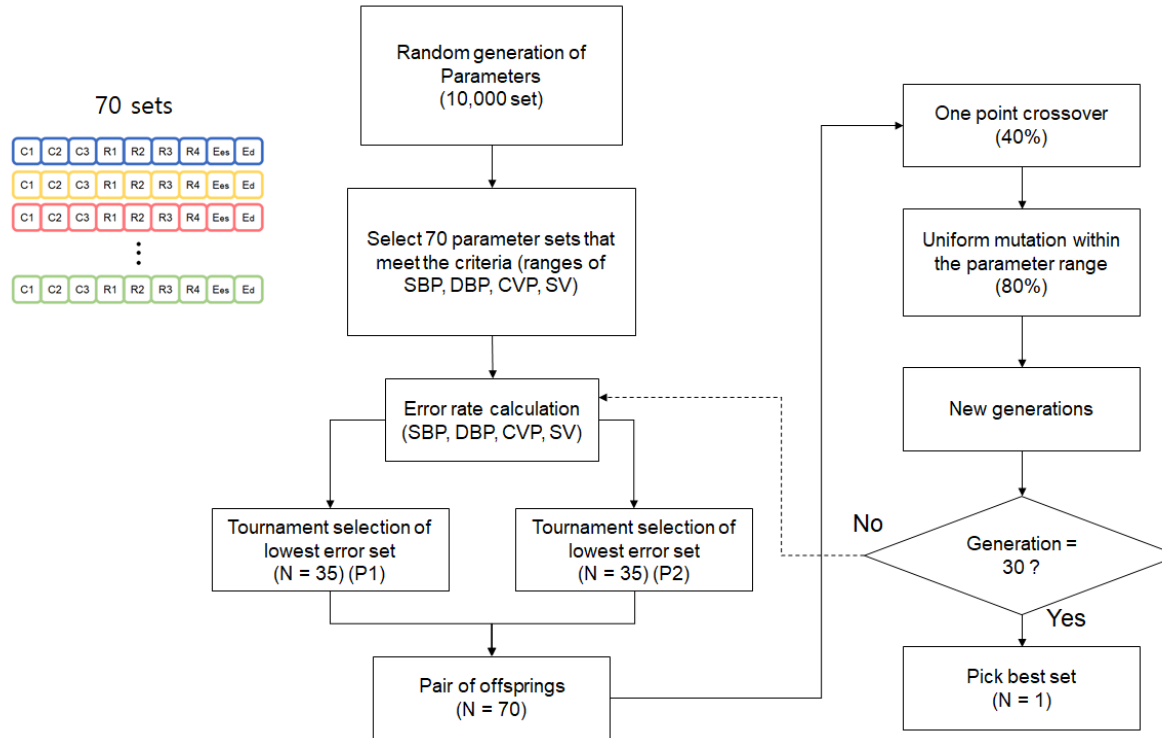
Figure 2.11 Flow chart of genetic algorithm.

CHAPTER 3

Results and Discussion

3.1 Modified CPR model based on general cardiovascular model

According to CPR physiology, the RAP peak pressure in the compression phase has almost the same value as the peak pressure of ABP [22]. Also, during compression, the pressure on the right side of the heart is equal to or higher than the pressure on the left side, limiting blood flow to the coronary arteries. Thus in the relaxation phase, coronary artery perfusion is relatively dominant [20, 50]. However, as these facts were not reflected in the original CPR model, we decided that the conventional model should be improved to reflect a better understanding of the current CPR physiology. We made two assumptions to improve the model. First, in order to increase the right side pressure as much as the left side, the atrium and the ventricle were compressed evenly between the sternum and the spine because the four cardiac chambers are located underneath the sternum anatomically (neglecting the compression gradients of the sternum's hinge motion) [59, 60], and the change in intrathoracic pressure caused by compression was also uniformly applied [80]. Therefore, unlike the original model, the thoracic factor was applied equally to the four chambers of the heart. Second, since the pressure of the central vena cava in the thoracic cavity is sensitively changed by spontaneous breathing or mechanical ventilation, it acts as a factor that greatly affects venous return. Therefore, we assumed that when the chest compression occurs by a strong external force, the intrathoracic vena cava should receive pressure changes in the intrathoracic pressure [81], and the model was modified to receive the intrathoracic pressure change by adding compartments of superior and inferior vena cava in the thoracic cavity. Based on these changes, we developed an improved hybrid model, and sought to verify its effectiveness by comparing it with the original model.
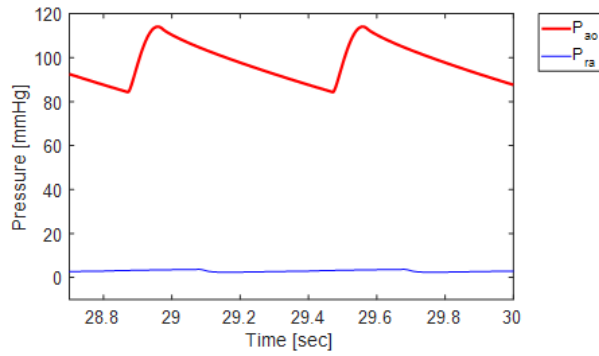
(A)
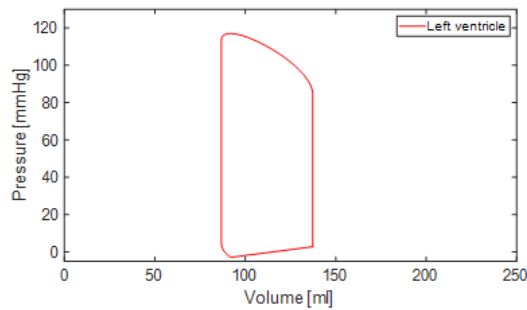
(B)

Figure 3.1 Validation of the normal condition of the developed model.

When the thoracic vena cava was added to the developed model, verification was first performed through normal conditions to ensure that appropriate cardiovascular parameters were configured. 100 beats per min for heart rate and 120 mmHg/25 mmHg for left and right ventricular pressure, respectively, were applied to represent normal conditions. As a result, we attained a cardiac output of 5.05 L/min and aortic blood pressure of 114/84 mmHg, which closes to typical physiologic conditions (Fig. 3.1).

3.1.1 Comparison results of animal experiments and simulations

To compare whether the developed model satisfies the current CPR physiology mentioned above, we compared the pressure waveforms and coronary blood flow of the two models. In addition, the pressure waveform obtained from animal experiments and the simulation results were compared.

The elastic modulus of the soft tissue through which the external force was transmitted to the thoracic cavity was 37 kPa, and the chest compression rate was 100 /min. Both models were simulated under the same conditions.

Figure 3.2 shows the pressure waveforms of the original and hybrid models, respectively. The original model has shown that during the compression phase, the right atrial pressure is much lower than that of the aorta, which led to primarily coronary blood flow during the compression phase. In contrast, the hybrid model has shown that in the compression phase, the right atrial pressure increased similarly to the aortic pressure, and in the relaxation phase, coronary blood flow predominated (Fig. 3.3).
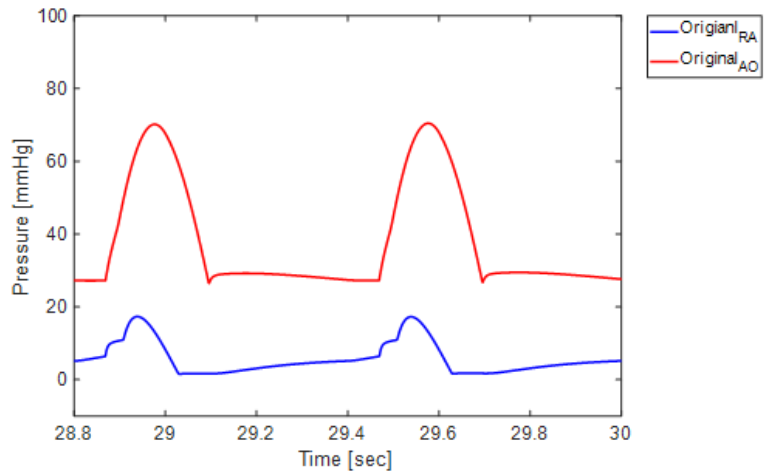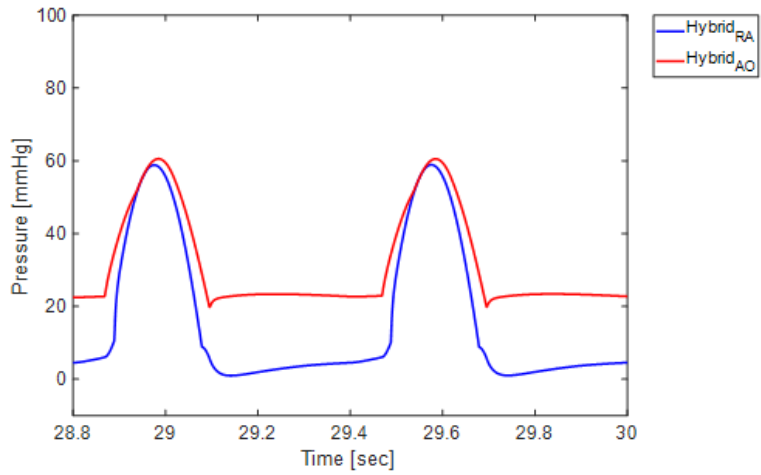
Figure 3.2 Aortic pressure and right atrial pressure for (A) the original model and (B) hybrid model.
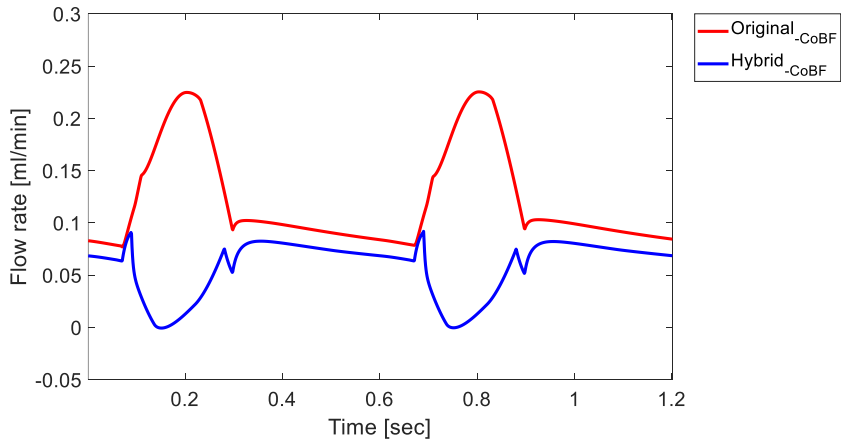
Figure 3.3 Coronary blood flow for the original model and the hybrid model.

In addition, both animal experiments showed that the CVP peak at compression was close to the ABP peak (Fig. 3.4). However, the model proposed in this section does not reflect the amplitude of the pressure waveform similar to those of the animal experiments because the cardiovascular parameters are configured based on the patient model of 70 kg, and the elasticity of the thorax is also a general value. Nevertheless, when comparing the pressure waveform and the coronary perfusion, the CPR model developed in this study can be said to be a general CPR model that can better reflect the current CPR physiology than the existing model.
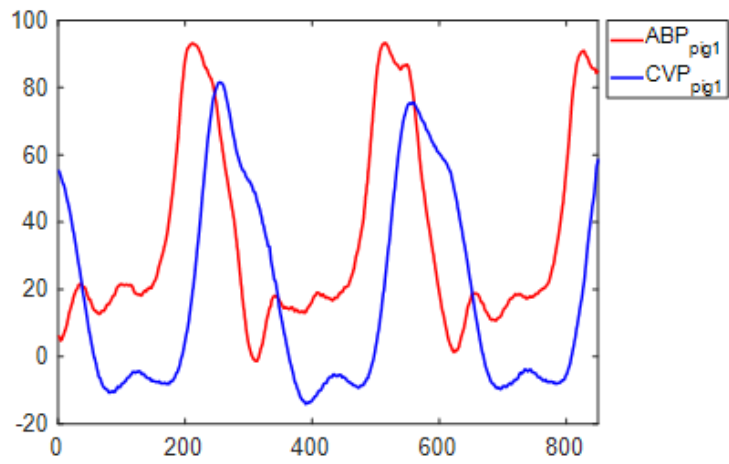
(A)
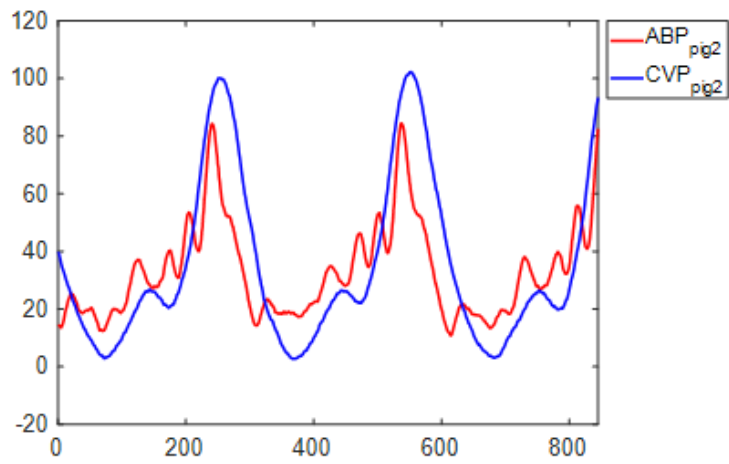
(B)

Figure 3.4 Pressure waveform obtained from animal experiments during CPR.

3.1.2 Hemodynamic effects on the various maneuvers
3.1.2.1 Comparison of CPR techniques

ACD–CPR + ITV is more effective in improving coronary artery perfusion than standard CPR (S–CPR). Therefore, to compare the CPP and coronary blood flow patterns of both models, Table 3.1 compares S–CPR and ACD–CPR + ITV of each model. CPP was calculated as the average value of the difference between aortic pressure and right atrial pressure in the relaxation phase, and the systemic perfusion pressure was calculated as the average value of the difference between aortic pressure and right atrial pressure over the entire cycle.

In the results, when ACD–CPR+ITV was applied, the cardiac output in the original model increased by about 10 %, and in the hybrid model by about 47 %. However, for CPP, the original model decreased by about 1.3 mmHg, while the hybrid model increased by about 8.9 mmHg. When comparing the mean coronary blood flow for the relaxation phase and full cardiac cycle, the hybrid model showed the coronary blood flow in the relaxation phase is higher than that in the full cardiac cycle, while the original model had higher coronary blood flow in the full cardiac cycle. Therefore, this result shows the difference in coronary perfusion patterns between the two models.

From these results, the original model showed a slight decrease in CPP [41], but the hybrid model showed increase by about 47 %. Since the original model has a more dominant coronary perfusion in the compression phase, even looking at the full cycle of coronary blood flow, the original model improved by about 16 % and the hybrid model by about 35 %. In many clinical studies of ACD–CPR+ITV, the application of ACD–CPR + ITV increases CPP by over 50 % on average, compared to S–CPR [23, 24]. Compared with these clinical results, it could be seen that the hybrid model presented in this study much better reflects the improvement of coronary perfusion.

Table 3.1 Comparison of changes in the hemodynamics of standard cardiopulmonary resuscitation (S–CPR) and active compression–decompression CPR with an impedance threshold valve device (ACD–CPR+ITV) for the original model and the hybrid model. Analytical parameters include Cardiac output (CO), systemic perfusion pressure (SPP), coronary perfusion pressure (CPP), relaxation phase coronary blood flow (CoBF), and mean coronary and cerebral blood flow (CeBF) for one cardiac cycle.

	Original Model		Hybrid Model	
	S–CPR	ACD–CPR+ITV	S–CPR	ACD–CPR+ITV
CO [L/min]	1.81	1.99	1.05	1.52
SPP [mmHg]	32.47	36.31	15.74	20.49
CPP [mmHg]	23.68	22.37	19.03	27.99
Relaxation CoBF [mL/min]	90.03	85.05	72.36	106.43
Mean CoBF [mL/min]	118.40	137.35	59.34	80.13
Mean CeBF [mL/min]	368.21	433.97	354.86	597.17

3.1.2.2 HUT and HDT

To compare the hemodynamic effects of changes in body position for the two models, the HUT angles were set to (30, 45, and 60)°, while the HDT angles were set to (-30, -45, and -60)°.

Figure 3.5 shows the stroke volume, the venous return with varying tilt angle. The stroke volume results show that as the HUT angle increased, the original model increased, while as the HDT angle increased, it had no changes. However, the hybrid model showed no significant difference from the supine position in both HUT and HDT. Therefore, this result shows the difference between the stroke volume change patterns of the two models. In addition, the venous return was compared through blood flow of vena cava in the thoracic cavity. From these results, the blood flow of IVC to RA increases with the HUT angle and shows little change in HDT, which shows that there is no difference between the two models. Also, the blood flow of SVC to RA decreases sharply with increasing HUT angles in both models. However, in HDT, the original model did not change in the supine position, but the hybrid model slightly increased, showing the difference in venous return between the two models. In addition, Figure 3.6 shows that CeBF and CPP increase as the head goes up(from HDT to HUT), and likewise in this result, CeBF and CPP also sharply changed in HUT, but slightly changed in HDT. Although there was no significant difference in CPP and CeBF between the two models, the hemodynamic changes according to the tilting angle were demonstrated through the modified model by showing similar results to the results of studying CPP and cerebral perfusion according to the tilt angle through animal experiments [52, 53].

In these results, both models change abruptly in HUT but almost no change in HDT, which is caused that the total compliance of blood vessels in the lower body is greater than that in the upper body. In general, the compliance of the lower body is larger than that of the upper body. And also, since the compartments of this study are more distributed in the lower body, it makes the total compliance of the lower body much larger than that of the upper body.

Therefore, it can be seen that the hemodynamics increases because the degree of accommodating the increased blood volume as gravity is applied in the direction of the lower body during the HUT is large. Conversely, in HDT, since the total compliance of the upper body is too small, there is a limit to the accommodating blood volume no matter how much the angle is increased, so it can be considered that the return flow does not increase.

Therefore, from these results, there was no difference in perfusion between the two models, but the difference in venous return was sufficiently demonstrated.
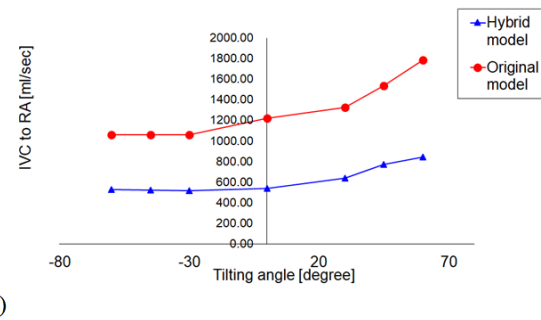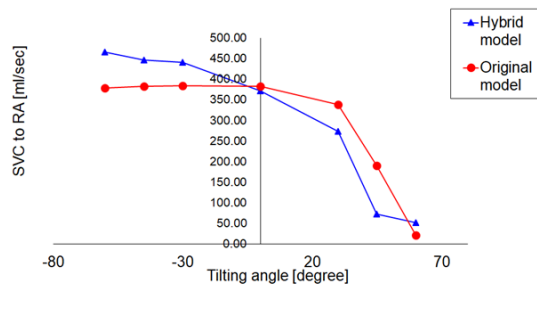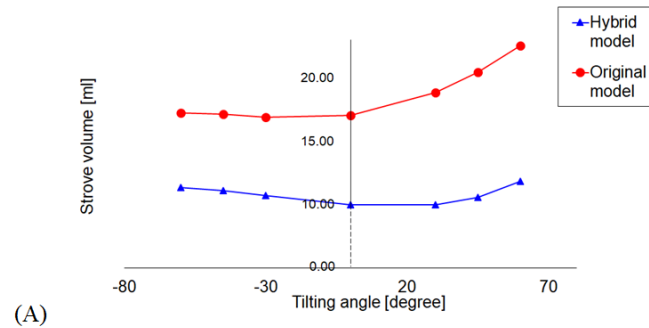
Figure 3.5 Changes in (A) stroke volume (SV), blood flow rate for (B) IVC (inferior vena cava) to RA (right atrium) and (C) SVC (superior vena cava) to RA (right atrium) according to the tilting angle. IVC had represented the thoracic IVC compartment in Hybrid model and the abdominal IVC compartment in Original model. Also, SVC had represented the thoracic SVC compartment in Hybrid model and the jugular compartment in Original model. Note the suppressed zeros on the ordinate axis in Figure 3.5(A).
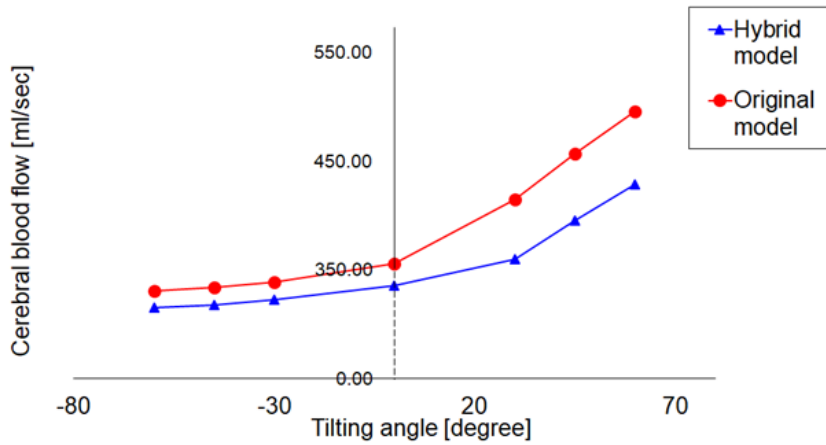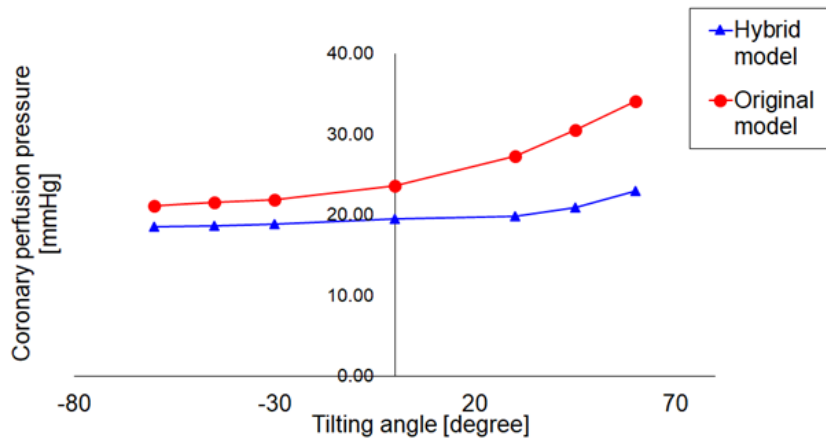
Figure 3.6 Changes in (A) cerebral blood flow (CeBF), and (B) coronary perfusion pressure (CPP) according to the tilt angle from the supine position for the original model and the hybrid model. Cerebral blood flow was calculated as the blood flow from the carotid artery to the jugular vein. Note the suppressed zeros on the ordinate axis in Figure 3.6(A).

3.2 Simulation-based approach to current issues in CPR using modified CPR model

Second, the hemodynamic effects for several issues arising during CPR were simulated based on the hybrid CPR model.

3.2.1 Hemodynamic effects on reduced elasticity of thorax

Repeated compression during CPR causes deformation of the thorax, and the thorax deformation appears in various ways, such as dislocation of cartilage joints or rib fractures. When the thorax is damaged, the stiffness of the sternum decreases, and the anteroposterior diameter of the sternum decreases [56, 82]. Decreased elasticity of the thorax may affect venous return by reducing the recoil of the chest return during the recoil phase [56, 76]. Therefore, in this study, to confirm the effects of the reduced elasticity of the thorax on the hemodynamic, the simulation was performed.

Figure 3.7 shows the pressure waveforms of ABP and CVP (RAP) when thorax elasticity is decreasing during CPR. This result shows that when the elasticity of the thorax decreases, the pressure amplitude changes more dominantly than the baseline value of the pressure waveform. Also, Figure 3.8 shows the pressure waveform in an animal experiment. As a result, even in animal experiments, the ABP and CVP peaks showed a notable decrease within 20 seconds after starting CPR. Thus, decreasing peaks of ABP and CVP in clinical or preclinical conditions under the assumption that the compression position has not changed may indicate a decrease in the elasticity of the thorax during CPR.
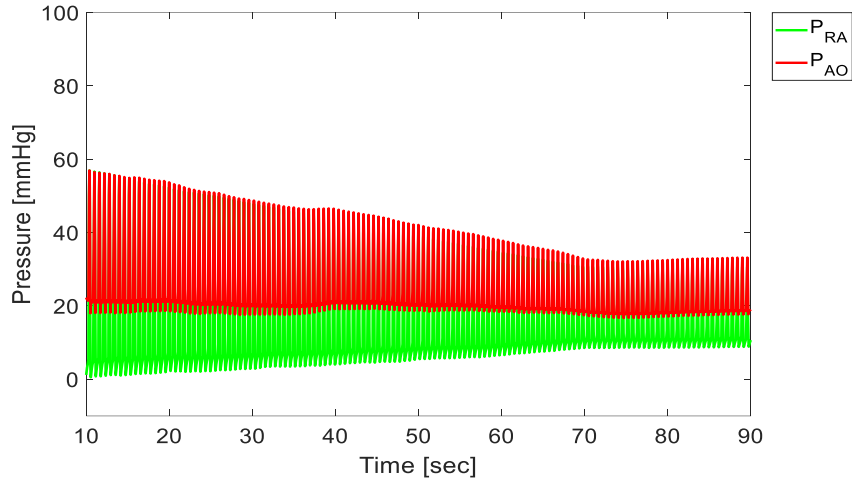
Figure 3.7 Pressure waveform when the thorax elasticity is decreasing during CPR.
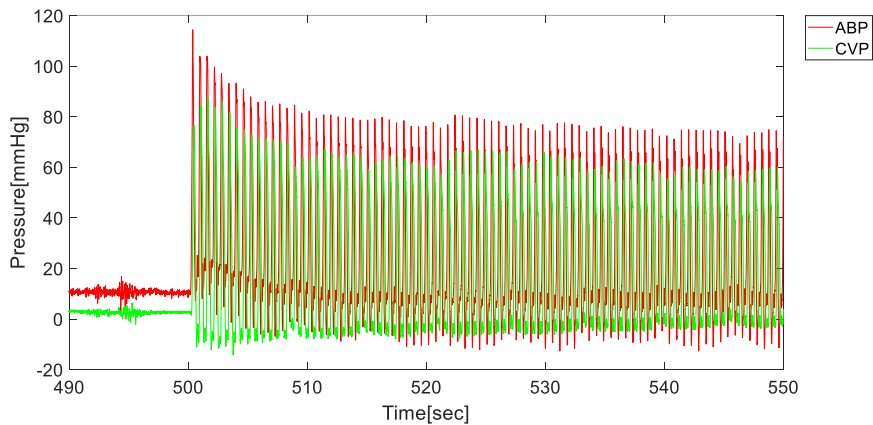
Figure 3.8 Pressure waveform of pig 1 during CPR animal experiments.

In addition, Figure 3.9 shows the carotid blood flow, coronary blood flow, and venous return during thoracic elasticity reduction. Carotid blood flow decreases as the elasticity decreases, not only the flow in the compression phase decreases, but also the flow in the recoil phase, the backflow from the carotid artery to the thoracic aorta, caused by the formation of negative pressure inside

the thoracic cavity. This result also showed that the decrease in thoracic elasticity limits hemodynamics during CPR by reducing coronary blood flow and venous return. Therefore, these results can be indicated that the negative pressure formation in the recoil phase is not properly achieved due to the decrease in thorax elasticity. Several studies have been conducted on the hemodynamic effects of chest elasticity reduction [83, 84]. These studies also suggested that many incomplete chest recoils occurred in the group with reduced thoracic elasticity due to chest injuries, leading to decreased coronary perfusion and poor hemodynamic results [56, 63, 83].

Therefore, the results presented in this study are similar to those of animal experiments, and it can be suggested that the reduction of thorax elasticity due to fracture and dislocation may reduce the effect of CPR. In addition, several recent studies have suggested that the compression depth recommended in the guideline of 5 – 6 cm is associated with increased injury [85], and the depth at which the maximum survival rate occurs is 4 – 5.5 cm [86]. Therefore, since the pressure waveform is the most easily accessible hemodynamic indicator for the patient, it is necessary to monitor the pressure waveform in a clinical or preclinical to perform compressions to a depth that can minimize chest damage.
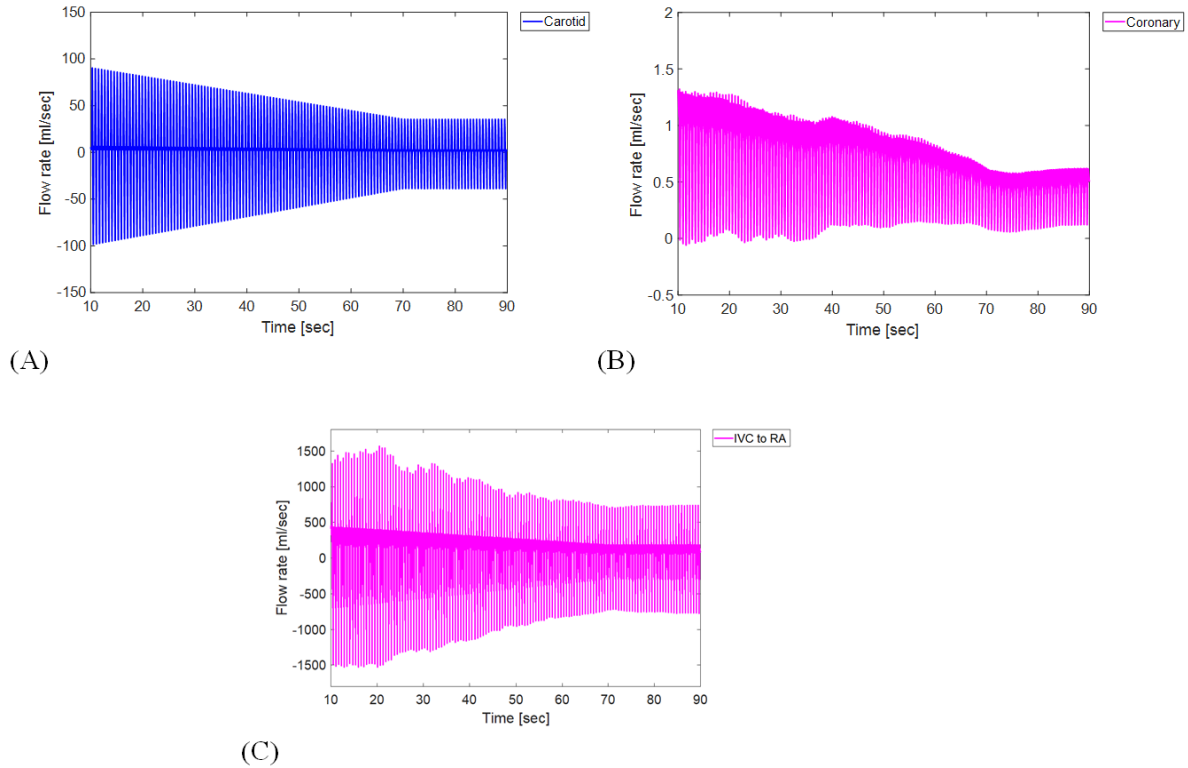
Figure 3.9 Blood flow rate when the thorax elasticity is decreasing during CPR. (A) Carotid blood flow, (B) Coronary blood flow, (C) blood flow rate of IVC to RA represent to venous return.

3.2.2 Coronary perfusion pressure for various VAR

A simple comparative study on the compression ratio of the ventricle and atrium was performed, which varied depending on the compression position. The current guideline's compression position is the midpoint of the inter-nipple line (INL), and the four cardiac chambers are anatomically located beneath that point [60, 61]. However, some clinical studies have suggested that the midpoint of INL may not be the optimal compression point because the maximal diameter of LV is located almost below the INL [59-61, 77]. Therefore, the compression ratio between the ventricle and atrium was simulated by modulating f_{tp}, and the change of CPP according to VAR was compared.

For example, if VAR (ventricle-atrium compression ratio) was 1.33, then f_{tp} of the ventricles is 1 (which means pure cardiac pump is applied to the ventricles in our model), and f_{tp} of the atriums is 0.75. If VAR = 1, then f_{tp} of the ventricles is 0.75, and f_{tp} of the atriums is 0.75.

Figure 3.10 shows that the CPP was the highest at VAR = 0.33 (f_{tp} of the ventricles is 0.25, and f_{tp} of the atriums and great vessels is 0.75) and it changed accordingly to the change in VAR. Figure 3.11 also shows the result of a decrease in stroke volume and CPP as the compression ratio of the atrial and great vessels, including the vena cava and aorta, increases for the same compression ratio of the ventricle. This result suggests that hemodynamics is inhibited as the atrium and major blood vessels' compression increases during CPR.
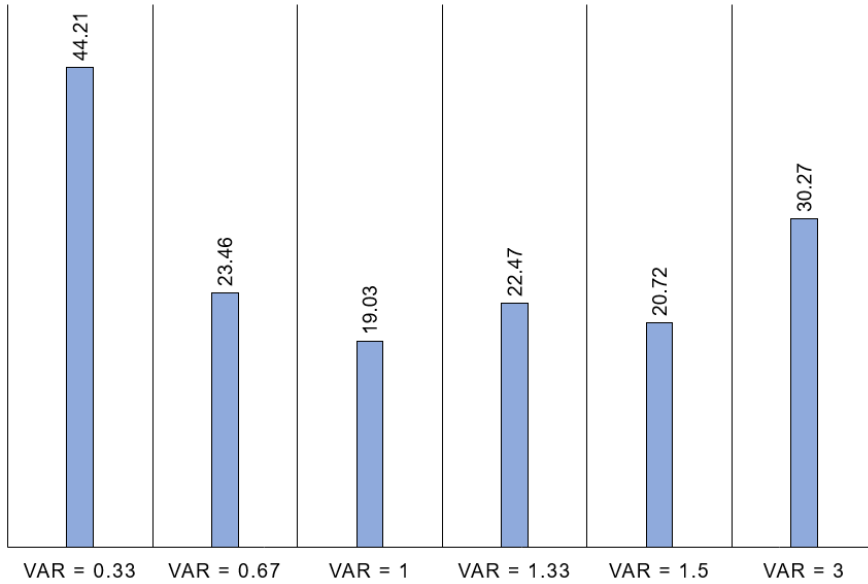
Figure 3.10 CPP changes in accordance to the ventricle-atrium compression ratio (VAR) and thoracic pump factors (f_{tp}) in the hybrid model. VAR = 1.33 (f_{tp} of the ventricles is 1, and f_{tp} of the atriums and great vessels is 0.75), VAR = 1 (f_{tp} of the ventricles is 0.75, and f_{tp} of the atriums and great vessels is 0.75), VAR = 1.5 (f_{tp} of the ventricles is 0.75, and f_{tp} of the atriums and great vessels is 0.5), VAR = 3 (f_{tp} of the ventricles is 0.75, and f_{tp} of the atriums and great vessels is 0.25), VAR = 0.67 (f_{tp} of the ventricles is 0.5, and f_{tp} of the atriums and great vessels is 0.75), VAR = 0.33 (f_{tp} of the ventricles is 0.25, and f_{tp} of the atriums and great vessels is 0.75).
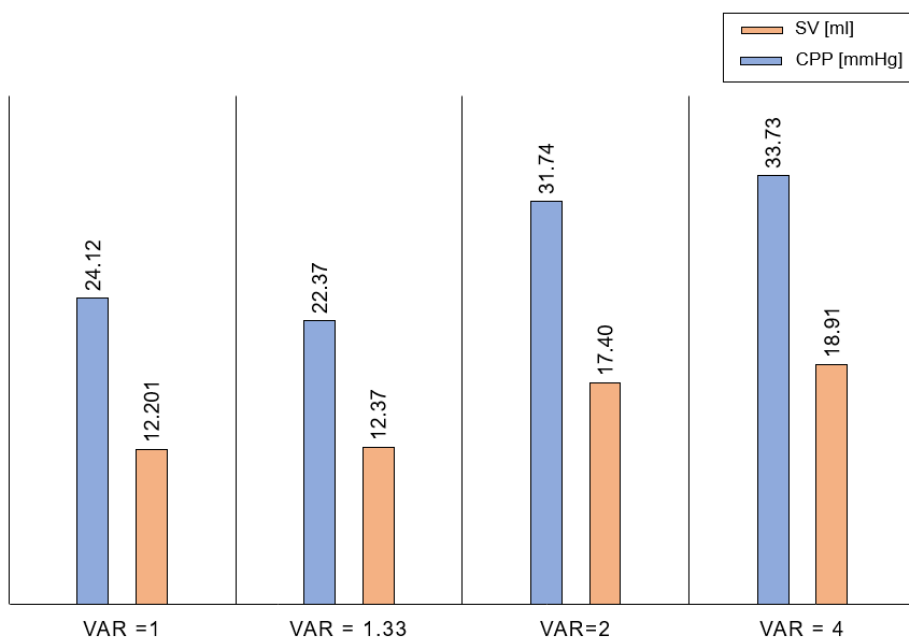
Figure 3.11 Comparison of coronary perfusion pressure (CPP) and stroke volume (SV) when different f_{tp} of atrium and great vessels as 1, 0.75, 0.5, 0.25 based on Ventricle's f_{tp} = 1.

The results show that the hemodynamics can vary considerably depending on VAR, and CPP is a potential indicator that can represent the optimal compression point [87]. These results mostly show that CPP is improved when ventricular pressure is high compared to compression of the atrium and large vessels, but the result of VAR = 0.33 shows a different pattern. This can be seen that coronary perfusion was increased due to a large aortic pressure. However, in Figure 3.12, it can be seen that the pressure of the pulmonary artery is relatively increased compared to when VAR = 3. Excessive increase in pulmonary pressure caused by compression may cause lung damage such as pulmonary edema [43], which may negatively affect. Therefore, although it can serve as a guide for the compression position through CPP, it is necessary to provide a guide in consideration of the anatomical position in the

thoracic cavity sufficiently. In addition, since the thoracic pump factor delivered to the compartments in the thoracic cavity may vary depending on the compression position and the sternum's compression gradient, further studies on this must be performed.

(A)

(B)
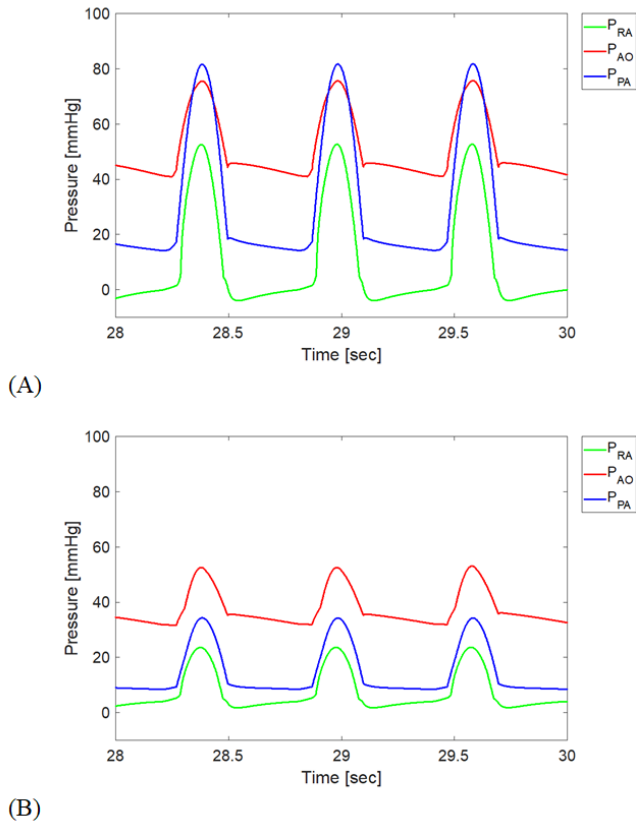
Figure 3.12 Comparison of pressure waveform when VAR = 0.33 (A) and VAR = 3.

3.3 Parameter estimation of simple cardiovascular model for patient-specific CPR model

Finally, in this section, to present the possibility of a personalized CPR model, parameters for the patient-specific cardiovascular model were estimated, and CPR was applied to them. First, 10 target hemodynamic indices (SBP, DBP, CVP, SV) were randomly generated to verify the parameter estimation through the genetic algorithm (GA). For the diversity of the generated data, the ranges were set as 100–150 mmHg of SBP, 60–90 mmHg of DBP, 1–10 mmHg of CVP, and 30–60 ml of SV. For CVP, the mean CVP was used in the same way because it was the value provided in the open dataset. The parameter estimation results for the simple cardiovascular system through the GA for the generated data are listed in Table 1. Consequently, the average error rate for each hemodynamic index does not exceed 7% at the maximum, and it shows that the overall results are similar to the target values. In CVP, the error rate tends to be relatively large compared to other indices, but because it is expressed as a relative ratio with the target value, it can be observed that there is no significant difference from the actual target value.

Table 3.2 Comparison of 10 generated data and simulated results from generated parameters by genetic algorithm.

Index	Generated Data SBP [mmHg]	DBP [mmHg]	CVP [mmHg]	SV [ml]	Simulation Results SBP [mmHg]	DBP [mmHg]	CVP [mmHg]	SV [ml]	Error rate [%] SBP	DBP	CVP	SV
1	102.70	63.37	5.14	57.35	107.31	62.93	5.70	59.85	4.49	0.69	10.87	4.36
2	113.31	85.73	1.75	32.52	107.93	81.20	1.73	32.46	4.75	5.29	0.92	0.18
3	147.01	69.03	3.15	46.56	148.51	75.06	3.13	46.22	1.02	8.74	0.76	0.72
4	118.46	79.77	2.60	43.30	114.46	82.33	2.81	41.21	3.38	3.20	8.24	4.82
5	129.20	81.37	9.57	49.98	134.13	76.25	8.10	52.46	3.82	6.29	15.37	4.97
6	109.37	71.69	7.05	39.28	104.43	73.69	7.68	40.21	4.52	2.79	8.98	2.38
7	121.19	89.54	6.61	41.28	115.62	85.36	7.10	41.08	4.60	4.67	7.45	0.48
8	119.46	64.29	5.40	51.23	123.95	55.13	5.17	50.38	3.76	14.25	4.17	1.65
9	101.68	66.06	2.29	42.61	110.24	58.43	2.47	40.39	8.41	11.56	7.77	5.20
10	112.20	73.28	5.93	51.39	112.05	74.63	5.88	54.59	0.13	1.84	0.89	6.22
Average of Error rate									3.89	5.93	6.54	3.10
Standard deviation of Error rate									2.12	4.15	4.59	2.14

3.3.1 Verification of parameter estimation using open dataset

In this study, the PhysioNet's MIMIC II database [79] was used for the patient-specific cardiovascular model. The patient data, including cardiac output from the database were primarily selected, and among them, patients with excessively high CVP values were excluded (N=40). The database provided the cardiac output value, which in this study was converted into the SV by dividing with the heart rate and simulated with the corresponding heart rate for each patient model.
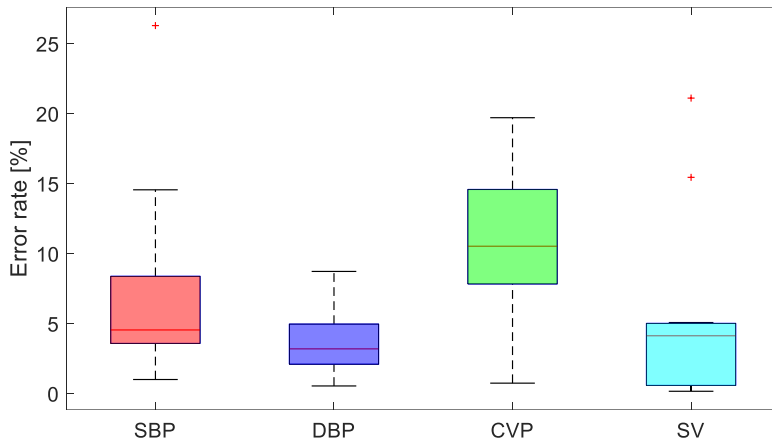
Figure 3.13 Box plot of error rate for open dataset results (N = 40).

The result of the parameter estimation using the open dataset is shown in a boxplot that presents the range of error rates for each hemodynamic index (Fig. 3.13). The average error rates and standard deviations are listed in Table 3.3. The mean and standard deviation of the error rate are observed to be larger than that of the randomly generated data.

Table 3.3 The average and standard deviation of error rate for the results of open datasets (N = 40).

	Error rate [%]			
	SBP	**DBP**	**CVP**	**SV**
AVG.	9.20	12.66	16.36	6.10
STD.	6.67	8.00	6.97	4.80

In SBP, the largest error rate is 25%, and the SV is 20%, which has a considerably high error rate. One cause of this could be the wide distribution of the patient's hemodynamic indices in the open dataset. Owing to the patients' varying age ranges and pathological conditions, the dataset includes patients significantly outside the range of normal cardiovascular values. In the initial population, because parameter sets with a normal cardiovascular range were selected, optimization could be difficult within 30 generations for individuals who are far out of the normal range even if mutation occurs [88]. However, a sufficiently low error rate could be reached as the number of optimization generations increases. Furthermore, setting the range of the initial population in consideration of the range of pathological conditions can make improvements. Another cause could be that the upper and lower limits of the set of parameters are limited, limiting the value of the offspring change through mutation, so that the appropriate parameter values cannot be reached. It is impossible to set the actual parameter range of the cardiovascular system according to various age groups and pathological conditions. However, if a broader range of mutation bounds is set, optimization with a lower error rate is possible.

Because the GA is optimized through generations, the change of the value of each individual (parameter sets) according to the generation for the result of the target hemodynamic index (SBP = 107.5, DBP = 70.3, CVP = 8.0, SV = 45.68), having the lowest error rate among the open dataset results, was represented through a heatmap. For each error rate, the results were 0.85, 6.5, 0.11, and 0.91%. Figure 3.14 shows a heat map for the SBP, Figure 3.15 is for the DBP, and Figure 3.16 is for the CVP. In these results, all individuals were converged to the value closest to the target value during generation passes. Figure 3.17 shows the pressure waveform result when each individual is applied to the cardiovascular system model, and the value of 30 generations is the pressure waveform for the finally converged result.

Figure 3.18 shows the heat map for SV, and Figure 3.19 shows the pressure-volume loop (PV loop) when each individual is applied to the cardiovascular system, and the difference between the parameter values of each individual and final parameter values as a percentage. The PV loop represents the work done by the heart, and a larger PV loop (Fig. 3.19 (A)) indicates that the work done by the heart increases, whereas a smaller one (Fig. 3.19 (B)) indicates that the work done by the heart decreases, which shows that the PV loop is affected not only by the heart's compliance but also by the pressure and resistance of the surrounding blood vessels.

As observed from these results, the points of convergence to the final value differ depending on the hemodynamic index. This is presumably because the cardiovascular system is a closed loop; thus, changes in the parameters affect adjacent compartments. Additionally, these results verify that different patients have different sets of cardiovascular parameters and that a patient-specific cardiovascular model can be constructed accordingly (Table 3.4).
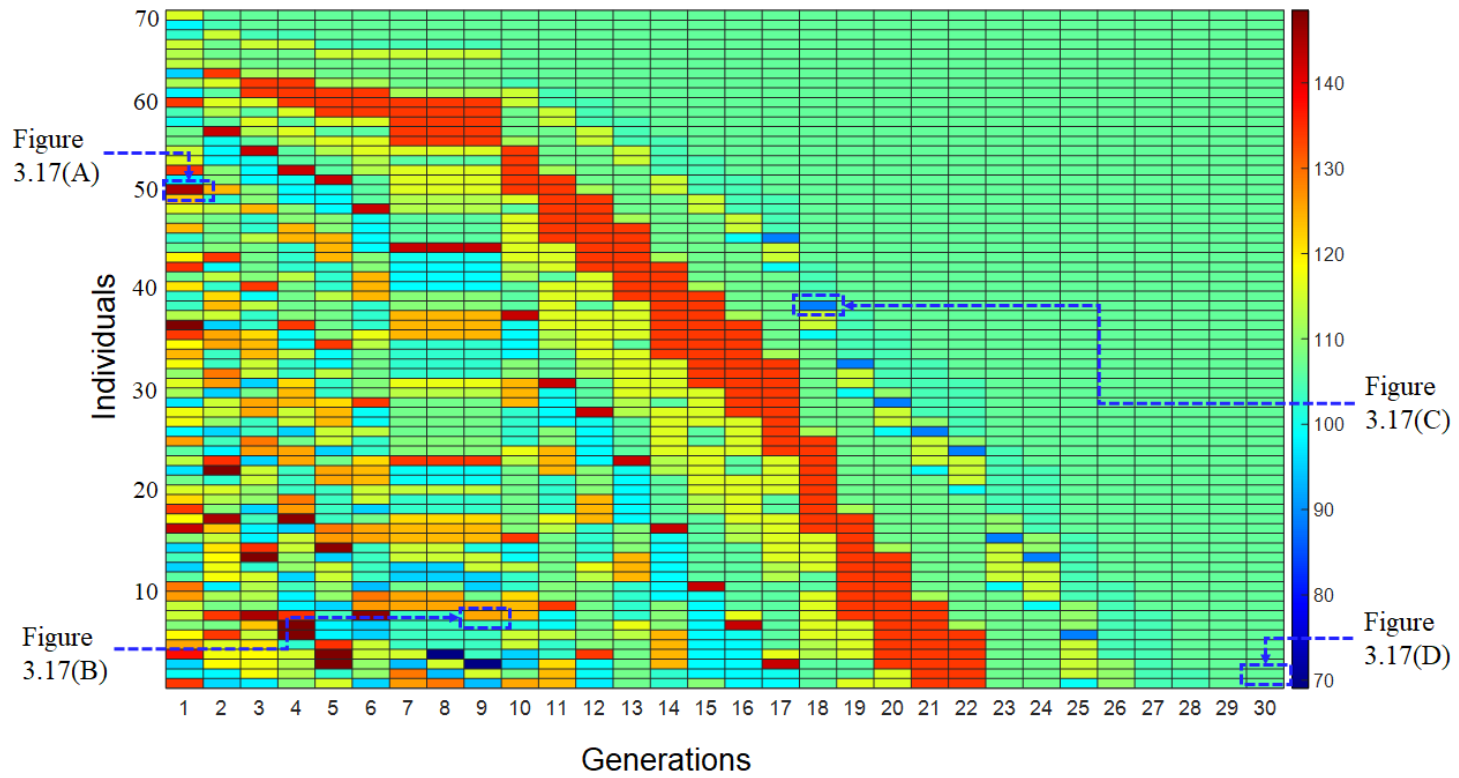
Figure 3.14 Changes in SBP value due to changes in individuals according to generation. The color bar represents the range of SBP.
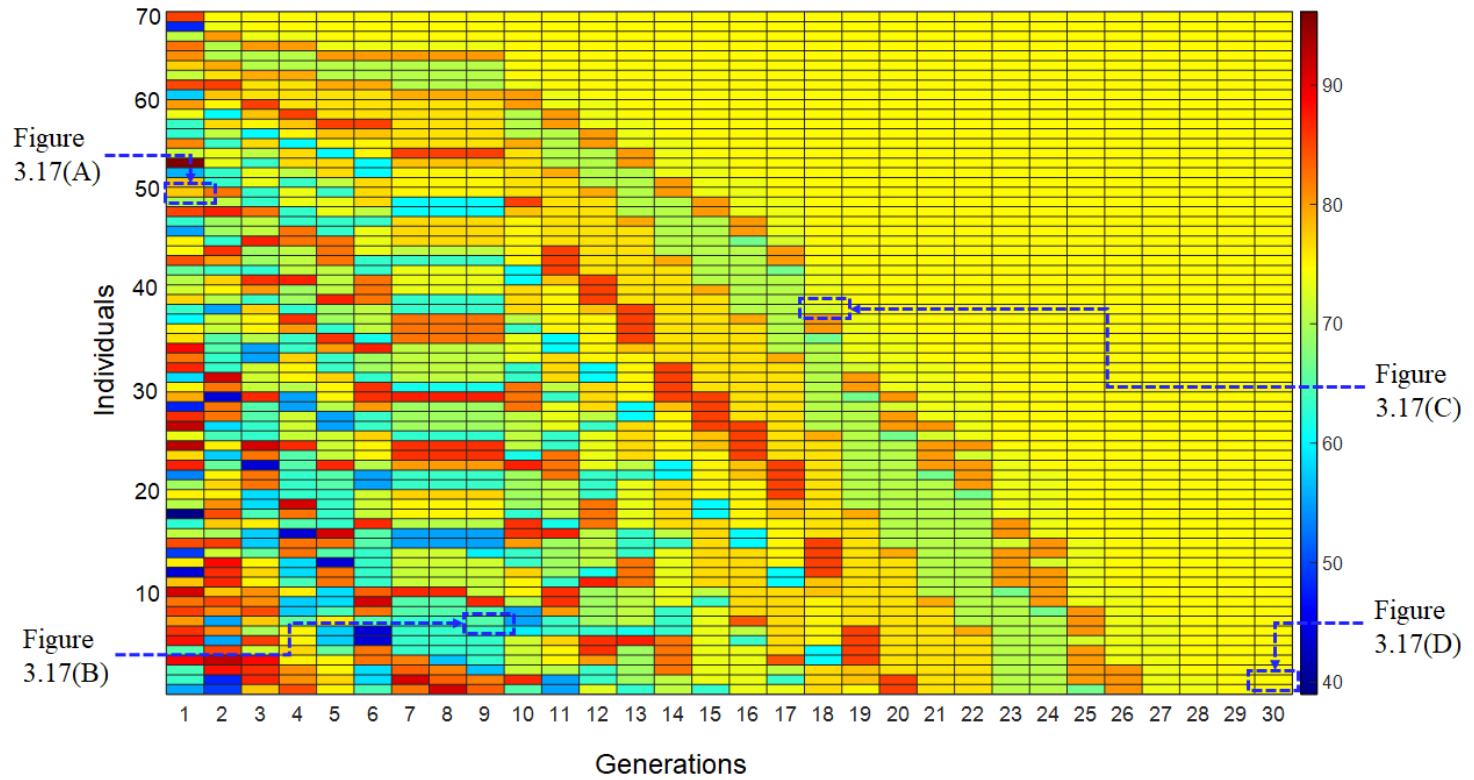
Figure 3.15 Changes in DBP value due to changes in individuals according to generation. The color bar represents the range of DBP.
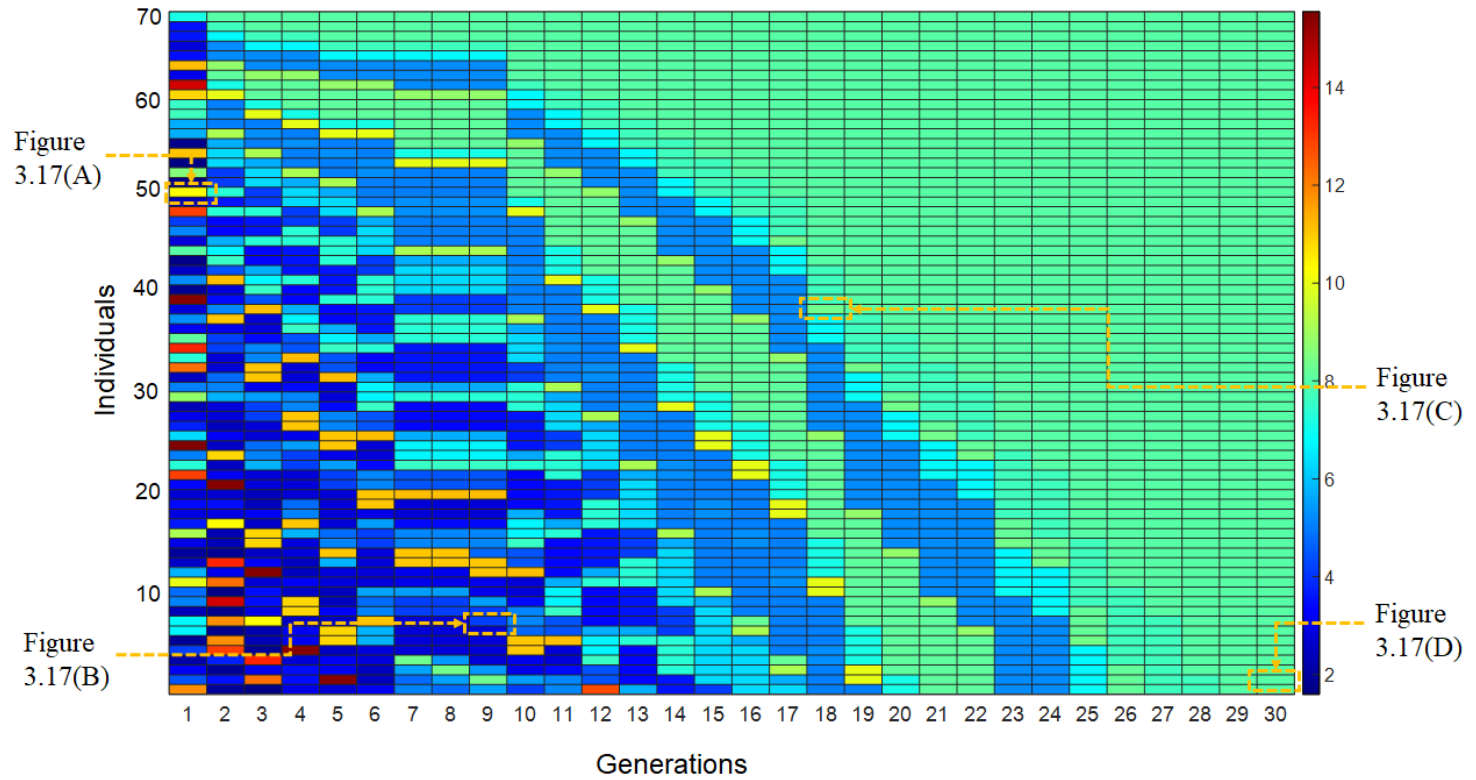
Figure 3.16 Changes in CVP value due to changes in individuals according to generation. The color bar represents the range of CVP.
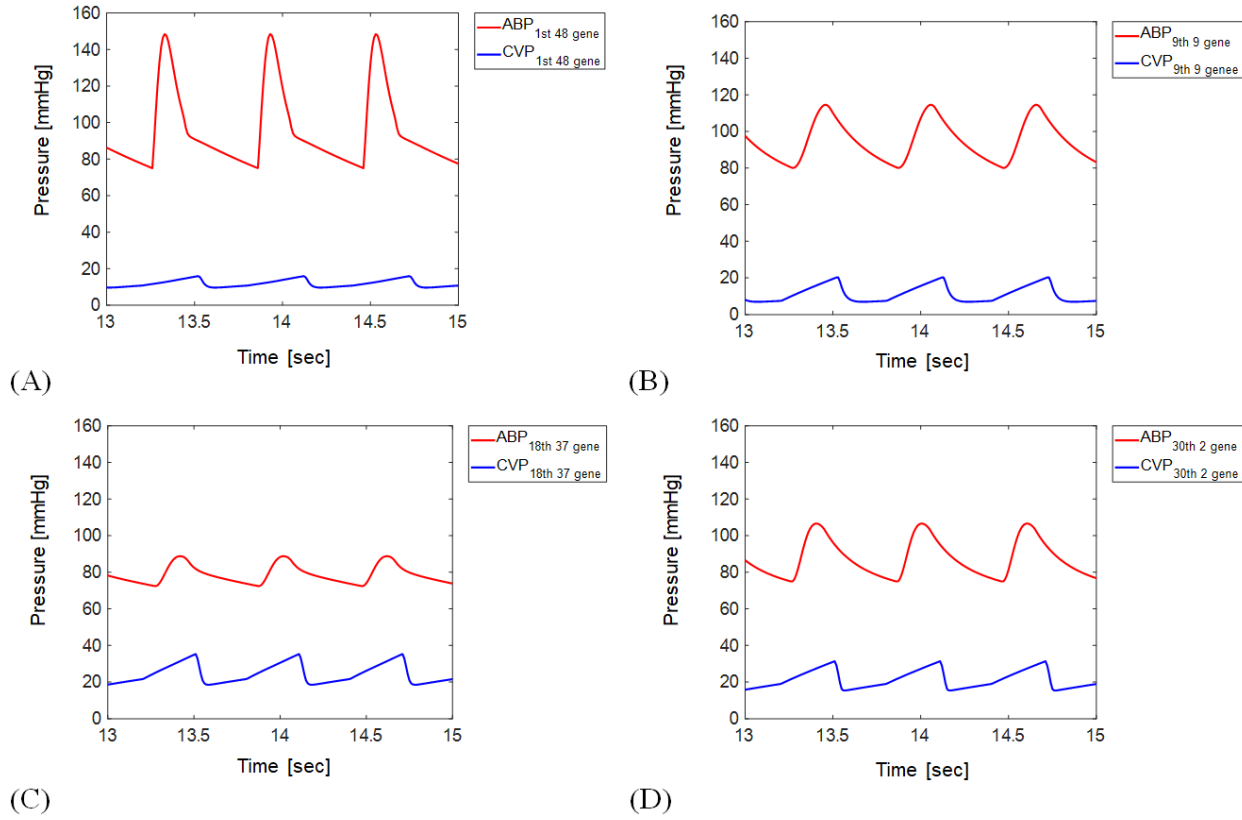
Figure 3.17 Pressure waveform of specific gene (individual) results.
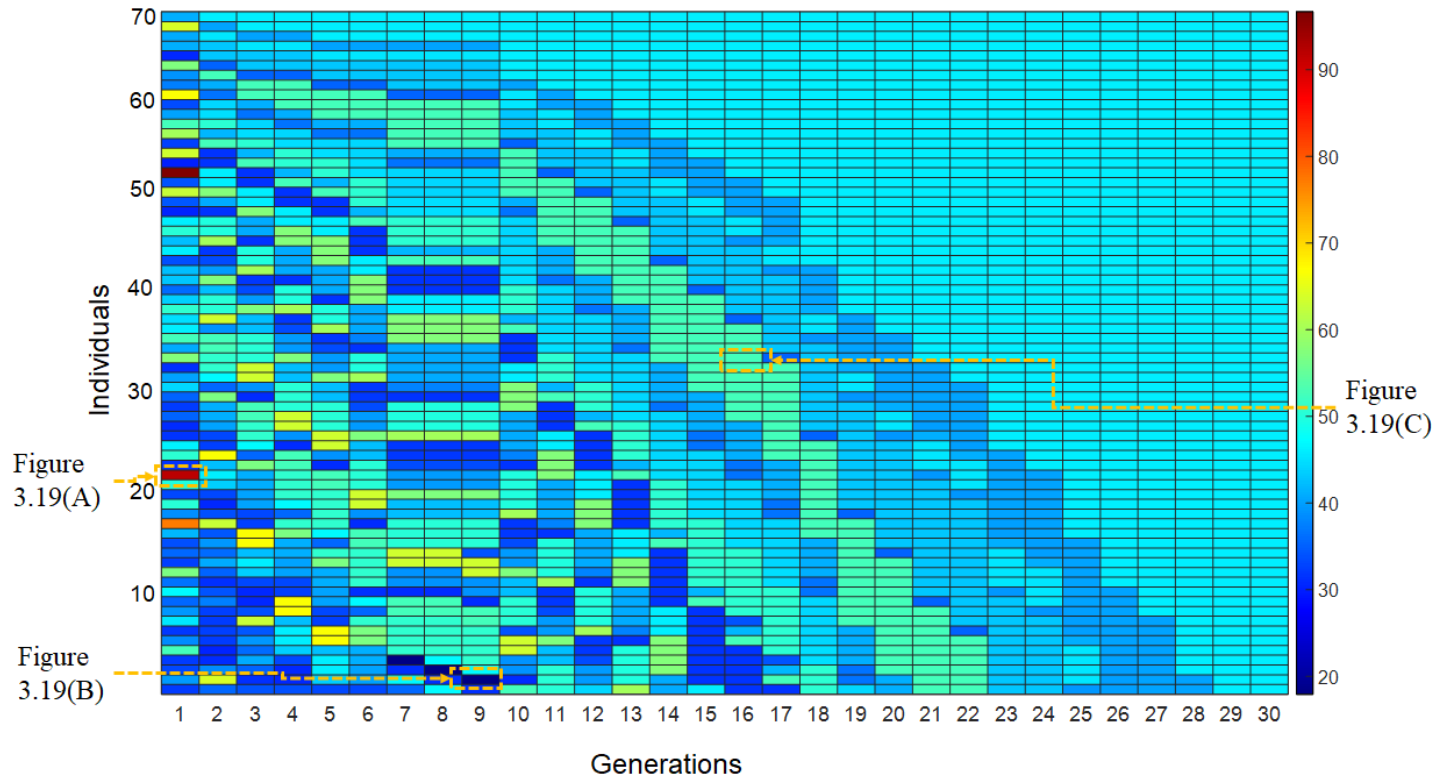
Figure 3.18 Changes in SV value due to changes in individuals according to generation. The color bar represents the range of SV.

(A)

(B)

(C)
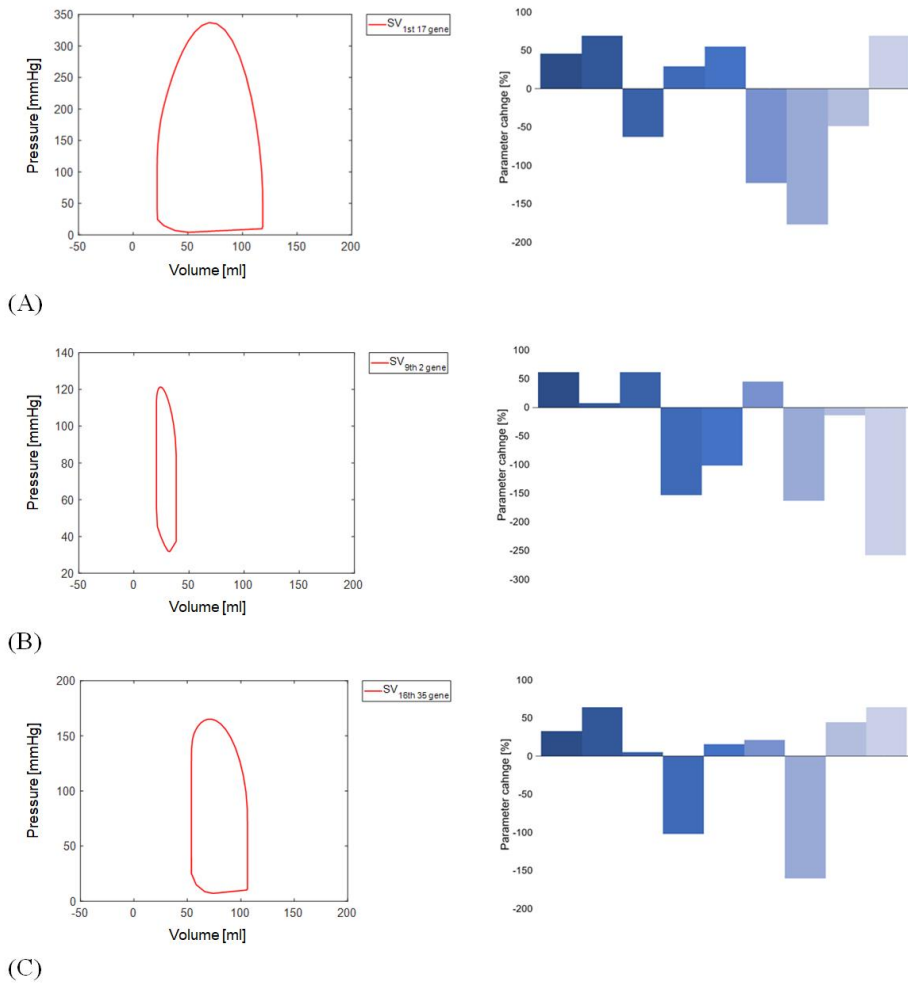
Figure 3.19 Pressure volume curve and percent change for optimal parameter and for each SV.

Table 3.4 Estimated parameter sets for the open dataset

Estimated parameter for cardiovascular system									Target hemodynamic index			
C1	C2	C3	R1	R2	R3	R4	Ees	Ed	SBP	DBP	CVP	SV
0.3943	4.3179	2.5541	0.2600	0.2517	0.0265	0.0037	4.4389	0.3227	139.00	64.30	9.00	55.55
0.5731	1.7013	1.6420	0.4461	0.5412	0.1106	0.0129	2.7043	0.0965	135.60	75.80	8.20	63.54
0.5932	2.4023	1.3296	0.1071	0.2525	0.5108	0.0268	7.0063	0.2977	112.10	54.10	15.70	68.64
0.7777	2.6137	1.5811	0.1803	0.4542	0.1611	0.0043	4.9489	0.2036	122.90	63.70	12.00	70.50
0.2331	3.0674	1.0420	0.2057	0.3652	0.7500	0.0167	3.7698	0.3506	110.80	58.40	11.90	43.23
0.2484	3.4827	2.3103	0.2916	0.1650	0.6154	0.0165	7.5989	0.4551	125.60	62.60	8.60	56.50
0.7140	0.7199	0.9240	0.3015	0.5080	0.0599	0.0164	1.7928	0.1510	109.70	60.60	10.00	47.11
0.4289	0.7505	2.8364	0.1523	0.2428	0.4513	0.0179	6.5391	0.2187	114.80	54.50	6.70	71.74
0.3671	4.5149	2.1523	0.1639	0.4704	0.4009	0.0093	2.8637	0.1130	106.70	51.60	8.40	55.56
0.9599	4.0775	1.4950	0.2676	0.3712	0.2068	0.0073	7.9919	0.4000	113.70	60.20	12.00	52.50
0.1612	2.7190	1.0571	0.2242	0.5895	0.6789	0.0256	3.3924	0.0512	110.50	59.90	12.10	48.25
0.3453	4.8758	1.7575	0.1803	0.1374	0.5430	0.0236	4.3460	0.4678	108.20	57.70	9.90	51.00
0.7431	4.7720	0.9204	0.4172	0.2231	0.3331	0.0171	1.0385	0.0893	99.00	54.60	10.00	42.63
0.1204	0.6872	1.1743	0.1183	0.5589	0.6781	0.0034	4.6771	0.1775	117.00	61.30	11.00	51.01

0.8613	4.7852	1.7397	0.2209	0.6429	0.1410	0.0050	4.9350	0.2720	105.70	70.30	8.00	45.68
0.0976	3.7632	0.5927	0.4299	0.7486	0.6384	0.0234	1.9356	0.0609	127.50	63.10	15.10	36.11
0.8049	2.3616	0.8645	0.0926	0.5242	0.2963	0.0024	6.6492	0.6354	117.80	68.30	14.10	49.24
0.9599	4.0775	1.4950	0.2676	0.3712	0.2068	0.0073	7.9919	0.4000	112.60	67.10	13.30	56.14
0.7888	4.0348	1.7648	0.3243	0.7763	0.5123	0.0194	4.7056	0.0692	118.40	69.00	6.80	50.16
0.6134	0.8239	1.2441	0.3507	0.1698	0.0674	0.0198	2.9841	0.3465	100.10	62.50	9.90	53.00
0.8559	1.3700	1.5002	0.2218	0.1670	0.7258	0.0063	5.4519	0.2547	109.50	56.60	10.80	74.88
0.3555	2.5277	2.7542	0.1804	0.1215	0.3382	0.0094	3.2860	0.3233	98.50	50.30	7.30	68.65
0.6145	2.9679	0.6790	0.1102	0.7215	0.3899	0.0179	5.1058	0.2395	124.50	61.10	17.70	41.16
0.7898	0.0085	6.0599	0.6274	0.3142	0.7898	0.0085	6.0599	0.6274	124.50	61.10	17.70	41.16
0.2554	0.4248	0.5702	0.0818	0.4764	0.7598	0.0133	4.9861	0.3991	111.10	54.80	18.30	44.21
0.4729	1.0546	1.0505	0.1568	0.2306	0.7565	0.0208	6.5489	0.5984	109.20	52.20	13.40	45.95
0.2635	1.8310	2.2498	0.5796	0.2431	0.3040	0.0092	5.5676	0.6408	126.70	53.50	6.40	39.71
0.1507	4.1952	1.1974	0.2816	0.2849	0.7886	0.0034	0.6876	6.0954	136.70	64.00	10.60	36.53
0.2330	4.9498	0.5415	0.2419	0.2178	0.4809	0.0116	2.8683	0.2343	131.10	53.60	13.80	47.85
0.0976	3.7632	0.5927	0.4299	0.7486	0.6384	0.0234	1.9356	0.0609	135.00	55.00	14.60	37.97
0.6275	4.5712	1.7203	0.2857	0.2770	0.6225	0.0017	2.4851	0.1306	131.50	59.30	8.50	52.95

0.2171	3.2819	0.4453	0.1935	0.9108	0.7706	0.0104	7.5178	0.5939	106.80	66.10	17.90	31.97
0.6512	4.1626	0.6359	0.1836	0.1387	0.6690	0.0006	5.3178	0.6221	121.00	57.40	18.20	44.69
0.6145	2.9679	0.6790	0.1102	0.7215	0.3899	0.0179	5.1058	0.2395	130.50	66.70	17.20	42.78
0.0976	3.7632	0.5927	0.4299	0.7486	0.6384	0.0234	1.9356	0.0609	116.80	52.60	15.90	33.77
0.2932	4.2498	2.0344	0.2729	0.4732	0.1857	0.0004	6.0270	0.3969	129.70	56.10	10.20	50.89
0.3042	3.4362	1.1933	0.4995	0.7518	0.7612	0.0009	3.6695	0.0608	134.50	65.30	12.90	42.87
0.2961	4.0809	1.5027	0.2002	0.5473	0.2626	0.0158	7.1143	0.4440	124.60	59.10	7.80	43.80
0.4756	4.7390	0.6251	0.2133	0.2981	0.4311	0.0036	1.9707	0.1713	112.00	59.60	19.30	51.70
0.6190	1.7526	0.9187	0.0680	0.2548	0.7165	0.0102	7.7281	0.4320	105.70	58.70	18.50	64.09

Furthermore, this study attempted to estimate the parameters for each pig model through the pressure waveform obtained in the previous animal experiments. Because there is no true value for the SV in the animal experiments, the parameters were estimated using the maximum and minimum peaks for CVP and ABP as the target hemodynamic indices (SBP, DBP, maxCVP, minCVP). Therefore, the changed target hemodynamic index was applied to the fitness equation to estimate the parameters of the pig model. For the target hemodynamic indices of each pig model, an average of five cycles was applied, and parameter estimation was performed for 30 generations in the same manner.

(A)

(B)
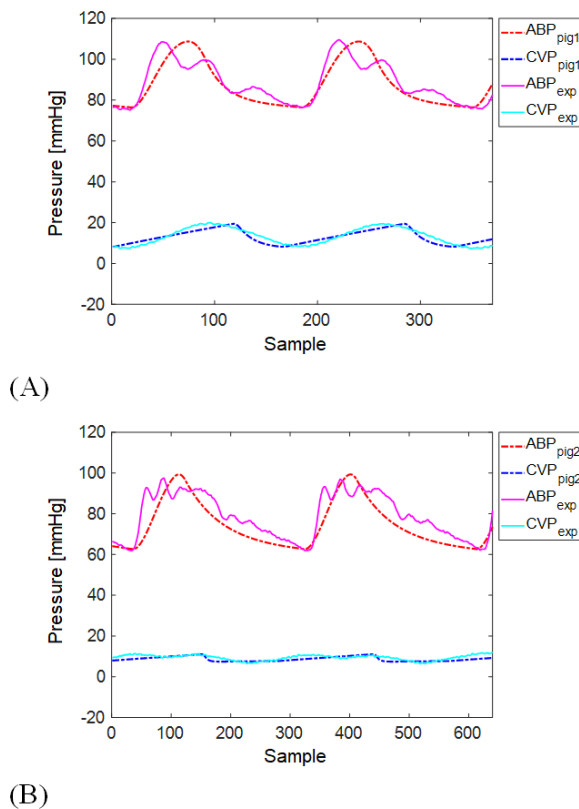
Figure 3.20 Pressure waveform of pig model vs Parameter estimated simulation model. (A) Pig 1, (B) Pig 2.

Figure 3.20 shows the comparison results of the pressure waveform for the simulation results estimated with the parameters and animal experiments. Table 3.5 shows the error rates for the target hemodynamic indices of each pig model.

Table 3.5 Error rates of target hemodynamic indices for each pig model.

	Error rate [%]			
	SBP	**DBP**	**maxCVP**	**minCVP**
Pig 1.	2.02	3.62	0.14	14.53
Pig 2.	3.25	3.54	3.11	1.86

The results show that the pressure waveform of the cardiovascular model implemented through parameter estimation of the two pig models tends to that of the actual one. However, it does not reflect the waveform of the dicrotic notch in the ABP. This is because the inertia value of the ABP was not reflected, and the cardiovascular system was constructed through the simplest compartments to minimize the estimation of unknown parameters. Furthermore, high-frequency oscillation can be observed in the systolic phase of the pressure waveform obtained from Pig 2 (Fig. 3.20(B)). This artifact can occur by the pressure transducer system used to invasively measure blood pressure [89-91]. One of the frequencies generated by the cardiovascular system overlaps with the natural frequency of the transducer, causing the underdamped/resonance phenomenon. Therefore, this non-physiological oscillation was not considered in this study. However, a recent study showed that this underdamped oscillation occurs in approximately 30% of critically ill patients [92]. Therefore, because this artifact may have clinical relevance to the cardiovascular condition, it is necessary to understand the sufficient correlation between the cardiovascular condition and measured artifact.

Nevertheless, this study proved that even if the parameters were estimated considering a simple cardiovascular system, the cardiovascular state

can be sufficiently simulated. Additionally, Pig 1's minCVP error rate (14.53%) was high compared with the other values. However, because all the minCVP values are exceedingly low, even a slight difference results in a relatively large error rate.

These results verified that parameters could be estimated not only from the open dataset but also from the actual animal model. Furthermore, because it takes less than 1 min to estimate parameters for each individual, it could be possible to estimate parameters for the data acquired in real-time and provide a personalized cardiovascular model.

3.3.2 Application to patient-specific CPR model

In this study, a personalized CPR model was proposed based on a patient-specific cardiovascular model. Therefore, it was intended to verify that pressure waveforms due to compression may be differently formed according to the state of the cardiovascular parameters. A personalized CPR model was simulated by applying the CPR model to animal models and one patient of the open dataset.

First, the modified CPR model was applied by selecting the four individuals (parameter sets) with the lowest error for the target hemodynamic index from the open dataset results (Fig. 3.21). These results showed that the pressure waveform changes remarkably according to the parameter set composed of each individual. Moreover, this indicated that CVP increases by as much as the ABP peak during compression, but those higher or lower than ABP are affected by the cardiovascular parameters. Therefore, fore these results, it can be suggested that hemodynamics may have different patterns according to the patient's cardiovascular system. Figure 3.22 shows the result of applying VAR differently when applying CPR to the cardiovascular system model composed of the finally converged parameter set. In this result, even if the same cardiovascular parameters are configured, it showed that the pressure waveform changes significantly when the compression position is different, and the hemodynamics can be influenced [93]. Because the elasticity of the thorax

cannot be predicted from the results, the simulation was performed by applying the same elasticity. However, when the elasticity of the thorax is changed, it should be considered that the pressure waveform may also be changed.
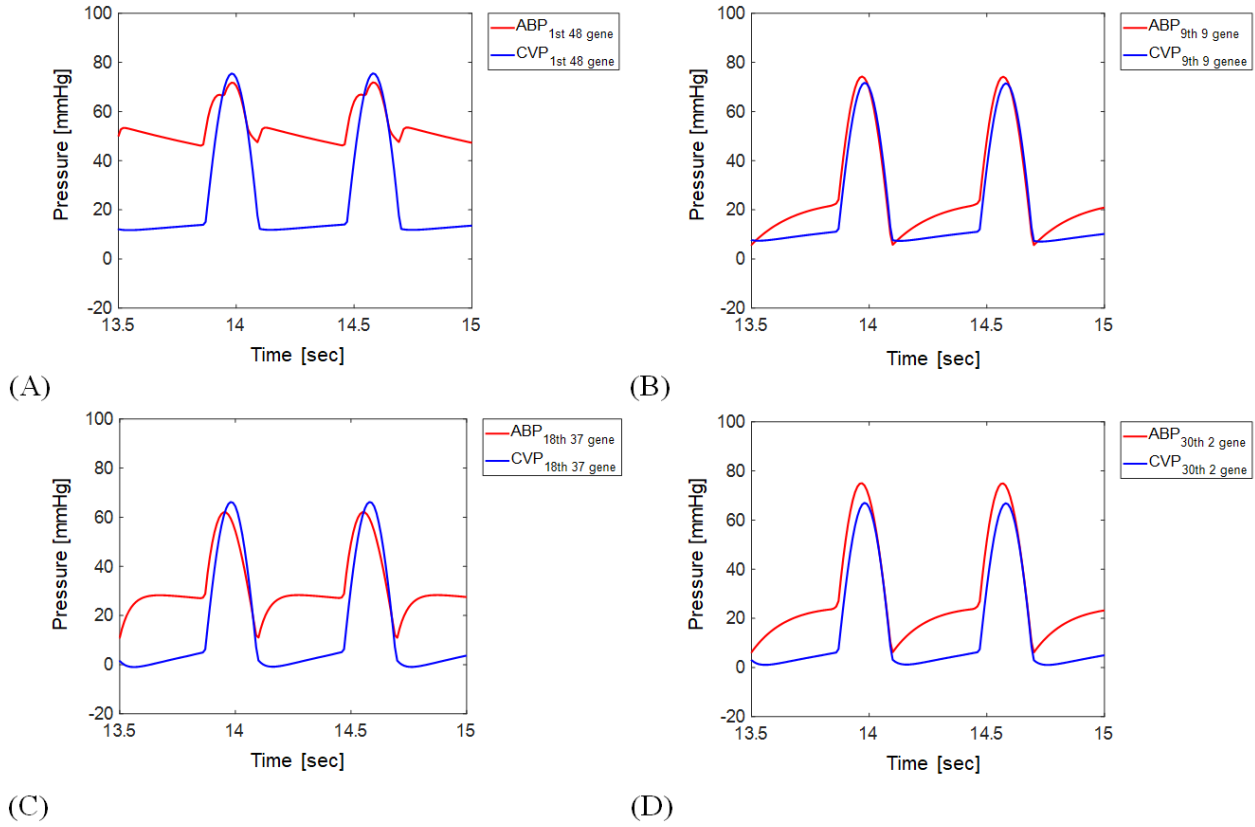
Figure 3.21 CPR models for cardiovascular models with different parameter sets
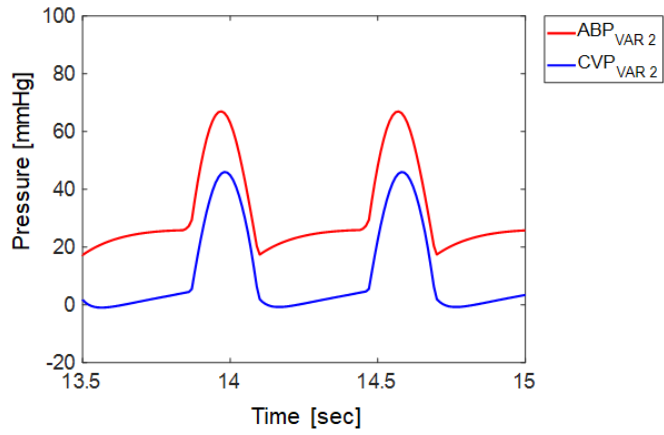
(A)
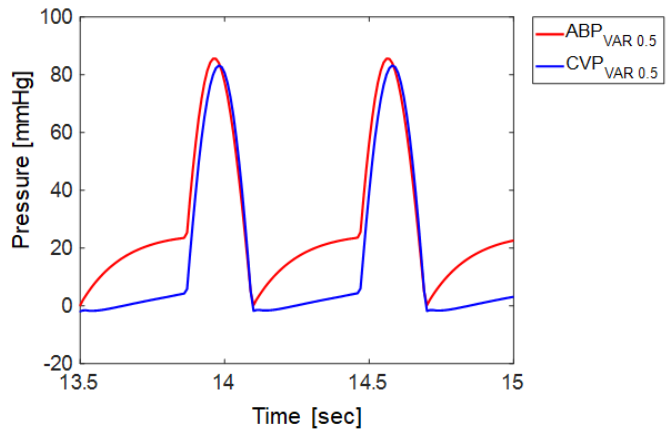
(B)
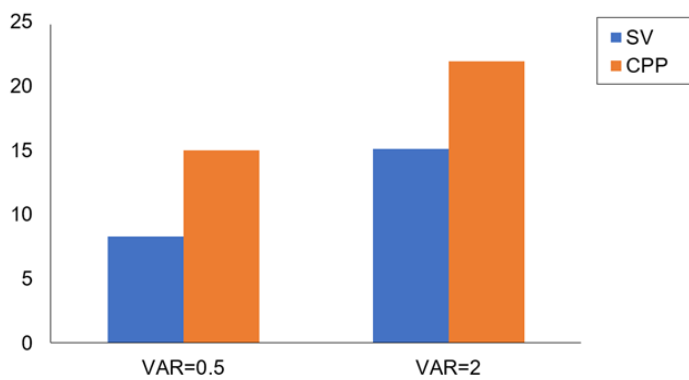
(C)

Figure 3.22 30th 2gene's (finally converged parameter set) pressure waveform according to VAR.

The CPR model was applied to the cardiovascular model for each pig, and the pressure waveforms in the animal experiments and simulation results of the parameters estimated from those were compared. (Fig. 3.23)

When the VAR is low, the CVP rises as much as the ABP, and the CPP is decrease. Conversely, when the VAR is high, the CVP becomes lower than the ABP, and the CPP increases [58, 87]. Based on the results of the VAR study in Section 2.2, in the CPR waveform of the pig model, it can be predicted that Pig 1 has a high VAR, whereas Pig 2 has a low VAR. Therefore, the VAR was applied differently to the CPR models of the two pigs. Additionally, when the same compression depth and thoracic elasticity (37kpa) were applied to the CPR models of both pigs, the pressure transmitted to the cardiovascular system tended to be too low in both models. Therefore, because the peak value of the pressure waveform is affected by the elasticity of the thorax [84, 85], the thoracic elasticity of each pig model was arbitrarily adjusted within the range of the elastic modulus of the mediastinal organs to be similar to the pressure waveform in the animal experiments [94, 95]. As a result, it was shown that the results of the CPR model of Pig 1 and Pig 2 had similar trends with the animal experiments. As shown in this result, it is possible to predict the current compression position through the CPP and degree of CVP higher or lower than the ABP. Additionally, it indicates that even when the same compression depth is transmitted, the overall pressure peak formation may vary depending on the elasticity of the thorax. Therefore, it was verified that the pressure and blood flow rate during CPR are affected by the individual's cardiovascular state, the elasticity of the thorax, and the compression position. Based on these, the possibility of a personalized CPR model was demonstrated through a patient-specific cardiovascular model with changes in the compression position and thoracic elasticity.
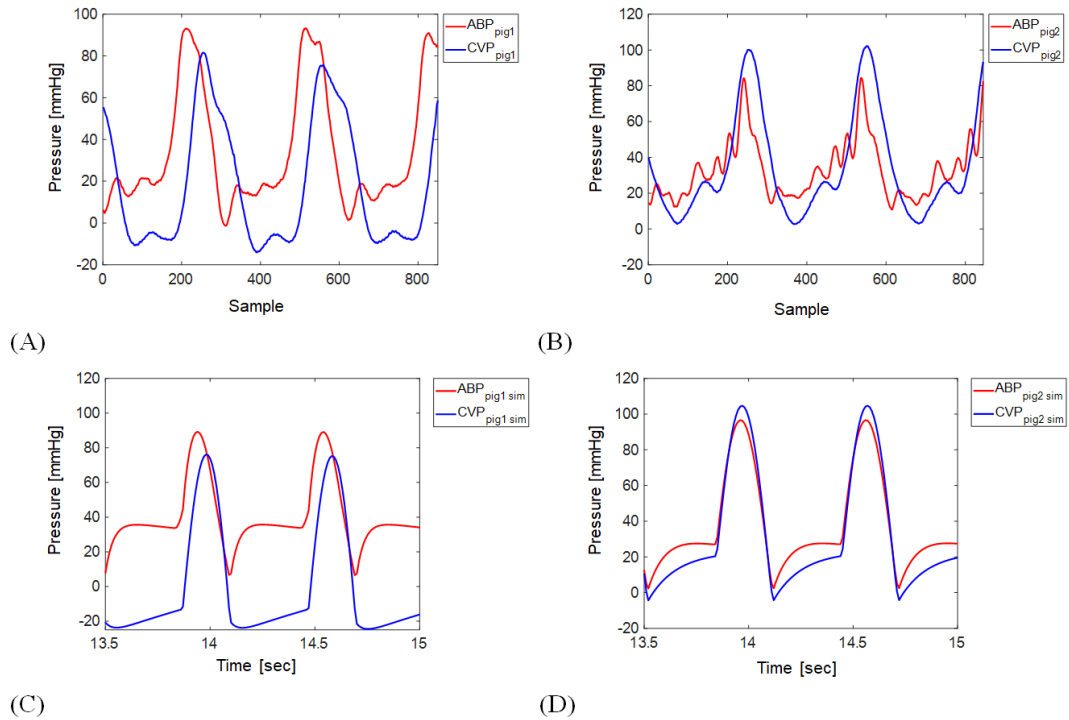
Figure 3.23 Pressure waveform of pig-specific parameter estimated CPR model. (A), (B) is real pressure waveform of pig1, 2. (C), (D) is simulation results of pig 1, 2. Pig 1 was simulated with E = 100 kPa, tpF = 0.4, tpF_v = 1. Pig 2 was simulated with E = 45kPa, tpF = 1, tpF_v = 0.5

To verify whether the optimal CPR strategy and the worst CPR strategy for each pig model can be determined through the developed personalized pig CPR, the simulation was performed with the various CPR condition. For each individualized pig model, the hemodynamics were compared at 4–6 cm of depth and 80–140/min compression rate, varying by 1 cm and 20 cpm (compression per minute), respectively. The depth was adjusted by changing the force applied to the compression (320N for 4cm, 400N for 5cm, and 480N for 6cm). The VAR was compared with the VAR value obtained from the results of the personalized pig CPR model, the value inverse of the VAR value, and the VAR 1 that refers to the compression of all hearts and blood vessels.

In the Pig 1 model, the CPP and CO increased with the increasing compression rate within each depth only at VAR 2.5. However, in VAR 0.4 and VAR 1, the CPP and CO increased as the compression rate decreased (Fig. 3.24). The lowest hemodynamics were observed at the compression position of VAR 0.4, depth of 4 cm, and compression rate of 140, thus it can be considered as the worst CPR strategy with regards to hemodynamics. The best CPR strategy in terms of hemodynamics is the VAR 1, depth of 6 cm, and 80 cpm. However, under this condition, the venous pressure was 220/-52 mmHg, and the aorta pressure was 188/56 mmHg; this demonstrates the results of excessively elevated venous and arterial pressures. Because it is a simple model, the pulmonary arterial pressure cannot be determined, but there may be a risk of adverse effects during CPR. Therefore, if a condition in which the venous pressure is lowered is selected, the depth may be reduced in the same VAR, or the condition maybe 6 cm and 140 cpm at VAR 2.5, in which the pressure of the vessels is reduced. In the Pig 2 model (Fig. 3.25), the CO increased as the compression rate increased under all compression position and depth conditions. However, in the CPP, when VAR=0.5, the CPP tends to decrease as the compression rate increases within each depth. Therefore, the CPR strategy with the worst hemodynamics of pig 2 is at VAR 0.5, 4 cm, and 120 cpm based on the CPP, or at VAR 0.5, 4 cm, and 80 CPM based on CO. Conversely, the best CPR strategy is the VAR 2, 6 cm, 140 cpm. By comparing the CPR strategies

of the two pigs, it can be observed that the hemodynamic effect increases as the compression depth increases, but the compression rate is affected by the compression position. However, the optimal compression depth may vary depending on the compression position when considering the pulmonary arterial pressure and venous pressure.

Figure 3.26 shows the hemodynamic results according to the thoracic elasticity, compression rate, and compression depth based on the Pig 1 model. In this result, the overall hemodynamics tends to decrease as the thoracic elasticity decreases, as in the previous results. In the Pig 1 model, when the VAR is 2.5, it shows that the CPP increases as the compression rate and depth increase, even when the elasticity of the thorax decreases. However, in VAR 1 and VAR 0.4, the CPP increases as the compression rate decreases for all compression depths, and the maximum CPP appears at VAR 1, 6 cm, and 80 cpm conditions. Therefore, it can be considered that the decrease in the thoracic elasticity affects the overall decrease in the pressure amplitude, but does not significantly affect the compression condition. However, because the optimal compression condition changes when the compression position is changed, it indicates that a combination of the appropriate compression position and compression conditions is required.

Therefore, through these results, it can be deduced that the hemodynamics according to the compression position, depth, and rate vary according to the cardiovascular condition, and the worst CPR strategy and optimal CPR strategy are different. Additionally, it is shown that the compression position with the best hemodynamics can be different depending on the cardiovascular state when considering at the hemodynamic improvement alone, and the optimal compression rate varies according to the compression position. Therefore, because optimal CPR conditions vary according to the hemodynamic conditions and compression position, this result can indicate that the CPR strategy should be different according to each patient. However, it is impossible to confirm the pulmonary arterial pressure in this model, thus, it is necessary to confirm through further studies whether the optimal strategy that improves hemodynamics obtained from this study is the best CPR condition.

Furthermore, because the structures of the thoracic cavity and cardiovascular system of the human are different from those of the pig model, it is also necessary to review whether the results based on the animal models can be equally applied to humans.
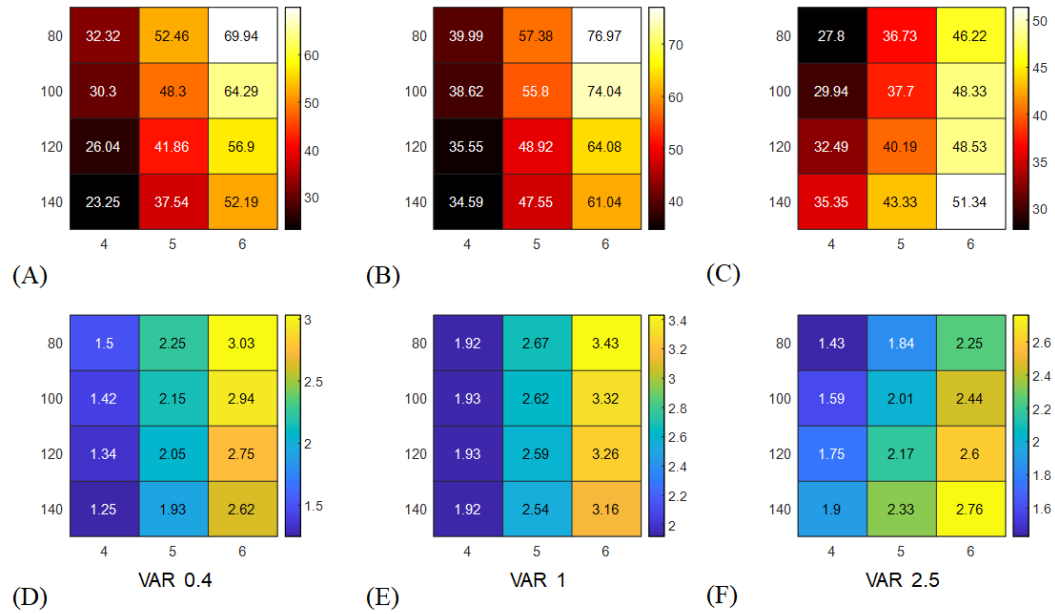
Figure 3.24 Each heatmap is the hemodynamic changes in the personalized Pig 1 model according to change the compression rate and compression depth at a fixed compression position (VAR). In each heat map, the y-axis is the compression rate and the x-axis is the compression depth. The column of the figure represents the VAR. (A) – (C) is the coronary perfusion pressure (CPP, mmHg), (D) – (F) is the cardiac output (CO, L/min).
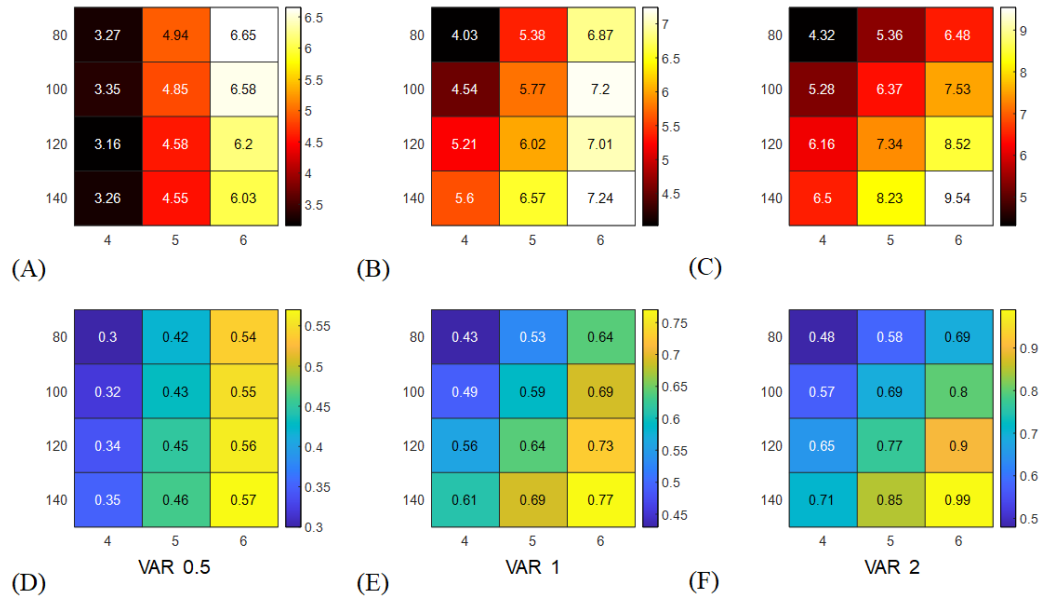
Figure 3.25 Each heatmap is the hemodynamic changes in the personalized Pig 2 model according to change the compression rate and compression depth at a fixed compression position (VAR). In each heat map, the y-axis is the compression rate and the x-axis is the compression depth. The column of the figure represents the VAR. (A) – (C) is the coronary perfusion pressure (CPP, mmHg), (D) – (F) is the cardiac output (CO, L/min).
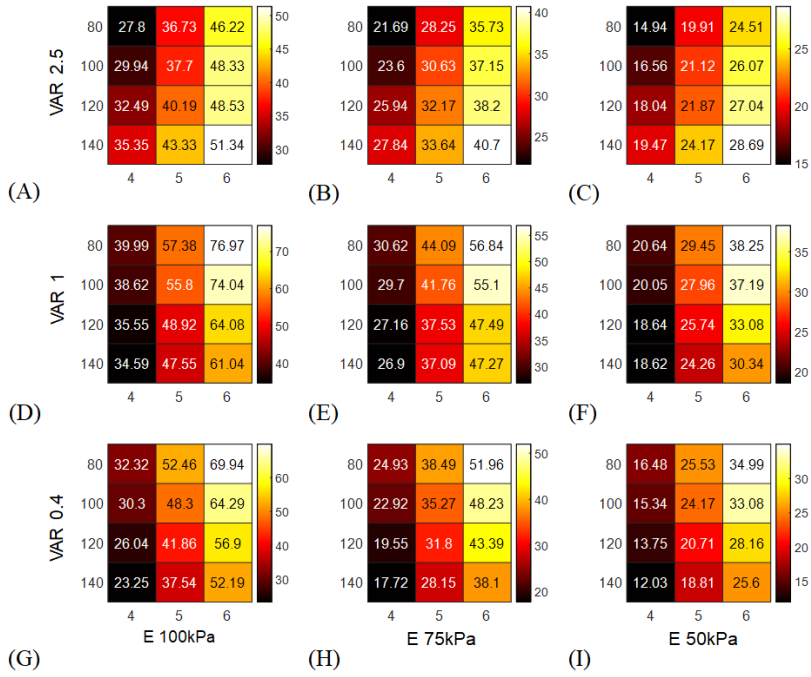
Figure 3.26 CPP changes in the personalized Pig 1 model according to the thorax elasticity, compression rate, and compression depth. In each heat map, the y-axis is the compression rate and the x-axis is the compression depth. The column of the figure represents the thoracic modulus of elasticity of 100 kPa, 75 kPa, and 50 kPa, respectively, and the row is VAR (2.5, 1, 0.4).

3.4 Limitations

This study has several limitations. First, the study was conducted only in the hemodynamic aspect through animal and simulation models. The recovery of ROSC during CPR is not enough to simply improve hemodynamics. Even if the hemodynamic indicators of CPR are improved, it does not guarantee that they have a positive effect on the neurological outcome, and the negative effects of lung damage that may be caused by chest compression cannot be ruled out [96]. However, if the hemodynamic index is improved, it indicates that the circulation of the entire body and blood flow to the heart has been properly performed [97, 98]. Therefore, the hemodynamic indices are the most fundamental for consideration during CPR. Therefore, this study could be the basis for a mathematical model study that can adequately reflect the hemodynamic effects during CPR. Another limitation is that, in HUT and HDT modeling, only systemic circulation was considered, and the relative distance was applied based on the thoracic cavity. Because the hydrostatic pressure is potential energy and depends on the reference point, further research is necessary to reflect the hydrostatic pressure for the distance of each pulmonary and systemic compartment from the heart.

Furthermore, the model used for parameter estimation did not consider pulmonary circulation. Several animal experiments have suggested that longer CPR times or strong compression may affect lung damage such as pulmonary edema [43, 99]. Therefore, considering this, it is necessary to simulate pulmonary circulation in a personalized cardiovascular model. However, in this study, it was impossible to estimate the parameters for the right heart, pulmonary artery, and pulmonary vein of the pulmonary circulation because the animal and open data had only the ABP and CVP. Moreover, in the animal model, because the SV value is unknown, it is impossible to know whether the heart elastance obtained through parameter estimation is properly reflected. Therefore, if there is a blood flow index such as the cardiac output or carotid

blood flow that can represent it, a more accurate parameter estimation will be possible.

The end-diastolic compliance of the heart estimated in the normal condition was applied to the compliance of the heart when simulating cardiac arrest in a personalized CPR model. In the Pig 1 model, the ABP and CVP was 19.6 mmHg during cardiac arrest, and the Pig 2 model had ABP and CVP of 12.6 mmHg. However, the blood pressure during arrest measured in the animal model was slightly different from the simulation results, showing that Pig 1 had an ABP of 14.1 mmHg and a CVP of 9.5 mmHg, whereas Pig 2 had an ABP of 23.4 mmHg and a CVP of 22.3 mmHg. This is because the compliance of the heart and blood vessels varies according to age and disease as well as blood pressure and volume [100, 101]. When cardiac arrest occurs, the blood pressures approach equilibrium because no volume changes occur in the overall cardiovascular system. In this case, because the values of the pressure and volume are different from the normal conditions, the vascular compliance in cardiac arrest may have different values from the normal condition. Because the venous pressure changes significantly during CPR, cardiovascular parameters during CPR may also differ from those estimated in the normal condition. However, although there are many studies on changes in the vascular compliance in various pathological conditions [102], there are no studies conducted on changes in the cardiovascular parameters from the normal condition to the cardiac arrest condition or during CPR. Therefore, studies on the estimation of cardiovascular parameters in cardiac arrest that can reflect the appropriate cardiac arrest status in future studies should be conducted.

The final limitation is that the elasticity of the thorax was arbitrarily applied in the personalized CPR model for each pig model. It is impossible to compare because there is no evidence to confirm whether it reflects the actual thoracic elasticity of the pig. However, in the study for the changes in the elasticity of the thorax, it can be confirmed that the change in the elasticity affects the amplitudes of the ABP and CVP. Therefore, this study can support the evidence for changing the elasticity of the thorax according to the change in the pressure waveform.

CHAPTER 4

Conclusion

4.1 Dissertation summary

First, this study presented a hybrid model of the hybrid pump mechanism that best reflects CPR physiology, by simulating various CPR situations and comparing the differences in hemodynamic characteristics, such as the CPP and SV, with those in the existing model. Furthermore, it was verified through comparison with the animal model that the modified model reflects the current CPR physiology more accurately than the existing model does.

Second, simulations were performed on the reduction of elasticity and optimal compression position, which are current issues in CPR. The decrease in the elasticity of the thorax is reduced by initiating CPR and by chest injuries such as dislocations and rib fractures. Therefore, in this study, the elasticity was simulated as decreasing linearly with time, and accordingly, it was confirmed that the peaks of the ABP and CVP significantly decrease as the elasticity decreases. Similar results were observed for the decrease in the peak pressure of the ABP and CVP at the beginning of CPR in the animal experiments. Additionally, the simulation results showed that when the elasticity decreases, the carotid blood flow, coronary blood flow, and venous return decrease as well. Therefore, these results suggest that the reduction in the elasticity of the thorax can be confirmed through the reduction in the ABP and CVP peaks. In addition, recent studies have suggested that the current uniform compression position may not be appropriate, because the position of the heart may vary among patients and as the blood flow may be restricted because the current compression position compresses the atrium more than the ventricle. Therefore, in this study, a simple simulation was performed by adjusting the thoracic pump factor of the compression ratio of the ventricles and atria to determine the hemodynamic difference according to the compression position. Consequently, when the atrium was more compressed than the ventricle, SV and CPP decreased, indicating that the hemodynamics were limited. Moreover, it was

shown that the CPP has the potential to assist in determining the compression position, considering that the CPP varies according to the compression position.

Finally, this study sought to present the potential of a personalized CPR model through a patient-specific cardiovascular model. Because each person has different cardiovascular conditions, the elasticity of the thorax varies with age and gender, and the position of the heart varies with body type; these personalized factors must be considered to provide optimal CPR quality. However, it is difficult to determine the main cause because all factors interact with each other in clinical application. Therefore, in this study, a patient-specific cardiovascular model was established through parameter estimation with a genetic algorithm, and the effect of each factor was verified by applying it to CPR. Further, to compare the personalized pig CPR model with animal experiments, a pig-specific cardiovascular system model was established based on the results of the animal experiments, and the CPR model was applied. It was verified whether the optimal CPR strategy appeared differently for each pig in the personalized CPR model, and the strategy for CPR in terms of hemodynamics was determined for each pig model. From these results, it was shown that the pressure waveform in the animal experiments and the results of the personalized pig CPR model were similar. It was also inferred that the personalized CPR model and CPR strategy could be established through the cardiovascular parameters, the elasticity of the thorax, and the compression position.

In this study, starting with the improvement of the general CPR model, a method to provide a personalized CPR model was proposed, providing insight into hemodynamics during CPR. Therefore, this study can serve as a basis for research that can contribute to improving patient-specific CPR strategies and new CPR guidelines.

4.2 Future works

Modeling-based CPR research should focus on the development of a patient-specific CPR model based on the results of this study and on creating patient-specific CPR strategies accordingly. First, it is necessary to measure the change in the thoracic elasticity during CPR in an animal model that can support a simulation of the decrease in the elasticity of the thorax and a subsequent analysis of the hemodynamic change that follows. The elasticity is estimated from the chest compression data; based on this data, the optimal compression depth that can minimize hemodynamic changes according to the elasticity change should be determined. Moreover, few clinical or preclinical studies can support studies on the compression positions. Therefore, a compression position capable of improving hemodynamics must be determined through research on various compression positions. Finally, patient-specific models must be improved. The patient-specific model presented herein was developed using simple compartments. However, because pulmonary circulation plays an important role in CPR, it needs to be considered. Hence, the right heart and pulmonary artery parameters must be defined; however, it is difficult to measure all of these parameters and collect the data in practice. Therefore, it is necessary to construct a more delicate cardiovascular model by estimating the unknown parameters based on readily available data.

In clinical application, it is difficult to estimate the parameters and find the optimal conditions through feedback on various CPR conditions because time is crucial when a patient needs CPR. Therefore, to apply a personalized CPR model to a patient based on this study, a model that can immediately derive an optimal CPR strategy by interacting with various patient individual parameters and cardiovascular models must be developed. Therefore, based on a patient that can obtain hemodynamics data, a personalized CPR model should be established for each patient with hemodynamics and individual parameters, including weight, gender, and age. Furthermore, it is necessary to acquire hemodynamic data for various CPR conditions to build a learning model to obtain an optimal CPR strategy. By developing such a learning model, it will

be possible to build an optimal CPR strategy database for various patients. Furthermore, this CPR strategy database allows the improvement of the personalized CPR model into immediately providing an optimal CPR strategy using the patient's blood pressure and several patient-specific parameters.

* In the materials and methods, sections 2.1.1, 2.1.2, and 2.2.2 and their corresponding results, 3.1.1, 3.1.2, and 3.1.3, were published as a research article previously in Computer Methods and Programs in Biomedicine (Dong Ah Shin, Jung Chan Lee, "Mathematical model of modified hybrid pump mechanism for cardiopulmonary resuscitation", 2021) [87].

References

[1] Vincent J-L. Understanding cardiac output. Critical care. 2008;12:1-3.

[2] Klabunde R. Ventricular Pressure-Volume Relationship. Richard E Klabunde Available: https://wwwcvphysiologycom/Cardiac%20Function/CF0252013.

[3] Klabunde R. Effects of Preload, Afterload and Inotropy on Ventricular Pressure-Volume Loops. Ricard E Klabunde Available: https://wwwcvphysiologycom/Cardiac%20Function/CF024 2013.

[4] Dong S-J, Hees PS, Huang W-M, Buffer Jr SA, Weiss JL, Shapiro EP. Independent effects of preload, afterload, and contractility on left ventricular torsion. American Journal of Physiology-Heart and Circulatory Physiology. 1999;277:H1053-H60.

[5] Klabunde R. Frank-Starling mechanism. Richard E Klabunde Available: http://www cvphysiology com/Cardiac% 20Function/CF003 htm Accessed2013.

[6] Berlin DA, Bakker J. Understanding venous return. Intensive care medicine. 2014;40:1564-6.

[7] Beard DA, Feigl EO. Understanding Guyton's venous return curves. Am J Physiol Heart Circ Physiol. 2011;301:H629-H33.

[8] Delicce AV, Basit H, Makaryus AN. Physiology, frank starling law. 2017.

[9] Klabunde R. Venous Return - Hemodynamics. Richard E Klabunde Available: https://wwwcvphysiologycom/Cardiac%20Function/CF0162013.

[10] Rashkind WJ, Lewis DH, Henderson JB, Heiman DF, Dietrick RB. Venous return as affected by cardiac output and total peripheral resistance. American Journal of Physiology-Legacy Content. 1953;175:415-23.

[11] Keener JP, Sneyd J. Mathematical physiology: Springer; 1998.

[12] Hoffman J, Spaan J. Pressure-flow relations in coronary circulation. Physiological reviews. 1990;70:331-90.

[13] Paradis NA, Martin GB, Rivers EP, Goetting MG, Appleton TJ, Feingold M, et al. Coronary perfusion pressure and the return of spontaneous circulation in human cardiopulmonary resuscitation. JAMA. 1990;263:1106-13.

[14] J. Gordon Betts KAY, James A. Wise, Eddie Johnson, Brandon Poe, Dean H. Kruse, Oksana Korol, Jody E. Johnson, Mark Womble, Peter DeSaix. Blood Flow, Blood Pressure, and Resistance. https://openstaxorg/books/anatomy-and-physiology/pages/20-2-blood-flow-blood-pressure-and-resistance2013.

[15] Varon J, Fromm RE. Cardiovascular facts and formulas. Acute and critical care formulas and laboratory values: Springer; 2014. p. 1-23.

[16] Neumar RW, Shuster M, Callaway CW, Gent LM, Atkins DL, Bhanji F, et al. Part 1: executive summary: 2015 American Heart Association guidelines update for cardiopulmonary resuscitation and emergency cardiovascular care. Circulation. 2015;132:S315-S67.

[17] Wik L, Hansen T, Fylling F, Vaagenes P, Steen F. Three minutes of basic cardiopulmonary resuscitation (CPR) of pre-hospital ventricular fibrillation (VF) patients increases the number of patients who restore spontaneous circulation (ROSC). Circulation: LIPPINCOTT WILLIAMS & WILKINS 530 WALNUT ST, PHILADELPHIA, PA 19106-3621 USA; 2001. p. 765-.

[18] Brooks SC, Anderson ML, Bruder E, Daya MR, Gaffney A, Otto CW, et al. Part 6: alternative techniques and ancillary devices for cardiopulmonary resuscitation: 2015 American Heart Association guidelines update for cardiopulmonary resuscitation and emergency cardiovascular care. Circulation. 2015;132:S436-S43.

[19] Paradis N, Martin G, Goetting M, Rosenberg J, Rivers E, Appleton T, et al. Simultaneous aortic, jugular bulb, and right atrial pressures during cardiopulmonary resuscitation in humans. Insights into mechanisms. Circulation. 1989;80:361-8.

[20] Maier GW, Tyson Jr G, Olsen C, Kernstein K, Davis J, Conn E, et al. The physiology of external cardiac massage: high-impulse cardiopulmonary resuscitation. Circulation. 1984;70:86-101.

[21] Babbs CF, Voorhees W, Fitzgerald K, Holmes H, Geddes L. Relationship of blood pressure and flow during CPR to chest compression amplitude:

evidence for an effective compression threshold. Annals of emergency medicine. 1983;12:527-32.

[22] Lurie KG, Nemergut EC, Yannopoulos D, Sweeney M. The physiology of cardiopulmonary resuscitation. Anesth Analg. 2016;122:767-83.

[23] Steinberg MT, Olsen J-A, Eriksen M, Neset A, Norseng PA, Kramer-Johansen J, et al. Haemodynamic outcomes during piston-based mechanical CPR with or without active decompression in a porcine model of cardiac arrest. Scand J Trauma Resusc Emerg Med. 2018;26:31.

[24] Demestiha TD, Pantazopoulos IN, Xanthos TT. Use of the impedance threshold device in cardiopulmonary resuscitation. World J Cardiol. 2010;2:19.

[25] Kwon Y, Debaty G, Puertas L, Metzger A, Rees J, McKnite S, et al. Effect of regulating airway pressure on intrathoracic pressure and vital organ perfusion pressure during cardiopulmonary resuscitation: a non-randomized interventional cross-over study. Scandinavian journal of trauma, resuscitation and emergency medicine. 2015;23:1-10.

[26] Ewy GA. The mechanism of blood flow during chest compressions for cardiac arrest is probably influenced by the patient's chest configuration. Acute Med Surg. 2018;5:236-40.

[27] Cipani S, Bartolozzi C, Ballo P, Sarti A. Blood flow maintenance by cardiac massage during cardiopulmonary resuscitation: Classical theories, newer hypotheses, and clinical utility of mechanical devices. J Intensive Care Soc. 2019;20:2-10.

[28] Vlachopoulos C, O'Rourke M, Nichols WW. McDonald's blood flow in arteries: theoretical, experimental and clinical principles: CRC press; 2011.

[29] Westerhof N, Lankhaar J-W, Westerhof BE. The arterial windkessel. Medical & biological engineering & computing. 2009;47:131-41.

[30] Tsanas A, Goulermas JY, Vartela V, Tsiapras D, Theodorakis G, Fisher AC, et al. The Windkessel model revisited: a qualitative analysis of the circulatory system. Medical engineering & physics. 2009;31:581-8.

[31] Brunberg A, Heinke S, Spillner J, Autschbach R, Abel D, Leonhardt S. Modeling and simulation of the cardiovascular system: a review of applications,

methods, and potentials/Modellierung und Simulation des Herz-Kreislauf-Systems: ein Überblick zu Anwendungen, Methoden und Perspektiven. 2009.

[32] Ursino M. Interaction between carotid baroregulation and the pulsating heart: a mathematical model. American Journal of Physiology-Heart and Circulatory Physiology. 1998;275:H1733-H47.

[33] Avanzolini G, Barbini P, Cappello A, Cevenini G. CADCS simulation of the closed-loop cardiovascular system. International journal of bio-medical computing. 1988;22:39-49.

[34] De Pater L, Van den Berg J. An electrical analogue of the entire human circulatory system. Medical electronics and biological engineering. 1964;2:161-6.

[35] Segers P, Stergiopulos N, Westerhof N, Wouters P, Kolh P, Verdonck P. Systemic and pulmonary hemodynamics assessed with a lumped-parameter heart-arterial interaction model. Journal of engineering mathematics. 2003;47:185-99.

[36] Shim EB, Sah JY, Youn CH. Mathematical modeling of cardiovascular system dynamics using a lumped parameter method. The Japanese journal of physiology. 2004;54:545-53.

[37] Heldt T, Shim EB, Kamm RD, Mark RG. Computational modeling of cardiovascular response to orthostatic stress. J Appl Physiol. 2002;92:1239-54.

[38] Babbs CF, Weaver JC, Ralston SH, Geddes LA. Cardiac, thoracic, and abdominal pump mechanisms in cardiopulmonary resuscitation: studies in an electrical model of the circulation. The American journal of emergency medicine. 1984;2:299-308.

[39] Babbs CF. CPR techniques that combine chest and abdominal compression and decompression: hemodynamic insights from a spreadsheet model. Circulation. 1999;100:2146-52.

[40] Babbs CF. Effects of an impedance threshold valve upon hemodynamics in standard CPR: studies in a refined computational model. Resuscitation. 2005;66:335-45.

[41] Babbs CF. Design of near-optimal waveforms for chest and abdominal compression and decompression in CPR using computer-simulated evolution. Resuscitation. 2006;68:277-93.

[42] Koeken Y, Aelen P, Noordergraaf GJ, Paulussen I, Woerlee P, Noordergraaf A. The influence of nonlinear intra-thoracic vascular behaviour and compression characteristics on cardiac output during CPR. Resuscitation. 2011;82:538-44.

[43] Zhang Y, Karemaker JM. Abdominal counter pressure in CPR: What about the lungs? An in silico study. Resuscitation. 2012;83:1271-6.

[44] Zhang Y, Jiménez-Herrera M, Axelsson C, Cheng Y. Not bad: passive leg raising in cardiopulmonary resuscitation-a new modeling study. Frontiers in physiology. 2017;7:665.

[45] Shin DA, Park J, Lee JC, Do Shin S, Kim HC. Computational simulation of passive leg-raising effects on hemodynamics during cardiopulmonary resuscitation. Comput Methods Programs Biomed. 2017;140:195-200.

[46] Yan S, Gan Y, Jiang N, Wang R, Chen Y, Luo Z, et al. The global survival rate among adult out-of-hospital cardiac arrest patients who received cardiopulmonary resuscitation: a systematic review and meta-analysis. Critical Care. 2020;24:1-13.

[47] Goodwill AG, Dick GM, Kiel AM, Tune JD. Regulation of coronary blood flow. Compr Physiol. 2011;7:321-82.

[48] Scarsoglio S, Gallo C, Saglietto A, Ridolfi L, Anselmino M. Impaired coronary blood flow at higher heart rates during atrial fibrillation: Investigation via multiscale modelling. Comput Methods Programs Biomed. 2019;175:95-102.

[49] SABISTON JR DC, Gregg DE. Effect of cardiac contraction on coronary blood flow. Circulation. 1957;15:14-20.

[50] Wagner H, Hardig BM, Steen S, Sjoberg T, Harnek J, Olivecrona GK. Evaluation of coronary blood flow velocity during cardiac arrest with circulation maintained through mechanical chest compressions in a porcine model. BMC Cardiovasc Disord. 2011;11:73.

[51] Otlewski MP, Geddes LA, Pargett M, Babbs CF. Methods for calculating coronary perfusion pressure during CPR. Cardiovasc Eng. 2009;9:98.

[52] Debaty G, Do Shin S, Metzger A, Kim T, Ryu HH, Rees J, et al. Tilting for perfusion: head-up position during cardiopulmonary resuscitation improves brain flow in a porcine model of cardiac arrest. Resuscitation. 2015;87:38-43.

[53] Kim T, Shin SD, Song KJ, Park YJ, Ryu HH, Debaty G, et al. The effect of resuscitation position on cerebral and coronary perfusion pressure during mechanical cardiopulmonary resuscitation in porcine cardiac arrest model. Resuscitation. 2017;113:101-7.

[54] Kralj E, Podbregar M, Kejžar N, Balažic J. Frequency and number of resuscitation related rib and sternum fractures are higher than generally considered. Resuscitation. 2015;93:136-41.

[55] Azeli Y, Lorente Olazabal JV, Monge García MI, Bardají A. Understanding the Adverse Hemodynamic Effects of Serious Thoracic Injuries During Cardiopulmonary Resuscitation: A Review and Approach Based on the Campbell Diagram. Front Physiol. 2019;10:1475.

[56] Liao Q, Sjöberg T, Paskevicius A, Wohlfart B, Steen S. Manual versus mechanical cardiopulmonary resuscitation. An experimental study in pigs. BMC cardiovascular disorders. 2010;10:1-8.

[57] Jiang L, Min J, Yang F, Shao X. The optimal chest compression point on sternum based on chest-computed tomography: A retrospective study. Hong Kong Journal of Emergency Medicine. 2020;27:197-201.

[58] Anderson KL, Castaneda MG, Boudreau SM, Sharon DJ, Bebarta VS. Left ventricular compressions improve hemodynamics in a swine model of out-of-hospital cardiac arrest. Prehospital Emergency Care. 2017;21:272-80.

[59] Shin J, Rhee JE, Kim K. Is the inter-nipple line the correct hand position for effective chest compression in adult cardiopulmonary resuscitation? Resuscitation
2007;75:305-10.

[60] Nestaas S, Stensæth KH, Rosseland V, Kramer-Johansen J. Radiological assessment of chest compression point and achievable compression depth in cardiac patients. Scand J Trauma Resusc Emerg Med. 2016;24:1-8.

[61] Papadimitriou P, Chalkias A, Mastrokostopoulos A, Kapniari I, Xanthos T. Anatomical structures underneath the sternum in healthy adults and implications for chest compressions. Am J Emerg Med. 2013;31:549-55.

[62] Lampe JW, Padmanaban S, Becker LB, Zanos TP. Towards Personalized Closed-Loop Mechanical CPR: A Model Relating Carotid Blood Flow to Chest Compression Rate and Duration. IEEE Transactions on Biomedical Engineering. 2019;67:1253-62.

[63] Chalkias A, Arnaoutoglou E, Xanthos T. Personalized physiology-guided resuscitation in highly monitored patients with cardiac arrest—the PERSEUS resuscitation protocol. Heart failure reviews. 2019;24:473-80.

[64] Cooper JA, Cooper JD, Cooper JM. Cardiopulmonary resuscitation: history, current practice, and future direction. Circulation. 2006;114:2839-49.

[65] Sebastian PS, Kosmopoulos MN, Gandhi M, Oshin A, Olson MD, Ripeckyj A, et al. Closed-loop machine-controlled CPR system optimises haemodynamics during prolonged CPR. Resuscitation Plus. 2020;3:100021.

[66] Gray RA, Pathmanathan P. Patient-specific cardiovascular computational modeling: diversity of personalization and challenges. Journal of cardiovascular translational research. 2018;11:80-8.

[67] Shi X, Cao L, Reed MP, Rupp JD, Hoff CN, Hu J. A statistical human rib cage geometry model accounting for variations by age, sex, stature and body mass index. Journal of biomechanics. 2014;47:2277-85.

[68] Alpert MA, Terry BE, Cohen MV, Fan TM, Painter JA, Massey CV. The electrocardiogram in morbid obesity. American Journal of Cardiology. 2000;85:908-10.

[69] Huang F, Ying S. On-line parameter identification of the lumped arterial system model: A simulation study. Plos one. 2020;15:e0236012.

[70] Bot CT, Kherlopian AR, Ortega FA, Christini DJ, Krogh-Madsen T. Rapid genetic algorithm optimization of a mouse computational model: benefits for anthropomorphization of neonatal mouse cardiomyocytes. Frontiers in physiology. 2012;3:421.

[71] Plaisance P, Lurie KG, Payen D. Inspiratory impedance during active compression-decompression cardiopulmonary resuscitation: a randomized evaluation in patients in cardiac arrest. Circulation. 2000;101:989-94.

[72] van Heusden K, Gisolf J, Stok WJ, Dijkstra S, Karemaker JM. Mathematical modeling of gravitational effects on the circulation: importance of the time course of venous pooling and blood volume changes in the lungs. Am J Physiol Heart Circ Physiol. 2006;291:H2152-H65.

[73] Williams ND, Wind-Willassen O, Wright AA, Mehlsen J, Ottesen JT, Olufsen MS. Patient-specific modelling of head-up tilt. Math Med Biol. 2014;31:365-92.

[74] Cherry BH, Nguyen AQ, Hollrah RA, Olivencia-Yurvati AH, Mallet RT. Modeling cardiac arrest and resuscitation in the domestic pig. World journal of critical care medicine. 2015;4:1.

[75] Lee D-Y, Kang S-M, Choi S-W. Utility of CPR Machine Power and Change in Right Atrial Pressure for Estimating CPR Quality. Scientific reports. 2019;9:1-7.

[76] Azeli Y, Lorente Olazabal JV, Monge García MI, Bardají A. Understanding the Adverse Hemodynamic Effects of Serious Thoracic Injuries During Cardiopulmonary Resuscitation: A Review and Approach Based on the Campbell Diagram. Frontiers in physiology. 2019;10:1475.

[77] Pickard A, Darby M, Soar J. Radiological assessment of the adult chest: implications for chest compressions. Resuscitation. 2006;71:387-90.

[78] Hwang SO, Zhao PG, Choi HJ, Park KH, Cha KC, Park SM, et al. Compression of the Left Ventricular Outflow Tract During Cardiopulmonary Resuscitation. Academic Emergency Medicine. 2009;16:928-33.

[79] Saeed M, Villarroel M, Reisner AT, Clifford G, Lehman L-W, Moody G, et al. Multiparameter Intelligent Monitoring in Intensive Care II (MIMIC-II): a public-access intensive care unit database. Critical care medicine. 2011;39:952.

[80] Rudikoff MT, Maughan WL, Effron M, Freund P, Weisfeldt ML. Mechanisms of blood flow during cardiopulmonary resuscitation. Circulation. 1980;61:345-52.

[81] Guerci AD, Halperin HR, Beyar R, Beattie C, Tsitlik JE, Wurmb EC, et al. Aortic diameter and pressure-flow sequence identify mechanism of blood flow during external chest compression in dogs. J Am Coll Cardiol. 1989;14:790-8.

[82] Arbogast KB, Maltese MR, Nadkarni VM, Steen PA, Nysaether JB. Anterior-posterior thoracic force-deflection characteristics measured during cardiopulmonary resuscitation: comparison to post-mortem human subject data. SAE Technical Paper; 2006.

[83] Niles DE, Sutton RM, Nadkarni VM, Glatz A, Zuercher M, Maltese MR, et al. Prevalence and hemodynamic effects of leaning during CPR. Resuscitation. 2011;82:S23-S6.

[84] Oh JH. Effects of cardiopulmonary resuscitation time on chest wall compliance in patients with cardiac arrest. Resuscitation. 2017;117:e1.

[85] Young N, Cook B, Gillies M. New resuscitation guidelines may result in an increased incidence of severe chest wall injury, and lead to prolonged length of stay in the Intensive Care Unit. Resuscitation. 2011;82:1355.

[86] Stiell IG, Brown SP, Nichol G, Cheskes S, Vaillancourt C, Callaway CW, et al. What is the optimal chest compression depth during out-of-hospital cardiac arrest resuscitation of adult patients? Circulation. 2014;130:1962-70.

[87] Shin DA, Lee JC. Mathematical model of modified hybrid pump mechanism for cardiopulmonary resuscitation. Computer Methods and Programs in Biomedicine. 2021:106106.

[88] Park J-B, Park Y-M, Won J-R, Lee KY. An improved genetic algorithm for generation expansion planning. IEEE Transactions on Power Systems. 2000;15:916-22.

[89] Ortega R, Connor C, Kotova F, Deng W, Lacerra C. Use of Pressure Transducers. The New England journal of medicine. 2017;376:e26-e.

[90] Moxham I. Physics of invasive blood pressure monitoring. Southern African Journal of Anaesthesia and Analgesia. 2003;9:33-8.

[91] Saugel B, Kouz K, Meidert AS, Schulte-Uentrop L, Romagnoli S. How to measure blood pressure using an arterial catheter: a systematic 5-step approach. Critical Care. 2020;24:1-10.

[92] Romagnoli S, Ricci Z, Quattrone D, Tofani L, Tujjar O, Villa G, et al. Accuracy of invasive arterial pressure monitoring in cardiovascular patients: an observational study. Critical Care. 2014;18:1-11.

[93] Cha KC, Kim HJ, Shin HJ, Kim H, Lee KH, Hwang SO. Hemodynamic effect of external chest compressions at the lower end of the sternum in cardiac arrest patients. The Journal of emergency medicine. 2013;44:691-7.

[94] Ishihara S, Ishihara K, Nagamachi M. Finite element estimation of pressure distribution inside the trunk on a mattress. International Journal of Automation and Smart Technology. 2015;5:217-23.

[95] Garoffolo G, Pesce M. Mechanotransduction in the cardiovascular system: from developmental origins to homeostasis and pathology. Cells. 2019;8:1607.

[96] Sack JB, Kesselbrenner MB. Hemodynamics, survival benefits, and complications of interposed abdominal compression during cardiopulmonary resuscitation. Academic Emergency Medicine. 1994;1:490-7.

[97] Lautz AJ, Morgan RW, Karlsson M, Mavroudis CD, Ko TS, Licht DJ, et al. Hemodynamic-directed CPR Improves Neurologic Outcomes and Mitochondrial Function in Heart and Brain. Critical care medicine. 2019;47:e241.

[98] Yu G, Kim Y-J, Lee S-H, Ryoo SM, Kim WY. Optimal hemodynamic parameter to predict the neurological outcome in out-of-hospital cardiac arrest survivors treated with target temperature management. Therapeutic hypothermia and temperature management. 2020;10:211-9.

[99] Truhlar A, Hejna P, Zatopkova L, Skulec R, Cerny V. Concerns about safety of the AutoPulse use in treatment of pulmonary embolism. Resuscitation. 2012;83:e133-e4.

[100] Safar ME, London GM. Arterial and venous compliance in sustained essential hypertension. Hypertension. 1987;10:133-9.

[101] Tozzi P, Corno A, Hayoz D. Definition of arterial compliance. American Journal of Physiology-Heart and Circulatory Physiology. 2000;278:H1407-H.

[102] Glasser SP, Arnett DK, McVeigh GE, Finkelstein SM, Bank AJ, Morgan DJ, et al. Vascular compliance and cardiovascular disease: a risk factor or a marker? American journal of hypertension. 1997;10:1175-89.

Abstract in Korean

국문 초록

심폐소생술의 생리학적 현상에 대한 이해를 위해 심폐소생술의 메커니즘과 이를 기반으로 한 수학적 모델링에 대한 연구들이 많이 진행되어왔다. 하지만, 기존의 수학적 모델이 아직까지 심폐소생술 중의 혈역학적 현상을 제대로 반영하지 못하고 있는 부분이 있다. 또한, 최근 심폐소생술 연구의 방향성은 환자 맞춤형으로 나아가고 있다. 하지만, 환자 맞춤형 심폐소생술은 환자 개인의 요소 및 주변 환경 요소들의 영향을 받기 때문에 임상환경에서 접근하는 것이 쉽지 않다. 따라서, 본 연구는 시뮬레이션 기반의 이론적 연구를 통해 심폐소생술 중의 혈역학에 대한 이해와 통찰력을 제공하고자 3 가지 목표를 기반으로 연구를 수행하였다.

첫번째는 현재 심폐소생술의 혈역학적 현상을 반영할 수 있는 개선된 일반화된 심폐소생모델을 개발하는 것을 목표로 하였다. 본 연구에서 제안하는 개선된 심폐소생모델은 기존 모델에 상대정맥과 하대정맥 구획을 추가하였고, "하이브리드 펌프" 메커니즘을 적용하였다. 기존 모델과 개선된 모델의 혈역학적인 현상을 비교하기 위해 다양한 기법에 대한 시뮬레이션 및 동물 모델로부터 얻은 데이터를 비교하였다. 동물 모델과 기존 모델, 개선한 모델의 압력 곡선 및 관상동맥관류압 등을 비교한 결과, 본 연구에서 개선한 모델이 현재의 심폐소생술 메커니즘을 더 잘 반영하는 심폐소생모델임을 검증하였다.

두 번째 목표는 개선한 모델을 기반으로 현재의 심폐소생술 방법으로부터 발생하는 이슈인 흉강의 탄성력 감소에 의한 부정적인 영향과 최적의 압박 위치에 대해 시뮬레이션을 통해 혈역학적인 해석을 제공하고자 하였다. 결과에서 흉강의 탄성력이

감소함에 따라 압박 중 최대 압력이 감소하며, 정맥 복귀 및 혈류 역시 감소하는 결과를 보였다. 압박 위치 변화는 심실과 심방의 압박 비율을 조절하여 시뮬레이션을 수행하였다. 이 결과에서 심실보다 심방이 더 많이 압박될 경우 1 회 박출량 및 관상동맥 관류 압이 감소하면서 혈역학이 제한되는 결과를 보여주었다. 따라서, 압박 중 최대 압력 변화와 관상동맥관류압의 변화는 흉강의 탄성력 변화 추정 및 압박 위치 가이드를 해줄 수 있는 잠재력을 가질 수 있음을 입증하였다.

마지막으로 환자 맞춤형 심폐소생술모델의 가능성을 제시하고자 하였다. 본 연구에서는 유전자 알고리즘을 통해 환자 개별에 대한 심혈관계 파라미터를 추정하였고, 환자마다 다른 심혈관계 파라미터 세트를 가짐으로써 맞춤형 심혈관계 모델을 구성할 수 있음을 검증하였다. 또한, 맞춤형 심혈관계 모델에 심폐소생모델을 적용하여 심혈관계 파라미터 구성에 따라 흉부 압박 시 혈역학적 영향이 달라짐을 검증하였다. 추가적으로 돼지 모델에서 다양한 압박 조건 변화에 대한 혈역학적 변화를 비교하였고, 이를 통해 맞춤형 모델을 통해 최적의 혈역학적 효과를 갖는 압박 조건을 제시할 수 있음을 보였다.

결론적으로 본 연구를 통해 제안하는 심폐소생 모델이 현재 심폐소생술에 의한 메커니즘을 더 잘 반영하는 일반화된 모델임을 보여주었고, 이를 통해 현재 심폐소생술 방법에 의한 이슈에 대해서 혈역학적인 해석이 가능함을 입증하였다. 또한, 이를 기반으로 환자 맞춤형 심폐소생 모델의 가능성 제시함으로써 맞춤형 심폐소생 모델링에 대한 연구의 기반이 될 수 있음을 보여주었다.

주요어: 수학적 모델링, 심폐소생술, 환자 맞춤형 심폐소생술, 최적의 압박 위치, 관상 동맥 관류압, 파라미터 추정

학 번: 2015-22886

Acknowledgement

감사의 글

박사학위 기간 동안 많은 분들의 도움과 응원이 있었기에 무사히 학위논문을 마무리할 수 있었고, 이 글을 통해 감사의 인사를 드리고자 합니다.

먼저 저의 지도 교수님이신 이정찬 교수님께 감사드립니다. 스스로 연구의 방향을 잡아갈 수 있도록 세심하게 지도해주신 덕분에 어설펐던 인턴 시절을 거쳐 박사학위를 받는 연구자로 성장할 수 있었습니다. 교수님의 가르침 아래 지식뿐만 아니라 연구의 의미와 연구자로서 가져야할 태도와 같이 연구자로써 많은 것을 배울 수 있었습니다. 앞으로도 교수님의 제자로써 부족함 없는 연구자가 되도록 성실히 연구에 임하겠습니다.

그리고 귀중한 시간 내주셔서 제 박사 학위 논문 심사를 해주신 김희찬 교수님, 서길준 교수님, 최성욱 교수님, 박중열 교수님께 감사드립니다. 특히, ECMO 과제를 수행하면서 실질적인 의료기기 개발 통해 의공학자로써 많은 지식을 얻을 수 있었던 좋은 기회를 주신 김희찬 교수님께 감사드립니다. 바쁘신 와중에도 연구에 열정적이신 서길준 교수님, 교수님과 함께 연구하면서 심폐소생술에 대한 많은 아이디어를 얻을 수 있었고 연구의 열정을 배울 수 있었기에 감사드립니다. 그리고 최성욱 교수님, 아무것도 모르던 학부생이었던 저를 지도해주시고 의공학자가 될 수 있는 기반을 마련해주신 덕분에 이렇게 의공학자로써 성장하여 박사학위를 받을 수 있었던 것 같습니다. 감사합니다. 마지막으로 저의 학위 논문에 대해 진심어린 조언을 해주신 박중열 교수님, 저의 부족한 점을 돌아볼 수 있었습니다. 조금 더 성숙한 연구자가 되도록 앞으로도 노력하겠습니다. 감사합니다.

우리 MBDL 연구실 동료들, 귀찮은 일임에도 마다하지 않고 도와주시는 현주 언니, 항상 열정적인 윤하 오빠, 무슨 일이든 믿고 맡길 수 있는 똑부러진 경진이, 자유로운 영혼 우상이, 사소한 말도 잘

경청해주는 성실한 찬훈이, 별 것 아닌 일에도 꼼꼼하게 신경 써주는 세심한 태우, 모두가 배려해주고 도와준 덕분에 학위 논문을 잘 마무리할 수 있었기에 고마움을 전하고 싶습니다. 그리고 지금 연구실에는 없지만 함께 연구해왔던 병탁이, 형수, 현수, 준희, 준식이, 희수에게도 함께 연구할 수 있어서 즐거웠고 고마웠다는 말 전하고 싶습니다.

그리고 연구실에서 함께 지냈던 MELAB 선배님들과 동료 연구원분들께도 감사드립니다. 바쁘신 와중에도 적극적으로 도움과 조언을 주신 노종민 선배님과 이사람 선배님께 감사드립니다. 그리고 함께 있는 동안 철없는 연구실 동생들 챙겨준 지흠 언니, 처음부터 끝까지 함께 해준 동기 희안이, 학위기간 동안 많은 일들이 있었지만 덕분에 정신적인 지지가 되어서 끝까지 잘 마무리할 수 있었던 것 같아서 특별히 고마움을 전하고 싶습니다.

마지막으로 저를 믿고 지지해주신 가족들에게 진심으로 감사의 말씀드립니다. 사랑하는 부모님, 어린 제 의견을 존중해주시고, 제가 가고자 하는 길을 항상 응원해 주셨기에 여기까지 올 수 있었던 것 같습니다. 너무 감사하고, 사랑합니다. 그리고 뒤쳐짐을 느낄 때 포기하지 않고 열심히 할 수 있도록 응원해준 언니와 동생, 형부, 존재만으로도 힘이 되는 우리 예쁜 조카들 준우, 세령이에게 너무 감사하고 사랑하다는 말 전하고 싶습니다.

이외에도 정신적 지지가 되어준 친구들, 특히 동고동락하며 힘이 되어준 희정이에게도 고맙다는 말 전하고 싶고, 지면으로 미처 언급하지 못하였지만, 함께 연구해왔던 모든 분들께 진심으로 감사하다는 말씀을 전합니다.